Title
The Role of Commercial Buildings in China's Renewable Electricity Future: Forecasting Load and Demand Response Potential

Author
Sifuentes, Froylan Emilfer

Publication Date
2018

Peer reviewed|Thesis/dissertation

The Role of Commercial Buildings in China's Renewable Electricity Future: Forecasting Load and Demand Response Potential

by

Froylan Emilfer Sifuentes

A dissertation submitted in partial satisfaction of the

requirements for the degree of

Doctor of Philosophy

in

Energy and Resources

in the

Graduate Division

of the

University of California, Berkeley

Committee in charge:

Professor Duncan S. Callaway, Chair
Professor Daniel M. Kammen
Professor Alexandra von Meier
Professor Thomas B. Gold

Fall 2018

Abstract

The Role of Commercial Buildings in China's Renewable Electricity Future:
Forecasting Load and Demand Response Potential

by
Froylan Emilfer Sifuentes

Doctor of Philosophy in Energy and Resources

University of California, Berkeley

Professor Duncan S. Callaway, Chair

As renewable energy continues to play a larger role in China's electricity grid, obstacles for increasing grid flexibility and reliability need to be addressed. Improved grid flexibility could be achieved by institutional changes, adding flexible supply, improving the reliability and efficiency of the transmission sector, or enhancing demand side flexibility. This dissertation focuses on the potential of demand response (DR) to provide flexibility in times of extreme need in a future with large penetration of renewables. It develops two different DR models that can be used to estimate DR impact for commercial buildings at the building level and at the national level, respectively.

Using a national level model, this dissertation characterizes the impact of DR events across the commercial sector to provide flexibility across four netload cases in 2030: hours of high and low netload, and hours of high down and up ramping. I describe the methodology to actuate DR by managing the buildings' HVAC system and explain the expected impact statistics. I find that for a 2030 basecase netload scenario with installed renewable capacity of about 1,200 GW, DR from the commercial sector can decrease peak netload between 7 and 12 GW, saving the system between 7 and 12 billion dollars in deferred capacity expansion. Extending demand response to the highest 1% of netload hours in the year, an average of 3 to 4 GW decrease in needed capacity during those hours is possible. This decrease is equivalent to a 276 to 377 GWh reduction in demand, and additional operation savings of between 21 to 28 million dollars. Calculating the cost and benefits of increasing netload at the lowest hours requires further analysis on the potential generation portfolio in 2030 that is likely to benefit from an increased operational baseload. In addition, DR can provide flexibility to alleviate extreme ramping down and up throughout the year. Actuating DR on the highest 1% ramping hours of the year can provide, on average, between 6 to 11 GW per hour and -14 to -27 GW per hour for the extreme down and up ramping hours of the year.

A mi familia.

Contents

Contents iii

List of Figures vii

List of Tables xi

Acknowledgments xv

1 Introduction 1
- 1.1 Chinese electricity growth . . . 2
- 1.2 Pollution problems and climate change . . . 3
  - 1.2.1 COP 21 . . . 3
- 1.3 Renewable energy plans . . . 4
  - 1.3.1 Integration issues . . . 5
- 1.4 Demand response . . . 5

2 Commercial Model 7
- 2.1 Introduction . . . 7
- 2.2 Motivation . . . 7
- 2.3 Assumptions . . . 9
  - 2.3.1 Building types and reference models . . . 9
  - 2.3.2 Climate considerations . . . 14
  - 2.3.3 Sub-Sectoral Estimates . . . 15
- 2.4 Scenarios . . . 17
  - 2.4.1 Efficiency Adoption, ξ . . . 19
  - 2.4.2 Operating Schedules, θ . . . 19
  - 2.4.3 Heating Electrification, χ . . . 20
  - 2.4.4 Summary of parameters . . . 20
- 2.5 Methodology . . . 21
- 2.6 Results . . . 23
  - 2.6.1 Aggregating across the country . . . 25
  - 2.6.2 Literature comparison . . . 25
- 2.7 Discussion . . . 26

2.7.1 Impact of parameters 26
2.8 Conclusion 27

3 Load Forecast Model **29**
3.1 Introduction 29
3.2 Assumptions 29
3.2.1 National and regional consumption, $C_{total,y}$ and $C_{region,y}$ 29
3.2.2 Daily demand share, $S_{total,d}$ 31
3.2.3 Sectoral demand share, $\epsilon_{sector,y}$ 33
3.2.4 Non-Controllable load 34
3.2.5 Controllable Commercial load, $L_{comm_c,r,y}$ 39
3.2.6 Regional and national load, $L_{total,r,y}$, $L_{CH,y}$ 39
3.3 Results 40
3.3.1 2015 vs 2030 basecase comparison 40
3.3.2 2030 load forecast across parameters 41
3.4 Discussion 42
3.5 Conclusion 43

4 Solar and Wind Scenarios **45**
4.1 Introduction 45
4.2 2020 Plans 46
4.2.1 Solar 46
4.2.2 Wind 46
4.2.3 Curtailment issues 49
4.3 Capacity Scenarios 49
4.3.1 Installation growth model 51
4.3.2 Potential 51
4.3.3 Provincial capacity factors 52
4.3.4 Scenario R_a: 2020 goals 52
4.3.5 Scenario R_b: Historic growth, with curtailment 56
4.3.6 Scenario R_c: Historic growth, reduced curtailment 56
4.4 Renewable Production 56
4.5 Conclusion 59

5 Netload Forecast Model **61**
5.1 Introduction 61
5.2 Model Description 61
5.3 Results 63
5.3.1 Netload statistics 63
5.3.2 Statistics variation and renewable scenarios 64
5.3.3 Average daily netload curves 64
5.3.4 Netload duration curves 66
5.3.5 Ramping duration curves 67

5.3.6 Impact of renewables on extreme case days . . . 68
5.4 Discussion . . . 72
5.4.1 Increased flexibility requirements . . . 72
5.4.2 Effect of renewable path . . . 73
5.4.3 Effect of parameters . . . 77
5.5 Conclusion . . . 78

6 Building DR for Regulation **79**
6.1 Introduction . . . 79
6.2 Model Description . . . 80
6.2.1 Wall Model . . . 80
6.2.2 Room Model . . . 81
6.2.3 VAV Terminal Box Model . . . 85
6.2.4 Fan Model . . . 85
6.2.5 Cooling Model . . . 87
6.3 System Simulation . . . 88
6.3.1 MPC Algorithm . . . 89
6.4 Model Testing . . . 90
6.4.1 Zero Mean Target . . . 90
6.4.2 Step Target . . . 91
6.5 Results and Discussion . . . 91
6.5.1 Temperature Comfort with Zero Mean Targets . . . 93
6.5.2 Performance with Step Change Targets . . . 94
6.5.3 Temperature Comfort with Step Targets . . . 95
6.6 Climate Parameters . . . 97
6.7 Conclusion . . . 99

7 Commercial Sector DR Potential **101**
7.1 Introduction . . . 101
7.2 Model description . . . 101
7.2.1 Netload algorithms . . . 104
7.2.2 Ramping algorithms . . . 105
7.2.3 Base case scenario . . . 106
7.3 Results . . . 107
7.3.1 DR impact statistics . . . 107
7.3.2 DR impacts on netload . . . 109
7.3.3 DR impact on ramping . . . 111
7.4 Discussion . . . 113
7.4.1 Impact Assessment . . . 113
7.4.2 Parameter sensitivity analysis . . . 116
7.4.3 Renewable Scenario Effect . . . 119
7.5 Scenario Comparison . . . 121
7.5.1 Netload Comparison . . . 121

7.5.2 DR Impact Comparison 124
7.6 Maximizing DR impact 126
7.6.1 Maximum high netload decrease 127
7.6.2 Maximum high ramping up decrease 127
7.6.3 Maximum high ramping down decrease 128
7.6.4 Key parameters in maximizing DR impact 129
7.7 Conclusion 129

Bibliography **131**

Appendix A Netload Parameters **141**

Appendix B Building Standards **143**

Appendix C Building Intensities **149**

Appendix D DR Flexibility Provision Potential **153**

List of Figures

1 Chinese and US operational schedules for the modeled office building in a weekday . . . 10
2 Chinese and US operational schedules for the modeled retail building in a weekday . . . 11
3 Chinese and US operational schedules for the modeled school building in a weekday . . . 12
4 Chinese and US operational schedules for a modeled guest room in a hotel building in a weekday . . . 13
5 Chinese and US operational schedules for a modeled inpatient room in a hospital building in a weekday . . . 14

6 Daily demand share, S_{total} . . . 32
7 Agricultural S_{ag}, Industrial S_{ind}, and Residential S_{res} hourly shares of daily totals . . . 35
8 Hourly shares of daily total from the non-controlable commercial component of the commercial sector,n $S_{comm_{nc},r}$, for the four different climate regions in China . . . 37
9 Hourly shares of daily total from the non-controlable commercial component of the commercial sector in the winter season, $S_{comm_{nc},r}$, for the four different climate regions in China . . . 38

10 Hourly shares of yearly national total case case load and netload for the three renewable penetration scenarios . . . 65
11 Load duration curve details on the lowest and highest 1% of hours in the year of base case load and netload for the three renewable penetration scenarios in 2030. . . . 66
12 Load duration-type curve details on the lowest and highest 1% of hours in the year of base case load and netload ramping for the three renewable penetration scenarios in 2030. . . . 67
13 Renewable production impact on the 24 hours around the lowest and highest netload hour for the netload model $NL(\xi_1, \theta_1, \chi_1, R_c)$ for load and netload across the three renewable penetration scenarios. . . . 69

14 Renewable production impact on the 24 hours around the lowest and highest netload ramping hour for the netload model $NL(\xi_1, \theta_1, \chi_1, R_c)$ for load and netload across the three renewable penetration scenarios. . 71
15 Extreme hourly ramps in netload with increasing renewables penetration level in China. Maximum ramp values as well as positive and negative ramps presenting 0.1% and 1% of exceedence level are shown. 74

16 Two later wall model diagram 81
17 Side view diagram of a room 82
18 Block diagram for the coupled wall - air mass model 84
19 Block diagram for the terminal box model 85
20 Block diagram for the fan model 86
21 Block diagram for cooling model 88
22 Block diagram for building's HVAC system 89
23 Tracking results for a single zero mean target trajectory within ±20% limits 92
24 Error as a function of target range for all runs. 92
25 Temperature deviations in the building as a result of following signal shown in Figure 23 93
26 Sample of tracking results for step target requests 94
27 $|\epsilon_{\%}|_2$ as a function of step target request 95
28 Temperature deviations in the building associated with a +10% step target 96
29 Temperature deviations in the building associated with a +20% step target 96
30 $|\theta|_2$ and $|\theta|_\infty$ as a function of step target 97
31 $P_{\theta>12.7^\circ C}$ and $P_{\theta>18.3^\circ C}$ for different US climate zones 99

32 DR impact on netload for base netload scenario for the lowest and highest netload hours of the year, in GW 110
33 DR impact on ramping for base netload scenario for the highest ramping down and up hours of the year, in GW per hour 112
34 Load duration curve details on the lowest and highest 1% of hours in the year for the base case netload (Scenario A) and a comparison netload scenario (Scenario B). 122
35 Netload scenarios comparison of the 24 hours around the lowest and highest netload hour for the netload model $NL(\xi_2, \theta_1, \chi_3, R_c)$, (Scenario B). 123
36 Ramping duration curve details on the lowest and highest 1% of hours in the year for the base case netload (Scenario A) and a comparison netload scenario (Scenario B). 124

37 Netload scenarios comparison of the 24 hours around the lowest and highest ramping hour for the netload model $NL(\xi_2, \theta_1, \chi_3, R_c)$, (Scenario B). 125

List of Tables

1 Climate regions in China 15
2 Fraction of commercial sector electricity consumption consumed by building type, in 2015, 2020 and 2030, across all climate regions, $\rho_{b,r,y}$ 16
3 Chinese Office building standards over time and across climate regions 18
4 Proportion of offices with datacenters, δ, between 2010 and 2030 19
5 Commercial building model parameters 21
6 Building intensity with 2005 standards, by climate region, in $\frac{kWh}{m^2}$ . . . 23
7 Building intensity of the base case scenario in 2030 for individual buildings and regional average, by climate region, in $\frac{kWh}{m^2}$ 24
8 Building intensity change, in percentage, from the 2005 standard case scenario to the 2030 base case scenario for individual buildings and regional average, by climate region, in $\frac{kWh}{m^2}$ 24
9 Average commercial sector, building intensity, $\frac{kWh}{m^2}$ 25
10 Percentage effect of changing a parameter from the average regional climate building intensity on the base case scenario 26

11 Model demand in TWh, at the national, climate region, and provincial level for years 2015, 2020, and 2030 31
12 Sectoral demand share of total electricity consumption in a given year . 33
13 2015 and basecase scenario 2030 load comparison across descriptive statistics. Percent change from 2015 load statistics 41
14 Descriptive statistics for all load models developed across all parameters 41
15 Percent change in load statistics from a variation in parameter 42

16 Solar and wind installed capacity in 2010 and 2016 in MW and yearly growth in this period in %. 46
17 Solar and Wind installed capacity in 2016, by province, MW 47
18 Provincial and national installed and planned solar capacity in 2016 and 2020, respectively, and yearly growth rate in MW and %, respectively . 48
19 Provincial and national installed and planned wind capacity in 2016 and 2020, respectively, and yearly growth rate in MW and %, respectively . 50
21 Cities and provinces with curtailment constraints between 2016 and 2020 development plans 51

22 Low and High Solar PV installation potential, respectively, by province, GW . . . 53
23 Low and High estimates for onshore wind, and offshore wind, installation potential, respectively, by province, GW . . . 54
24 Mean (μ) and standard deviation (σ) for hourly capacity factor data by province and renewable type . . . 55
25 Solar PV and wind capacity installations for the three different 2030 scenarios, by province, GW . . . 57
26 Installed renewables capacity and total yearly electricity production in 2030 under different scenarios . . . 59

27 Global parameters for the national hourly netload model . . . 62
28 Netload statistics for the base case load scenario $L(\xi_1, \theta_1, \chi_1)$ for the three different renewable penetration scenarios. . . . 63
29 Netload statistics change from base case load $L(\xi_1, \theta_1, \chi_1)$, for the three different renewable penetration scenarios, in percentage terms . . . 64
30 Netload statistics comparison between renewable scenario R_b and the other two renewable scenarios, holding base case load constant, in percentage terms . . . 74
31 Power plant CO_2 emissions and COE data . . . 76
32 Associated carbon emisssions and cost savings for the three different renewable scenarios . . . 76
33 Netload statistics effect of change in load parameters, holding renewable scenario R_b constant, in percentage terms . . . 77

34 Wall model parameters . . . 82
35 Room model parameters . . . 83
36 Fan model parameters . . . 86
37 Cooling model parameters . . . 87
38 $|\theta|_2$ and $|\theta|_\infty$ associated with zero mean target's within specified limits 93
39 Climate zones in representative cities . . . 98

40 Parameters for the base case netload scenario . . . 106
41 Statistics for base netload scenario . . . 107
42 DR impact statistics for the lowest and highest netloads in the year . . 108
43 DR impact statistics for the highest ramping up and down rates in the year . . . 109
44 Descriptive statistics for the impact of DR on the lowest and highest netload 1% of hours in the year, in GW or % terms) . . . 110
45 Descriptive statistics for the impact of DR on the highest ramping down and up 1% of hours in the year, in GW per hour or % terms) . . . 111
46 Power plant CO_2 emissions and COE data . . . 114

47 Effect of changing parameter on the mean demand response to a 1^oC temperature setpoint signal across different DR scenarios, as a percent of original response 116
48 Effect of different renewable scenarios on the mean demand response to a 1^oC centigrade temperature setpoint signal across different DR scenarios, as a percent of original response 119
49 Netload impact of a 1^oC temperature setpoint change across two different netload scenarios 126
50 Ramping impact of a 1^oC temperature setpoint change across two different netload scenarios 127
51 Maximum mean decrease in load in GW (μ) and as a percentage of netload ($\mu_{t,\%}$) across all hours affected by DR events across all parameters and renewable penetration scenarios studied 127
52 Maximum mean decrease in ramping up rates in $\frac{\text{GW}}{h}$ (μ) and as a percentage of ramping ($\mu_{t,\%}$) across all hours affected by DR events across all parameters and renewable penetration scenarios studied 128
53 Maximum mean decrease in ramping down rates in $\frac{\text{GW}}{h}$ (μ) and as a percentage of ramping ($\mu_{t,\%}$) across all hours affected by DR events across all parameters and renewable penetration scenarios studied . . . 128

54 Global parameters for the national hourly netload model 141

55 Chinese hospital building standards over time and across climate regions 144
56 Chinese hotel building standards over time and across climate regions . 145
57 Chinese office building standards over time and across climate regions . 146
58 Chinese retail building standards over time and across climate regions . 147
59 Chinese school building standards over time and across climate regions 148

60 Hospital building intensity, $\frac{kWh}{m^2}$ 149
61 Hotel building intensity, $\frac{kWh}{m^2}$ 150
62 Office building intensity, $\frac{kWh}{m^2}$ 150
63 Office with no data center intensity, $\frac{kWh}{m^2}$ 151
64 Retail building intensity, $\frac{kWh}{m^2}$ 151
65 School building intensity, $\frac{kWh}{m^2}$ 152

66 Definitions for DR flexibility provision statistics 153
67 DR flexibility provision: netload decrease, for high netload case and renewable scenario R_a, in GW 154
68 DR flexibility provision: netload decrease, for high netload case and renewable scenario R_a, in percentage deviation 155
69 DR flexibility provision: netload increase, for low netload case and renewable scenario R_a, in GW 155
70 DR flexibility provision: netload increase, for low netload case and renewable scenario R_a, in percentage deviation 156

71 DR flexibility provision: ramping decrease, for high ramping up case and renewable scenario R_a, in $\frac{GW}{h}$ 156
72 DR flexibility provision: ramping decrease, for high ramping up case and renewable scenario R_a, in percentage deviation 157
73 DR flexibility provision: ramping increase, for high ramping down case and renewable scenario R_a, in $\frac{GW}{h}$ 157
74 DR flexibility provision: ramping increase, for high ramping down case and renewable scenario R_a, in percentage deviation 158
75 DR flexibility provision: netload decrease, for high netload case and renewable scenario R_b, in GW 158
76 DR flexibility provision: netload decrease, for high netload case and renewable scenario R_b, in percentage deviation 159
77 DR flexibility provision: netload increase, for low netload case and renewable scenario R_b, in GW 159
78 DR flexibility provision: netload increase, for low netload case and renewable scenario R_b, in percentage deviation 160
79 DR flexibility provision: ramping decrease, for high ramping up case and renewable scenario R_b, in $\frac{GW}{h}$ 160
80 DR flexibility provision: ramping decrease, for high ramping up case and renewable scenario R_b, in percentage deviation 161
81 DR flexibility provision: ramping increase, for high ramping down case and renewable scenario R_b, in $\frac{GW}{h}$ 161
82 DR flexibility provision: ramping increase, for high ramping down case and renewable scenario R_b, in percentage deviation 162
83 DR flexibility provision: netload decrease, for high netload case and renewable scenario R_c, in GW 162
84 DR flexibility provision: netload decrease, for high netload case and renewable scenario R_c, in percentage deviation 163
85 DR flexibility provision: netload increase, for low netload case and renewable scenario R_c, in GW 163
86 DR flexibility provision: netload increase, for low netload case and renewable scenario R_c, in percentage deviation 164
87 DR flexibility provision: ramping decrease, for high ramping up case and renewable scenario R_c, in $\frac{GW}{h}$ 164
88 DR flexibility provision: ramping decrease, for high ramping up case and renewable scenario R_c, in percentage deviation 165
89 DR flexibility provision: ramping increase, for high ramping down case and renewable scenario R_c, in $\frac{GW}{h}$ 165
90 DR flexibility provision: ramping increase, for high ramping down case and renewable scenario R_c, in percentage deviation 166

Acknowledgments

A special thanks to my main advisor and mentor Prof. Duncan Callaway and the other members of my dissertation committee Profs. Dan Kammen, Alexandra von Meier and Thomas B. Gold. Also, thanks to my many collaborators: Gang He at Stony Brook University, Fritz Kahrl at E3, Wei Feng in the China Energy Group of the Lawrence Berkeley National Lab (LBNL), Rongxin Yin in Grid Integration Group of LBL, Taylor Keep at KATERRA, and Zhaoguang Hu formerly at the State Grid Energy Research Institute. Thanks to everyone in the ERG community, especially to Kay Burns who has supported me for almost as long as Duncan. Thanks to the EMAC research group for stimulating conversations and feedback.

This research was supported by a UC Berkeley Chancellor's Fellowship, the Boren and Blakemore Fellowships, and a National Science Foundation Graduate Research Fellowship under Grant No. DGE-1106400.

Chapter 1

Introduction

China is the world's largest energy consumer, coal producer and consumer, and carbon dioxide emitter. Over 60% of its total energy requirements are satisfied by coal [2]. In addition, China relies heavily on coal for electricity production [3]. This reliance on coal has not only led China to become the largest carbon dioxide emitter in the world [2] but has also raised new national security concerns [4]. Simultaneously, due to decreasing costs, government incentives, and a desire to ameliorate pollution[5], and climate change [6], China has also become the world's leader in installed capacity of renewable energy. The National Renewable Energy Law, passed in 2005 and revised in 2009, mandates an increased share in electricity production from renewable sources by 2020 [7]. China has set up ambitious renewable energy development target to have 20% of its primary energy from non-fossil sources by 2030 [8].

By the end of 2016, China's installed wind power capacity had reached 148 GW, up from 1.3 GW in 2005. Wind power has been the fastest growing renewable energy source nationally in the past 6 years and, according to the latest Five-Year plan, it is expected to surpass 210 GW of installed capacity by 2020 [9]. Similarly, solar photovoltaic (PV) capacity is expected to surpass 100 GW by 2020 with an additional 5 GW of installed concentrated solar capacity also expected by 2020 [10].

With increased participation in the procurement of electricity, renewable sources typically encounter grid integration issues [11] [12]. In California, an important consideration to achieve the renewable portfolio standards (RPS) has been the increase in system regulation requirements [13]. China shares some of these problems in integrating renewables with California [14], but due to large structural differences, such as over reliance on coal and a relative lack of gas infrastructure and resources, it also faces a different set of complex challenges [3] [15].

In this chapter we frame our research and elaborate on our motivations for developing an electricity load model [Chapter 3]. As an introduction, we contextualize the historical growth of electricity consumption in China and the interrelated issues of atmospheric pollution in Sections 1.1 and 1.2. In addition, we will contextualize this electricity consumption growth and associated pollution problems within China's commitments in COP21 to reduce carbon intensity and emissions, and increase renewable

capacity in Sections 1.2 and 1.3. In later chapter, the electricity load model is used to understand the flexibility requirements of the Chinese grid under different renewables penetration scenarios in 2030 [Chapter 5]. We make a case for flexibility provision using demand response (DR) to alleviate some of these constraints in Chapter 7.

1.1 Chinese electricity growth

Electricity consumption per capita in China has increased 13-fold between 1980 and 2014, rising from 281 kWh to 3927 kWh per person. By 2015, total national electricity consumption reached 6,000 TWh[16]. With over 70% of national electricity output produced by coal in 2015, China has met most of the historical growth in demand by electricity production from coal power plants. Nonetheless, the government plans for a flattening of coal generation by shifting to renewable power [17]. Most recently, in the beginning of 2017, China announced its intention to invest 360 billion USD in renewable energy [18] by 2020. Estimates for per capita electricity consumption in 2030 range widely from 5308 to 8292 kWh [19]. In Chapter 3 we develop a model of an hourly load forecast with a controllable commercial component (Chapter 2) using, in part, yearly demand estimates from [19].

In China, most of the population and economic output is concentrated in the urban eastern coastal provinces [20]. Consequently, the majority of electricity consumption occurs in these densely populated regions with high rates of urbanization [21]. As population and economic output continue to increase, these coastal regions are expected to maintain the lead in future electricity consumption, but the interior regions are expected to increase their share as well[22]. Furthermore, as China's economy moves from an export-oriented model to a consumer-based model, shifts in the economic and electricity consumption patterns will occur. In this work we will focus primarily in the increasing role of commercial buildings in electricity consumption, but also, their role in providing flexibility to the grid [Chapters 2-7].

Since the country's electricity system currently runs primarily on coal, their future climate emissions and ability to stay within a safe carbon budget depends on the prospects of producing electricity from renewable sources. In addition to climate change concerns, coal dependence presents other significant problems to Chinese development. First, coal producing regions, such as Shaanxi, Gansu, and Inner Mongolia are far away from load centers. Consequently, in order to power the eastern regions, coal has to be transported by freight, boat, or trucks, or alternatively, electricity generated in the coal producing regions is transmitted over vast distances. If the coal is burned nearby cities, pollution problems arise that increase mortality and morbidity, and reduce productivity [5].

1.2 Pollution problems and climate change

Chinese pollution problems are well known and documented in the media [23, 24, 25], affecting millions of lives every day, especially in Northern China and urban centers. Researchers have linked air pollution issues in Northern China to regional electricity production sources [26]. Research shows that pollution levels have a negative effect on the health of citizens of major cities, leading to increased health care costs and premature deaths [27, 28]. Partly due to these air pollution concerns, all levels of government have increased their interest in integrating larger amounts of renewables into their electricity grid. Unfortunately, pollution has also contributed to a reduction of renewable electricity production as studied by Mauzerall et al [29].

As coal-based electricity production in China has increased over the last thirty years, so have carbon dioxide emissions. China became the biggest carbon dioxide emitter in 2009, surpassing the United States. In 2015, national annual emissions reached approximately 10.5 Gt, accounting for close to 30% of the global total [30]. In an analysis done by CarbonBrief, after a three year plateau, carbon dioxide emissions rose about 2% in 2017 [31]. On a per capita basis, Chinese emissions continue to rise but still lag behind developed countries.

1.2.1 COP 21

Some researchers argue that coping with climate change should no longer be regarded as a cost for China, but rather as an opportunity to help deliver better national growth, environment, and energy infrastructure to its people[32]. In December 2015, China, together with 200 other countries agreed to take further steps to limit emissions contributing to climate change. In particular, China undertook several commitments. First, China committed to reducing carbon intensity by around 65% from 2005 levels by 2030. Second, China committed to increasing non-fossil-fuel energy to 20 percent of its energy mix, and third, they committed to reaching peak carbon emissions by 2030 [33]. Although the country has made significant progress since 2015 it showed a 2% increase in carbon emissions in 2017 [31]. Coal consumption remained relatively flat between 2013 and 2016, with some analysts claiming a peak in consumption [34], but as with carbon emissions, coal consumption also grew in 2017 [35].

In contrast to the relative small growth in coal consumption and carbon emissions, solar and wind energy utilization continues to grow at the fastest pace in the world [8]. A transition to cleaner energy will help China tackle its air pollution challenges and put the countrys future growth on a low-carbon pathway [33]. How China gets there depends on how ambitiously they implement their national efficiency and renewable energy plans.

An analysis by Climate Action Tracker contextualizes China's efforts to combat climate change [36], estimating that if current efforts are kept or increased for the next decade, it is likely that emissions will plateau to about 12 $GtCO_2e$ per year. If, however, coal consumption does not continue to decline, and instead stalls at todays

levels, and if no additional policies are introduced to limit other, non-CO_2greenhouse gases, China's total GHG emissions could continue to rise until at least 2030 [36]. In part, how the country achieves a total decrease in coal consumption depends on how fast renewable energy plays an increasing role in meeting national energy demand.

1.3 Renewable energy plans

China's renewable energy law, passed in 2005 and updated multiple times since then, stipulates a minimum contribution of 20% of energy production from renewable sources (including large hydro) to meet national energy needs by 2030 [7]. In order to achieve this national target of 20% non-fossil primary energy by 2030, an additional 800 to 1000GW of low-carbon power capacity needs to be deployed [42]. As mentioned earlier, in its most recent Five-Year Plan, the Chinese government has announced goals to expand solar and wind capacity to over 100 and 200 GW, respectively, by 2020 [10, 9]. This Five-Year Plan gets China a portion of the way towards their 2030 goals.

Increasing penetration of renewable intermittent electricity in the Chinese grid is driven, in part, by efforts to meet 2030 goals, combat pollution and climate change, as well as forward national strategies to become a world leader in this area. China's installed solar and wind capacity and production currently exceeds that of any other country, and meeting these goals would only further their global lead. Even after meeting their goals, there would be untapped potential for both solar and wind resource utilization in the country.

While China's 2030 goals may seem ambitious, the country has the resource potential to meet them. Studies on the potential of wind generated electricity in China show that the resources available could reduce dependency on coal to meet large amounts of national energy needs [37, 38]. Other studies on resource potential have focused on the practical questions of the integrating such large wind capacity into the grid [15]. Similarly, studies on the potential of solar generation in China show great prospects in reducing dependency on coal [39, 40, 41]. When accounting for all non-fossil sources, a comprehensive energy system study by the Deep Decarbonization Pathways project estimates that the share of these sources in total electricity generation could reach approximately 43% in 2030[32].

As the experiences in California, Denmark, and countries with large amounts of renewables in their electricity system show, there are integration issues that need to be throughly studied and addressed in order to integrate higher amounts of renewables. In Chapter 4 we explore different renewable pathways to 2030 and compare their impact on netload in Chapter 5. Two of the three renewable pathways developed in Chapter 4, in accordance with our scenario projections, propose solar and wind capacities that surpass the estimated 1000 GW of low-carbon power needed to meet the national 20% non-fossil primary energy target by 2030.

1.3.1 Integration issues

With installed solar and wind capacities of 130 and 160 GW, respectively, by the end of 2017, there seems to be little doubt that China will exceed its own national renewable capacity 2020 goals [43]. Their solar capacity goals have already been exceeded ahead of schedule, and wind capacity goals are nearly met. Nevertheless, when analyzing electricity production, we can see that capacity factors are unusually low [44] and monumental efforts will be required to integrate the estimated 800 to 1000 additional GW of non-fossil fuel power. Specifically, the capacity factor from wind is also around 20% [41], much lower than the typical 30% found in the United States[45].

Flexibility and reliability

According to a recent study by the Danish Energy Agency, China faces three kinds of flexibility challenges at present. First, prices do not provide incentive to provide flexibility. Second, Chinese power plants are not as flexible as their Danish counterparts. Third, the distance between load centers and production areas is large and leads to inefficiencies [46]. A reality of the Chinese electricity system is that the provinces with the largest solar and wind power potential are often far away from the load centers [40, 38]. Having low demand placed next to high supply locations often leads to transmission lines not being built, and therefore, around 10% of installed capacity is persistently unconnected to a transmission line at any point in time [44]. In response to these issues, transmission lines, and especially ultra-high voltage DC lines, are now being built across the country to connect high load centers on the coast to high supply regions, like Northwestern China.

As renewable energy continues to play a larger role in China's electricity grid, obstacles for increasing grid flexibility and reliability need to be addressed. Overall improved flexibility could be achieved by institutional changes, adding flexible supply, improving the reliability and efficiency of the transmission sector, and enhancing demand side flexibility. In this work, we focus specifically on the challenges and potential of demand response to provide flexibility to the Chinese grid in times of extreme need in a future with high penetration of renewables.

1.4 Demand response

Managing demand in times of critical need to alleviate grid constraints has been studied in a variety of contexts and locations. In China, Wang et al provides context for the potential utilization of demand response to alleviate electricity shortages [47]. Hu et al describes China's experience with demand side management and explores the barriers to, and the potential for, new demand-side investment [48]. Other studies focus on DR's potential in flexibility provision for the integration of renewables in other countries with large renewable portfolios [49]. In the US, studies have investigated how regions that depend on variable hydro-electric resources can enhance their flexibility through

demand management to help integrate new electricity generation from solar and wind sources[50].

Until recent years, the most commonly used form of demand curtailment in China was industry based, in which distribution and transmission networks serving industrial clients are required to shutdown, or at least run their own grid-independent plants. Efforts to study the ability of industrial loads to provide ancillary services have been done by Yao et al [51].

A more economically sensible, and less intrusive way of managing demand is through widespread sharing of demand response needs across many buildings [52, 53]. In the US, an often studied way of managing electricity demand relies on adjusting buildings' temperature setpoints in heating, ventilation, and air conditioning (HVAC) systems. A building usually has two temperature setpoints that frame the range of temperatures comfortable to occupants. If temperature in the building goes above the upper setpoint, the HVAC system cools, and if the temperature in the building dips below the lower setpoint, the HVAC system heats. In traditional DR, an increase in the upper setpoint, would lead to a decrease in power consumption in summer. In the winter, the same increase in upper setpoint would lead to an increase in power consumption. In contrast to traditional DR, continuous DR strategies allow systems to continuously manipulate temperature setpoints, and therefore the system's power consumption, to match a system operator's frequent requests rather than only large infrequent deviations from baseline [54].

In this work we aim to provide an analysis on the potential and impact of managing both traditional and continuous demand response from the commercial sector to provide flexibility and reliability services in a Chinese grid with increasing penetration of renewables. In Chapters 6 and 7 we present two different demand response models that can be used to estimate DR for commercial buildings at the building level and at the national level, respectively.

Chapter 2

Commercial sector electricity load model for China

2.1 Introduction

From 1990 to 2016, the commercial sector electricity consumption in China has seen a 2000% increase going from 38 to roughly 800 TWh. The corresponding share in electricity consumption from the commercial sector in the same period has grown from 4 to 13.4% of the total electricity consumption in their respective year [21].

Yearly electricity consumption growth has also been faster for the commercial sector than the total consumption growth of any other economic sector in the country. Between 2015 and 2016, the commercial sector consumption grew by 11.2%, while the yearly total electricity consumption grew by 4.9%. For the 2010-2017 period, yearly growth rates for the industrial, residential and commercial sectors have been 6.5, 8.4, and 10.6% respectively [21].

As the economy continues to evolve and the country transitions to a more consumer based growth, the commercial sector will continue to increase their share in electricity consumption. By 2030, we expect the commercial sector to consume 16.3% of the total electricity consumption[55].

In this chapter, our developed hourly load model for the Chinese commercial sector will be described. We first state our motivations to create such a model and state our assumptions in building it. We then describe the methodology used to construct it, including the individual building models used. Finally, we compare some of the model results with available data from other research sources.

2.2 Motivation

The commercial sector model described in this section is built for two main purposes. First, the model will be used to develop an hourly load forecast model to 2030. Second, the models will be used to estimate the demand response potential of the commercial

sector as the economic structure evolves and becomes more service oriented.

The main motivation to fulfill the first purpose, that is, to build a commercial sector model to aid in the forecast of load in 2030 comes from the lack of available and reliable hourly data to describe electricity demand on a regional and national basis. In the SWITCH China model, He et al constructed hourly load models based on monthly and hourly consumption shares across all load in the system [41]. Although these load models allow the SWITCH optimization to broadly analyze distinct parts of the yearly load curve, they fall short in accounting for changing proportions in the electricity load from the different industrial, residential and commercial sectors, and from the different building types in the commercial sector.

Buildings in the United States and China consumed 41% and 28% of the total primary energy in 2011, respectively [56]. We assume that buildings in China will continue to increase their energy consumption share and close the gap with their US counterparts. Economic restructuring will be a driving factor in changing the daily load shape and its load procuring requirements. In addition to its very significant expected load growth, with estimates having China consuming between 2 and 3 times more electricity in 2030 than in 2010 [57, 58], the load shape changes will lead to increased peak capacity and flexibility requirements. Although both residential and commercial sectors will increase in importance in future electricity consumption, this work only describes models for commercial buildings. The rationale behind this is that under the same data availability restrictions, it is more feasible to construct commercial building models that conform to published norms. Residential buildings vary much more significantly in vintage, applicable construction standards, and appliance ownership models.

Building physically-based building models for the commercial sector is important in order to understand future load shapes for several reasons. First, modifying the physical characteristics of the model will impact the load shape of a typical day in 2030. For example, having a very small load factor in the commercial sector, will in turn reduce the load factor of the total load in a given day if the industrial and residential load hourly models are unchanged. Having an available model to test and measure how much will the peak load and flexibility requirements change with changing sectoral proportions is of key interest. In this work, we will use non-parametric load curves to represent the hourly behaviors of agricultural, industrial and residential loads in aggregate. These load curves will be explained further in Chapter 3 below, and are based on work by Yao et al [51].

A second reason we feel motivated to build physically-based building models for the commercial sector is that, as is the case with commercial buildings, controlling a smaller group of loads more predictably seems more feasible in the foreseeable future than controlling large numbers of diverse residential buildings. Controlling loads in the residential sector for the purpose of flexibility provision is possible but it presupposes existing infrastructure needs larger than the needs in the commercial sector. Furthermore, China already has pilots of commercial and large buildings able to participate in demand response programs [59, 60]. Although smart appliances area available in the market, plans for implementing a large distribution of smart appliances or a transition

to smart appliances needed for large scale demand response programs in the residential sector were not found.

2.3 Assumptions

The commercial sector model is built using a bottom up approach with individual building models that are climate, efficiency standard and operational schedule dependent. This section will discuss the three main assumptions in the model. First, I will describe the individual building models that make up the backbone of this commercial sector model. Second, climate considerations will be described as they relate to the building models representing the commercial sector in China. Finally, I will discuss commercial sector electricity consumption proportions by building type and efficiency standards.

2.3.1 Building types and reference models

The commercial sector load is defined by the building electricity consumption from offices, retailers, malls, hospitals, service providers, and public buildings among others. In this study, the controllable commercial sector is described by a simplified model using six types of physically-based building models: offices with and without datacenters, retail buildings, hotels, hospitals and schools. All building models are modified versions of the Individual Standard 90.1-2013 Prototype Building EnergyPlus Models published by the Building Energy Codes Program of the U.S. Department of Energy and developed by researchers at Pacific Northwest National Laboratory (PNNL) [61]. All other details for the building models not covered in this section are presented on their PNNL prototype scorecards, available at [61]. How a building is constructed, what is the window to wall ratio, for example, affects what construction standards values are used.

EnergyPlus

EnergyPlus is a building energy simulation program developed by the U.S. Department of Energy's Building Technologies Office, and managed by the the National Renewable Energy Laboratory. Researchers, engineers and architects use EnergyPlus to study the impact of efficiency improvements on building operation and comfort for ASHRAE standards [62]. Furthermore, researchers have used EnergyPlus to model buildings and efficiency improvements across the globe [63, 64, 65]. In this work, EnergyPlus is used to simulate the six main types of commercial buildings in the Chinese sector: offices with and without datacenters, retail buildings, hotels, hospitals and schools. Reference prototype models were downloaded from [61] and are briefly described in the next sections.

Operational Schedules

The reference models used in this work come loaded with operational schedules defining the building's HVAC, lights, equipment's operation and occupants behavior (among other characteristics) as suggested by the American Society of Heating, Refrigerating and Air-Conditioning Engineers (ASHRAE). These operational schedules can be modified to test impacts of operational changes on energy consumption, comfort and construction [61] or to compare against standards and operational schedules in China [66]. In this work we are interested in situating these out-of-the-box building reference models onto a Chinese context and therefore provide a comparison between the operational schedules suggested by ASHRAE and those suggested by the Ministry of Housing of Urban and Rural Development (MOHURD) in China [67, 68]. In Section 2.6 the impacts of using the different operational schedules on the electricity consumption of the reference building will be presented and discussed.

Office Reference model

The office building reference model has twelve floors with a 40% window to wall ratio, and a basement that might host a datacenter depending on the type of office building. Each above ground floor has five climate controlled zones. The HVAC system that provides temperature and comfort regulation in these climate controlled zones consists of two cooling coils and pumps systems that provide cooling and a gas boiler that provides heating. The building's operational schedules for a given weekday proposed by ASHRAE and MOHURD standards are presented below.

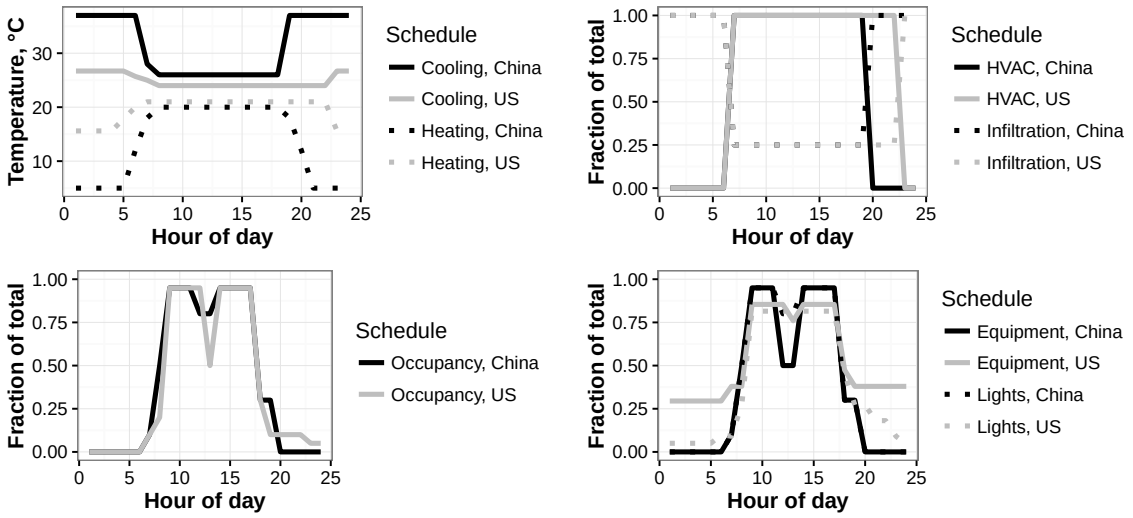

Figure 1: Chinese and US operational schedules for the modeled office building in a weekday

Figure 1 shows a representative set of operational schedules for both the ASHRAE

(US, in gray) and MOHURD (Chinese, in black) office buildings. Starting on the upper left and continuing clock-wise, we can see the building's cooling and heating temperature setpoints, the HVAC operational hours (and the corresponding assumed fraction of infiltration of outside air into the building), the equipment and lights load as a fraction of the designed maxima, and the occupancy throughout the day as a fraction of the maximum design occupancy.

From Figure 1, three main differences can be observed between the Chinese and US operational schedules. First, the US cooling and heating schedules fall within the Chinese schedules. This implies that buildings operating with Chinese schedules have a temperature controlled zone wider than those operating with US schedules. This difference would lead to wider temperature swings and lower engagement from the cooling and heating systems in the building. Second, HVAC systems are operated for longer hours each day in US buildings. Finally, equipment and lights are assumed to operate at higher intensities during the day in US buildings than in Chinese buildings.

Retail Reference model

The retail building model has one floor with five climate controlled zones and a 7% window to wall ratio. Cooling is provided by a packaged air conditioning unit, while heating for four of the five zones is provided by a gas furnace inside the packaged air conditioning unit. A stand alone gas furnace provides heating to the front entry zone. No cooling is provided to the front entry.

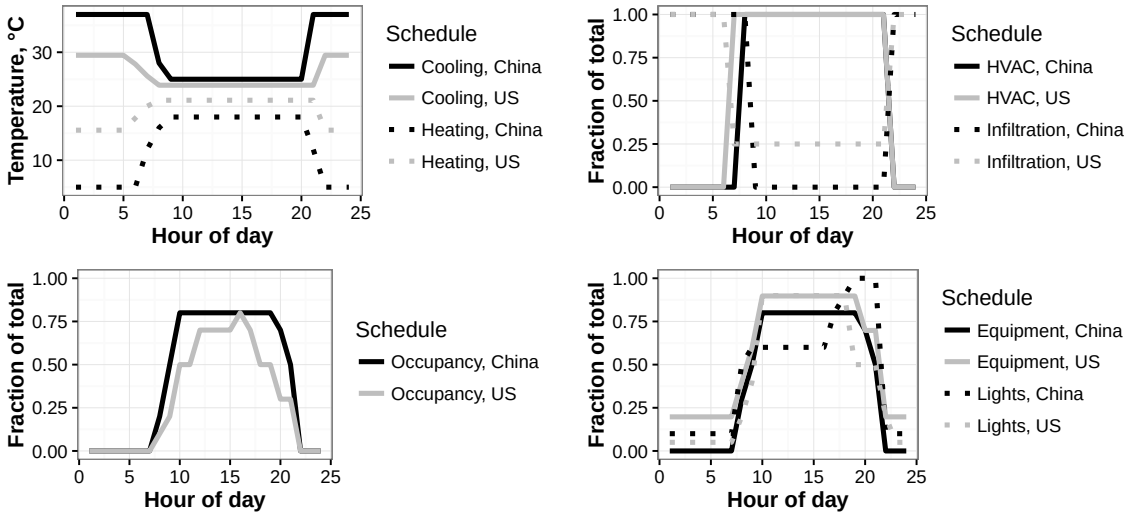

Figure 2: Chinese and US operational schedules for the modeled retail building in a weekday

From Figure 2, three main differences can be observed between the Chinese and US operational schedules. First, as with the office building's operational schedules, the US cooling and heating schedules fall within the Chinese schedules. This implies that

retail buildings operating with Chinese schedules have a temperature controlled zone wider than those operating with US schedules in turn leading to wider temperature swings and lower engagement from the cooling and heating systems in the building. Second, as with the office building's operational schedules, HVAC systems in retail buildings are operated for longer hours each day in the US case. Finally, occupancy is assumed to stay constant between business hours for the Chinese building. On the other hand, US buildings have a more punctuated occupancy profile during the day.

School Reference model

The school building model has 2 floors with a window to wall ratio of 33%. Heating is provided by both gas furnaces inside the packaged air conditioning units and a gas-fired boiler. Cooling is provided by the packaged air conditioning unit and an air-cooled chiller. In addition, the school building year schedule is different from other building types as it follows the school calendar as established by government. In contrast to other buildings, its operation is marked by two extended vacation periods between semesters.

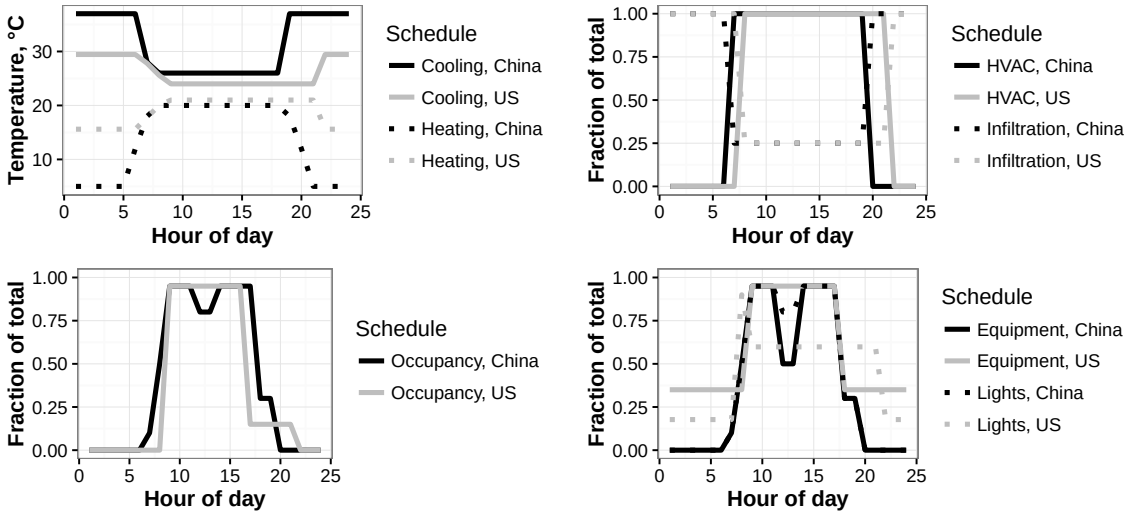

Figure 3: Chinese and US operational schedules for the modeled school building in a weekday

From Figure 3 we can point out almost the same differences between the Chinese and the US operational schedules for a typical weekday: higher temperature gap between cooling and heating setpoints for the Chinese case, longer HVAC operational hours, and higher intensity in equipment and lights plugs for both US operational schedules.

Hotel Reference model

The hotel building model has six above-ground floors and a basement with different window to wall ratios for each side of the building. On average, the window to wall ratio is 30.2%. The basement is a single conditioned climate zone, while all the above-ground floors consist of seven climate controlled zones each. The ground floor includes retail and lobby facilities, a cafeteria and a laundry room. From the second to the fifth floor are the guest floors, with each hosting 42 guest rooms. The top floor includes guest rooms, a banquet room, and a kitchen. Heating and cooling are provided by a gas-fired boiler and an air-cooled chiller, respectively.

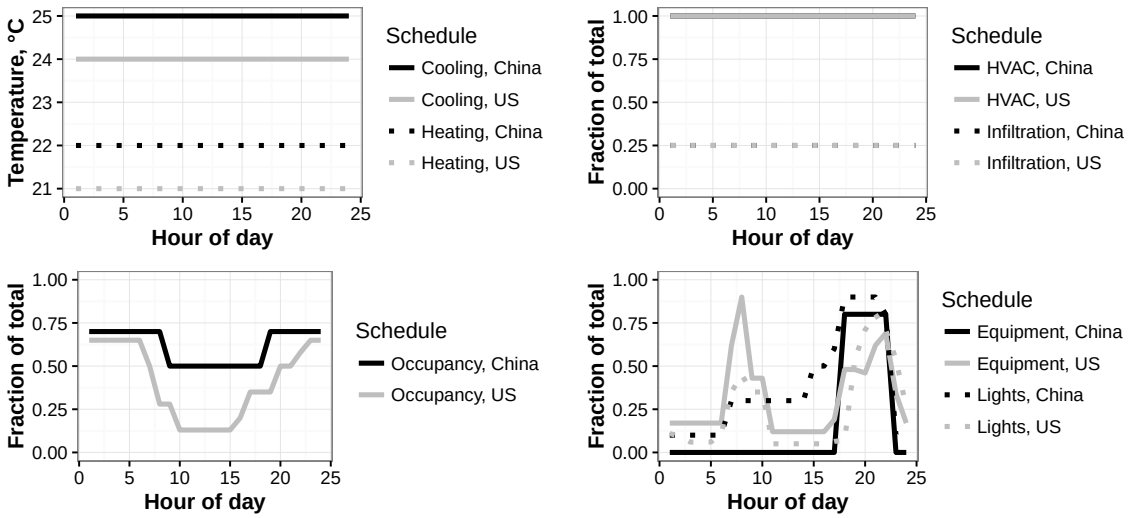

Figure 4: Chinese and US operational schedules for a modeled guest room in a hotel building in a weekday

From Figure 4 we can see important differences between the operational schedules of hotels and offices, retail buildings, or schools. First, temperature setpoints for guest rooms stay constant throughout the day for both the Chinese and the US operational schedules. Buildings have the same temperature gap between cooling and heating setpoints, but are shifted away from each other by a degree, depending if they follow Chinese or US schedules. HVAC operational hours are the same for both operational schedules types. Finally, occupancy is assumed to be lower, on average, for US hotels than for their Chinese counterparts.

Hospital Reference model

The hospital building model has 5 above-ground floors and a basement. All rooms, with the exception of the basement are conditioned and the building's average window to wall ratio is 16%. A gas boiler provides heating, while two water cooled centrifugal

chiller provide cooling to the conditioned zones across the buildings. Several variable-air-volume (VAV) units modulate air flow into the respective zones.

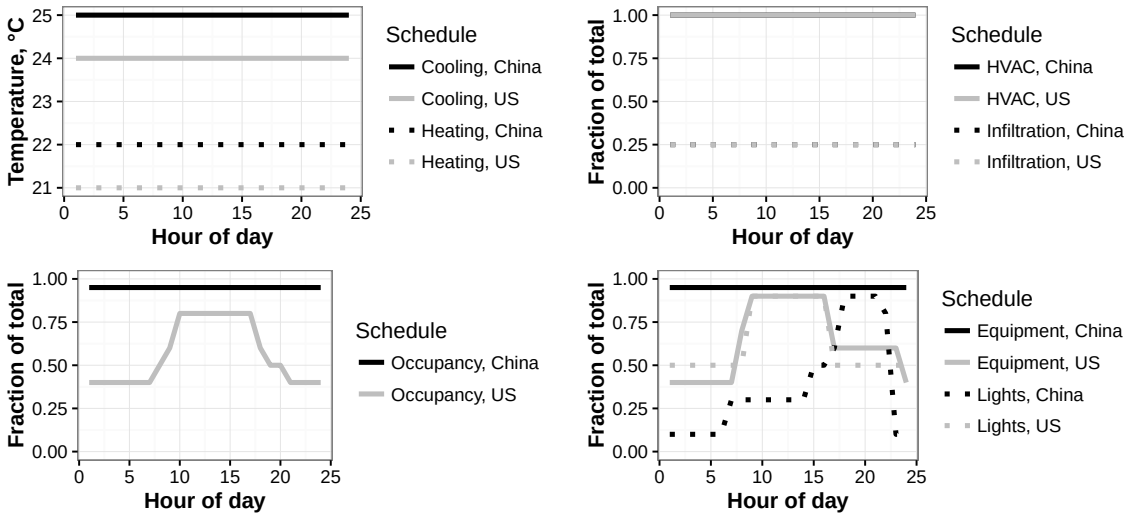

Figure 5: Chinese and US operational schedules for a modeled inpatient room in a hospital building in a weekday

From Figure 5 we can see similarities between the operational schedules of hospitals and hotels in both countries. Hospitals and hotels have the same cooling and heating temperature setpoints, and HVAC operational hours. The Chinese occupancy schedules differ from the US case in that it assumes a constant occupancy of its in-patient rooms, while US rooms see a high plateau in the middle of the day.

2.3.2 Climate considerations

To provide higher quality standards applicable to the different kinds of climates in the country, China's MOHURD classifies the country's climate into five different zones: Severe Cold, Cold, Hot Summer Cold Winter (HSCW), Hot Summer Warm Winter (HSWW), and Temperate (or Mild) [69, 70, 71].

In this study, only four climate zones are used to model the building's operation across the country. The temperate (or mild) climate region covers part of Sichuan and Yunnan provinces and are included within the HSCW region. For each climate zone, MOHURD develops and applies different standards for each commercial building type [67, 68]. Part of our motivation on which building models to choose from the database available from PNNL is the published availability of building standards from MOHURD. There are more building models available than there are published standards. We used all the models for which we can match published MOHURD building standards.

In order to model the appropriate climate within the EnergyPlus framework, the cities of Harbin, Beijing, Shanghai, and Guangzhou were chosen as representatives for

each of our climate regions: Severe Cold, Cold, HSCW, and HSWW. With appropriate climate files to inform the sizing requirement of the buildings in each region, as well as to provide more realistic outside temperature and humidity profiles, it is possible to situate the prototypes to their Chinese regional variation. Table 1 shows how all provinces and cities in China are grouped within the four climate zones aforementioned in our model.

Climate Zone	Provinces and cities included
Severe Cold	Heilongjiang, Inner Mongolia, Jilin, Liaoning, Qinghai, Tibet
Cold	Beijing, Gansu, Hebei, Henan, Ningxia, Shandong, Shanxi, Shaanxi, Tianjin, Xinjiang
HSCW	Anhui, Chongqing, Fujian, Guizhou, Hubei, Hunan, Jiangsu, Jiangxi, Shanghai, Sichuan, Yunnan, Zhejiang
HSWW	Guangdong, Guangxi, Hainan

Table 1: Climate regions in China

2.3.3 Sub-Sectoral Estimates

Commercial sector electricity consumption by building type, $\rho_{b,r,y}$

In order to construct a realistic bottom up model of the commercial sector in China by climate region, estimates for the shares of the total sector consumption from different building types in a given year are used. These sub-sectoral proportions are used to create a weighted average across the different building models described in Section 2.3.1 by climate region for any given year. Using data from [55], we calculated the fraction of the total commercial sector electricity consumption in a given year and climate region consumed by office, retail, hospital, hotel, and school buildings. The fraction of the total commercial sector consumption consumed by any other type of buildings is aggregated into its own category, 'Other'.

Table 2 shows the proportion of total sector consumption consumed by each modeled building type for a given year, between 2015 and 2030, and across all simulated climate zones. In general, we notice similar building electricity consumption shares across all climate zones. About 30% of the sector's total electricity is consumed by both types of office buildings. Hotels, schools and hospitals consume about 18, 15, and 6% of the commercial sector's total consumption with small variations across climate zones for any given year. Some trends as time progresses are noticeable, in particular, small increases in the fraction of total sector electricity consumed by offices from 2015 to 2030 across all climate zones are expected. On the other hand a more pronounced decline in the proportion of total sector electricity consumed by retail buildings is observed for the same period. Proportion of the total sector consumption consumed by the 'Other' building categories shows moderate increases between 2015 and 2030.

		Building type					
Climate Zone	Year	Office	Retail	Hospital	Hotel	School	Other
Severe Cold	2015	0.298	0.180	0.054	0.182	0.144	0.141
	2020	0.302	0.168	0.056	0.182	0.148	0.143
	2030	0.306	0.156	0.059	0.183	0.152	0.144
Cold	2015	0.298	0.180	0.053	0.181	0.145	0.142
	2020	0.302	0.168	0.055	0.182	0.147	0.143
	2030	0.306	0.156	0.058	0.184	0.149	0.144
HSCW	2015	0.298	0.180	0.053	0.181	0.146	0.142
	2020	0.301	0.169	0.056	0.182	0.149	0.143
	2030	0.305	0.157	0.059	0.184	0.152	0.144
HSWW	2015	0.297	0.182	0.053	0.181	0.145	0.142
	2020	0.301	0.172	0.055	0.182	0.147	0.143
	2030	0.305	0.159	0.058	0.184	0.149	0.144

Table 2: Fraction of commercial sector electricity consumption consumed by building type, in 2015, 2020 and 2030, across all climate regions, $\rho_{b,r,y}$

Standards over time

ASHRAE/PNNL energy codes and standards used in the reference model buildings for the commercial sector in the US do not map directly to building models applicable in China. The first national set of standards for commercial buildings in China was published by MOHURD in 2005 and updated with more stringent goals in 2014 [67, 68]. Throughout this work, for brevity's sake, we will refer to them by the year of their publication: 2005 or 2014 and drop the name of the Ministry in charge of publishing them.

Existing research on Chinese building standards focuses on how building standards are useful to develop better sustainable development goals and metrics[72] or to compare the impact of adopting ASHRAE operational schedules and standards in Chinese buildings [56]. Some researchers also provide suggestion on having more frequent updates for Chinese building standards [71].

Adopting this last suggestion for more frequent standards, and using linear interpolation between the published 2005 and 2014 standards, future standards for 2020 and 2025 are estimated for the following building construction parameters: wall, roof, and window heat transfer coefficients (U_{wall}, U_{roof}, U_{window}, respectively), window's solar heat gain coefficient ($SHGC$), outside air infiltration (f_{oa}, also knows as air tightness), boiler efficiency (η_b), COP, light and plug load intensities (β_l and β_e, respectively), and occupancy levels (σ_p).

According to the 2014 standards, different sizes in buildings, as well as geometries across different climate zones in China are subject to meet different building standards [68]. In Table 3 we show the value for the above mentioned parameters across different climate zones and through time for the office buildings used in our model. It is important to note that a larger building, or a building without windows, or a building with very different temperature setpoints would all require to meet different standards according to MOHURD. A more detailed description of the office model is presented in Section 2.3.1.

Using the same linear approximations, parameters across all other building type models in each climate zone in any given year are estimated to model efficiency gains by 2030. The efficiency standards tables for all buildings are presented in Appendix B. Two different scenarios for standard adoption in the commercial building sector in 2030 are studied. The first scenario assumes that developers and builders are subject to strict monitoring for compliance which in turn results in all buildings complying with the estimated 2020 standards for their respective climate zone. The second scenario assumes that developers and builders are subject to stricter monitoring for compliance which in turn results in a commercial sector that complies with the estimated 2025 standards for their respective climate zone.

Offices with data centers, δ

In this work, we assume that data centers in offices become more common in the future. As data centers become more common, the electricity consumption from these offices will also increase due to increased cooling loads.

We estimate the proportion of offices with datacenters to increase in the future. In Table 4 we can observe that by 2030, our model assumes that 25% of all office buildings will have a dedicated data center in the basement of the building. For this version of the model, we do not have different scenarios in data center penetration in buildings of any type. In future iteration of the model, other data center penetration scenarios might be explored.

2.4 Scenarios

In this model, the commercial sector is a function of three global variables that define the overall energy consumption in each building: efficiency standards adoption, operating schedules and electrification of heating (with symbols ξ, θ, and χ, respectively). Efficiency standard adoption scenarios capture two different efficiency standards compliance levels across the building stock. Building level operating schedules model the way each building, irrespective of its adopted efficiency standards, is operated. Finally, electrification of heating explores how the building provides heating to its conditioned zones. In this section we will describe the different scenarios for each of these global variables. In Section 2.6 we will explore how different scenarios give rise to different

	HSWW Standards				HSCW Standards				*Units*
	2005	2014	2020	2025	2005	2014	2020	2025	
U_{wall}	1.5	1.5	1.5	1.5	1.0	0.8	0.66	0.55	$\frac{W}{K \cdot m^2}$
U_{roof}	0.9	0.8	0.73	0.68	0.7	0.5	0.37	0.26	”
U_{window}	3.5	3.0	2.7	2.4	3.0	2.6	2.3	2.1	”
$SHGC$	0.45	0.35	0.28	0.22	0.5	0.4	0.33	0.28	–
f_{oa}	7.5	3.0	1.0	1.0	7.5	3.0	1.0	1.0	$\frac{m^3}{m^2 \cdot hr}$
η_b	0.89	0.89	0.91	0.91	0.89	0.89	0.91	0.91	–
COP_c	5.1	5.7	6.1	6.4	5.1	5.6	5.9	6.2	–
β_l	11	9	7.7	6.6	11	9	7.7	6.6	$\frac{W}{m^2}$
β_e	20	15	11.7	8.9	20	15	11.7	8.9	”
σ_p	8	10	11.3	12.4	8	10	11.3	12.4	$\frac{m^2}{person}$
	Cold Standards				Severe Cold Standards				
	2005	2013	2020	2025	2005	2014	2020	2025	
U_{wall}	0.6	0.5	0.43	0.38	0.45	0.38	0.33	0.29	$\frac{W}{K \cdot m^2}$
U_{roof}	0.55	0.45	0.38	0.21	0.35	0.28	0.23	0.19	”
U_{window}	2.7	2.4	2.2	2.0	2.5	2.2	2.0	1.8	”
$SHGC$	0.7	0.48	0.33	0.21	0.7	0.7	0.7	0.7	–
f_{oa}	7.5	3.0	1.0	1.0	7.5	3.0	1.0	1.0	$\frac{m^3}{m^2 \cdot hr}$
η_b	0.89	0.89	0.91	0.91	0.89	0.9	0.91	0.91	–
COP_c	4.7	5.2	5.5	5.8	4.7	5.0	5.2	5.4	–
β_l	11.0	9.0	7.7	6.6	11.0	9.0	7.7	6.6	$\frac{W}{m^2}$
β_e	20.0	15.0	11.7	8.9	20.0	15.0	11.7	8.9	”
σ_p	8	10	11.3	12.4	8	10	11.3	12.4	$\frac{m^2}{person}$

Table 3: Chinese Office building standards over time and across climate regions

Year	Offices with datacenters (% of total)
2010	-
2015	10
2020	15
2030	25

Table 4: Proportion of offices with datacenters, δ, between 2010 and 2030

commercial sector electricity consumption levels. In Chapter 3 we will expand our analysis on how different global variables affect the overall regional and national load. Finally, in Chapter 5, renewable generation will be introduced into the picture and see how the three global variables affect the national netload.

2.4.1 Efficiency Adoption, ξ

There are two efficiency standards adoption scenarios modeled in this work labeled 2020 and 2025 (ξ_1, and ξ_2, respectively). If buildings follow ξ_1 (2020 standards) standard adoption scenarios, then by 2030, the model assumes that buildings' construction (wall, roof, window, and equipment efficiency, etcetera) will comply with 2020 efficiency standards as presented in Table 3 (for the case of office buildings). Similarly, if ξ_2 (2025) standard adoption scenario is followed, then by 2030, the model assumes that buildings will comply with 2025 efficiency standards. The impact of following the two different efficiency scenarios outlined here will be presented in Section 2.6.

2.4.2 Operating Schedules, θ

Independently of how buildings are constructed, that is, what efficiency adoption scenario (ξ) is used, there are two building level operating schedules scenarios that buildings could adopt by 2030, θ_1 and θ_2. For scenario θ_1, buildings adhere to the operating schedules in the 2014 standards. In θ_2, buildings adhere to the operating schedules used in the US ASHRAE/ANSI 90.1-2012 commercial building prototypes in Section 2.3.1. As outlined in Section 2.3.1, θ_1 and θ_2 are different in terms of temperature setpoints in a day, and across days, HVAC operating schedules, and occupancy profile assumptions among other characteristics. For example, the difference in temperature setpoints between high and low occupancy hours (2 pm vs 2 am) is not that large for the θ_2 (US) schedules. In Chinese buildings, this difference in temperature setpoint can sometimes be as large as ten degrees centigrade for some building types.

Operational schedules can increase or reduce the energy intensity of a building. In addition, a building designer, and EnergyPlus, needs to know the time the HVAC system turns on, the temperature cooling and heating setpoints, as well as the occupancy profile in a variety of days in order to properly size the heating and cooling

equipment. Furthermore, different operating schedules can give rise to different comfort levels. Introducing operating schedules (θ) as a global variable across scenarios allows us to explore how will commercial sector load in China change if behaviors and comfort expectations of building users emulate those in the United States.

As mentioned before, operating schedules (θ) and efficiency adoption decisions (ξ) are independent. A building can be operating with the US schedule θ_2 and in compliance with efficiency standards adoption scenario ξ_1, or operating with the Chinese operating schedule (θ_1) and in compliance with efficiency standards ξ_2 (2025). The impact of adopting either operating schedule will be discussed in more detail in Section 2.6.

2.4.3 Heating Electrification, χ

By default, all reference building models use gas as their heating fuel. Nevertheless, as China pursues electrification of their commercial sector in order to reach their clean air and renewable energy goals and in compliance with the required fundamental changes in the energy system for a deep decarbonization[73], we expect that the building sector's heating consumption will shift towards electricity and away from coal or gas as the main fuel by 2030 [74, 75, 76]. In order to study the effects on load, netload, and demand response of such a shift, we propose three different heating electrification scenarios of the commercial sector to 2030.

The first heating electrification scenario, χ_1, assumes that all buildings use electricity as their main heating fuel with a heating efficiency equal to that of a traditional gas boiler, or about 90%. The second scenario, χ_2, assumes no electrification of heating in the building sector. That is, buildings continue to use gas or coal as their main heating fuel. The third scenario, χ_3, assumes that heating is provided with a heating pump 2.5 times more efficient than a traditional gas boiler.

As mentioned before with variables ξ and θ, heating electrification scenarios (χ) are independent from the other two. The impact of pursuing different heating electrification options will be discussed in more detail in Section 2.6 of this chapter.

2.4.4 Summary of parameters

To summarize the needed parameters to define a set of commercial building models we provide Table 5 below for quick reference.

Parameter	Value: Description
ξ, Efficiency standards	ξ_1: Buildings follow 2020 standards in 2030 ξ_2: Buildings follow 2025 standards in 2030
θ, Operation schedules	θ_1: Buildings follow Chinese operational schedules guidelines θ_2: Buildings follow US operational schedules guidelines

χ, Heating electrification	χ_1: Heating is provided by low efficiency electric boilers χ_2: Heating is provided by gas or coal boilers χ_3: Heating is provided by high efficiency electric heat pumps

Table 5: Commercial building model parameters

2.5 Methodology

In this section we describe the steps taken to model the hourly load from the commercial sector derived from the individual building models discussed in Section 2.3.1 and the sub-sectoral estimates discussed in Section 2.3.3. For every climate region, we define a building's electricity load as a function of three main variables, or scenarios, as shown in Equation 2.5.1.

$$L_{b,r,y} = f_{b,r,y}(\xi, \theta, \chi) \tag{2.5.1}$$

where $L_{b,r,y}$ is the electricity load for building b, in climate region r in year y, $f_{b,r,y}$ is the model describing the same building, in the same region and year and ξ, θ, and χ represent the three global decision variables or scenarios available as described in Section 2.4.

For any given building, climate region, and year (b, r, and y, respectively), and for scenarios ξ, θ, and χ every building model output provides hourly energy consumption from all different equipment or services in the building including HVAC electricity, heating gas, lights, total building electricity and gas consumption. Using these time-series, we can calculate the hourly electricity load, $L_{b,r,y}$, for a given building, climate region, and year with Equation 2.5.2.

$$L_{b,r,y} = C_{e,nh,b,r,y}(\xi, \theta) + H(\chi) \cdot \eta_{boiler,b,r,y}(\xi) \cdot C_{gas,h,b,r,y}(\xi, \theta) \tag{2.5.2}$$

where $C_{e,nh,b,r,y}(\xi, \theta)$ is the hourly electricity consumption from all processes other than heating as a function of the efficiency (ξ) and operational schedule (θ) scenarios, $H(\chi)$ is the heating exchange factor as a function of the heating electrification χ scenario chosen, $\eta_{boiler,b,r,y}(\xi)$ is the boiler efficiency as a function of the efficiency (ξ) scenario, and $C_{gas,h,b,r,y}(\xi, \theta)$ is the hourly energy consumption from gas to provide heating as a function of ξ and θ, for any given building, region, and year (b,r,and y, respectively).

After a building model is run, its respective electricity intensity (in $\frac{kWh}{m^2}$) is calculated by summing across its hourly electricity load and dividing it by its floor space area, A_b, as in Equation 2.5.3.

$$i_{b,r,y} = \frac{\sum_{h=1}^{8760} L_{b,r,y}(h)}{A_b} \tag{2.5.3}$$

As shown in Equation 2.5.1 above, $L_{b,r,y}$ is a function of the three global variables or scenarios. By extension, $i_{b,r,y}$ is also a function of the same three variables (ξ, θ, and χ). We can now formulate a definition for the average intensity of commercial sector with Equation 2.5.4.

$$\bar{i}_{r,y} = \sum_{b \in B} \rho_{b,r,y} \cdot i_{b,r,y}(\xi, \theta, \chi) \tag{2.5.4}$$

where $\bar{i}_{r,y}$ is the average building intensity from the commercial sector built from the individual models described in 2.3.1 (defined here as set B), as a function of the three global variables, $\rho_{b,r,y}$ is the proportion of the yearly electricity consumption consumed by building type b (as discussed in Section 2.3.3) and the total commercial sector consumption in region r and year y, and $i_{b,r,y}$ is electricity intensity of building b, in region r, and year y as a function of (ξ, θ, and χ).

In order to track the impact of efficiency gains, operational schedules, or electrification scenarios at the commercial sector level, we define a baseline average intensity in climate region r as the average intensity when global variables equal ξ_1, θ_1, and χ_1 respectively as shown in Equation 2.5.5.

$$\bar{i}_{baseline,r,y} = \sum_{b \in B} \rho_{b,r,y} \cdot i_{b,r,y}(\xi_1, \theta_1, \chi_1) \tag{2.5.5}$$

We aggregate the electricity consumption from each of the individual models into a regional electricity density model as in Equation 2.5.6.

$$\Gamma_{r,y}(h) = \sum_{b \in B} \frac{\rho_{b,r,y} \cdot L_{b,r,y}(h)}{A_b} \tag{2.5.6}$$

where $\Gamma_{r,y}(h)$ is the hourly weighted sum, across all buildings in set B, of the hourly building load models, $L_{b,r,y}(h)$, in region r and year y, $\rho_{b,r,y}$ is the ratio between the yearly electricity consumption from building type b and the total commercial sector consumption in region r and year y, and A_b, is the total floor area of building b.

By combining Equations 2.5.5 and 2.5.6 and introducing two new parameters, $\epsilon_{comm,y}$ and $C_{r,y}$, we can now define an hourly load for the commercial sector built from the individual building models. We label this commercial sector load as controllable (with the subscript $_c$), since as we will see in Chapter 7 we can control the load of these buildings to provide flexibility to the electric grid. The commercial sector controllable load in region r and year y is then defined in Equation 2.5.7

$$L_{comm_c,r,y}(h) = \frac{\Gamma_{r,y}(h)}{\bar{i}_{baseline,r,y}} \cdot (1 - \rho_{other,r,y}) \cdot C_{r,y} \cdot \epsilon_{comm,y} \tag{2.5.7}$$

where $L_{comm_c,r,y}$ is the hourly demand of the controllable commercial sector, $\Gamma_{r,y}(h)$ is the regional electricity density function as defined in Equation 2.5.6, $\bar{i}_{baseline,r,y}$ is the baseline average intensity, as defined in Equation 2.5.5, $\rho_{other,r,y}$ is the ratio between the yearly electricity consumption from building types not built from the individual

models in set B and the total commercial sector consumption in region r and year y. The new parameters $C_{r,y}$ and $\epsilon_{comm,y}$ represent the total electricity consumption across all sectors , and the ratio of electricity consumption consumed by the commercial sector and the total electricity consumption across all sectors of the economy in region r and year y, respectively. Equation parameters $C_{r,y}$ and $\epsilon_{comm,y}$ will be described in more detail in Chapter 3.

2.6 Results

In this section, we present the results of our commercial building models for each building type and climate region in terms of yearly building intensity, $\frac{kWh}{m^2}$. We present results of only two scenarios for comparison purposes. With two efficiency standard (ξ), two operational schedules (θ), three heating electrification scenarios (χ) across four climate regions and six different building models we developed a total of 288 building models. For brevity's sake, in this section we only present the full results at the building level for buildings under sets of scenarios. The individual building's electricity intensity across different set of parameters and climate zones in 2030 are presented in Appendix C.

Table 6 shows the estimated individual building intensities across all climate zones for buildings complying with the 2005 standards. These building models all have heating that is provided by traditional gas or coal boilers and operational schedules that follow MOHURD recommendations and not their American counterparts.

Building	Climate region			
	Severe Cold	Cold	HSCW	HSWW
Hospital	396.1	376.4	380.0	394.8
Hotel	249.0	214.1	233.5	247.8
Office	128.8	104.0	96.9	100.2
Retail	162.2	149.0	139.2	153.4
School	101.3	116.3	96.7	104.8

Table 6: Building intensity with 2005 standards, by climate region, in $\frac{kWh}{m^2}$

The second set of presented results in Table 7 provide the yearly individual building intensities for the base case scenario across the four climate zones for buildings with low-efficiency heating electrification (χ_1) that have MOHURD recommended operation schedules (θ_1) meeting the estimated 2020 standards (ξ_1).

Among the building types modeled across both scenarios, hospitals have the highest energy consumption footprint with 350 - 400 $\frac{kWh}{m^2}$. School buildings have the lowest energy consumption with intensities ranging from 70 to 80 $\frac{kWh}{m^2}$ for the improved 2020 standards across all climate regions. Office building's building intensities vary greatly between those with and without datacenter with ranges between 80 - 210 $\frac{kWh}{m^2}$ across

Building	Climate region			
	Severe Cold	Cold	HSCW	HSWW
Hospital	386.0	361.5	352.6	361.9
Hotel	199.3	173.6	183.8	200.5
Office (with datacenter)	211.0	194.2	189.4	194.3
Office (no datacenter)	109.9	90.9	82.4	84.2
Retail	120.7	114.7	98.9	109.4
School	70.7	81.0	68.8	73.9
Average	152.1	139.1	132.9	140.8

Table 7: Building intensity of the base case scenario in 2030 for individual buildings and regional average, by climate region, in $\frac{kWh}{m^2}$

all climate regions. Retail and hotel buildings electricity intensities hover around 100-120 and 170-200 $\frac{kWh}{m^2}$, respectively for the improved 2020 standards across all climate regions.

We can calculate the average regional building intensity by using the sub-sectoral estimates presented in Section 2.3.3. On average, the region with the lowest overall average commercial sector intensity is the one with the mildest climate, Hot Summer Cool Winter (HSCW), with a 132 $\frac{kWh}{m^2}$. The region with the highest average commercial sector intensity is the northernmost region of Severe Cold climate with 152 $\frac{kWh}{m^2}$. Overall, given our assumptions for building distributions across all climate regions, the average building intensities are within 20% of each other.

Building	Climate region			
	Severe Cold	Cold	HSCW	HSWW
Hospital	-2.6	-4.0	-7.2	-8.3
Hotel	-20.0	-18.9	-21.3	-19.1
Office (with datacenter)	63.9	86.7	95.4	93.9
Office (no datacenter)	-14.7	-12.6	-15.0	-15.9
Retail	-25.6	-23.0	-28.9	-28.7
School	-30.3	-30.4	-28.9	-29.5

Table 8: Building intensity change, in percentage, from the 2005 standard case scenario to the 2030 base case scenario for individual buildings and regional average, by climate region, in $\frac{kWh}{m^2}$

In Table 8 we show the decrease in building intensity between building models that comply with the 2005 and the estimated 2020 building standards. We see that the linear approximation of standard improvement does not have a large effect on hospital buildings. In addition, offices with datacenter show an increase in energy consumption of between 60-95% with respect to offices in 2005. The lowest increase in offices with datacenter occurs for buildings in the Severe Cold climate since they need the least

amount of extra cooling among all climate regions. In general, buildings that comply with the estimated 2020 efficiency standards will be between 20 to 30% more efficient than those meeting 2005 standards, depending on the building type and climate region. The biggest decrease in energy consumption occurs for schools in cold climates with a 30.4% efficiency improvement.

2.6.1 Aggregating across the country

With electricity demand data at the province level, and assuming that provinces fit neatly into climate regions, as presented in Chapter 3, we can estimate the overall commercial sector building intensity for each set of parameters used to model the buildings. Table 5 is offered for reference in the definition of parameter values.

Scenario	2020 (ξ_1)	2025 (ξ_2)
$\theta_1\chi_1$	138.4	134.4
$\theta_1\chi_2$	118.5	114.8
$\theta_1\chi_3$	125.1	121.3
$\theta_2\chi_1$	154.7	150.4
$\theta_2\chi_2$	129.2	125.2
$\theta_2\chi_3$	137.7	133.6

Table 9: Average commercial sector, building intensity, $\frac{kWh}{m^2}$

In scenarios where heating (χ) is provided by electricity ($\chi_{1,3}$), the intensities from each building, and the commercial sector overall increases. In colder climates the heating electrification scenario has a bigger impact on the intensity of the commercial sector. In general, commercial buildings that operate with ASHRAE/PNNL recommended schedules (θ_2) consume about 10% more energy in a year than buildings that operate with MOHURD recommendations (θ_1). In the absence of heating electrification (χ_2), buildings in the warmest climate (HSWW) have the highest energy intensity of all commercial buildings. Compliance to Efficient standards by 2030 (ξ_2) lead to an average decrease in commercial sector building intensity of 4 $\frac{kWh}{m^2}$ as compared to the BAU standards (ξ_1).

In Section 2.7 we perform a sensitivity analysis for each of the possible variations across parameters available in our model (ξ,θ,χ) with comparison with the basecase scenario.

2.6.2 Literature comparison

Although there are comparative studies on energy performance done on office buildings in China across multiple climate regions ([71, 69]) there is no definitive comparison available for all building types modeled in this work. Feng et al built a series of Chinese reference office building models using surveys of existing buildings as well as

design drawings of newly constructed ones. Their average intensity for the three modeled buildings using 2005 standards is almost 160 $\frac{kWh}{m^2}$. The Cold climate model using 2005 standards had a energy intensity of about 140 $\frac{kWh}{m^2}$. When compared with the Cold climate office model used in this work it appears as if our model severely under estimates its energy consumption since our model does not take into account building's heating load as it is assumed that for the 2005 standards buildings in Northern China are provided by heat from district heating. Research from Da Yan at Tsinghua aggregates heating and non-heating load across all buildings in China. It estimates a range between 53-80 $\frac{kWh}{m^2}$ for heating provision in Beijing[77]. Adding this heating energy consumption, our model energy consumption now surpasses that from Feng et al by 10-20%.

Research on the energy consumption of buildings across China rely on data aggregation that does not suit our direct needs. For example, in Da Yan's research it is estimated that the public and commercial buildings have an electric building intensity of around 55 $\frac{kWh}{m^2}$. When heating is added, buildings have an average energy consumption of 170 $\frac{kWh}{m^2}$ [77]. As seen from Table 9 our 2030 commercial sector building intensity average ranges from 120 to 150 $\frac{kWh}{m^2}$ depending on the parameters used to construct the buildings across all climate regions and excluding scenarios without electrification of heating. This range of potential average building intensity seems like a plausible future if efficiency in building construction, operation, and heating provision is pursued.

2.7 Discussion

As discussed in Section 2.4 our commercial building hourly model is a function of the parameters or scenarios chosen. In this section we examine the impact of modifying a parameter at a time on the electricity intensity climate region average for the basecase scenario (ξ_1,θ_1,χ_1).

2.7.1 Impact of parameters

Climate Region	Parameter change			
	$\Delta\xi$	$\Delta\theta$	$\chi_1 \rightarrow \chi_2$	$\chi_1 \rightarrow \chi_3$
Severe Cold	-2.0	12.3	-27.4	-18.3
Cold	-3.3	14.9	-16.5	-11.0
HSCW	-2.7	9.5	-10.3	-6.9
HSWW	-3.7	8.8	-5.9	-3.9

Table 10: Percentage effect of changing a parameter from the average regional climate building intensity on the base case scenario

In general, as seen in Table 10, differences in efficiency standards as defined in Section 2.3.3 have a small effect on the average climate region commercial building intensity. A shift from 2020 to 2025 standards compliance by 2030 ($\Delta\xi$) only reduces electricity consumption by 2 to 4% from the basecase scenario depending on the climate region we compare. On the other hand the other two parameters (θ,χ) have a much larger impact on the electricity consumption in buildings. For example, changing the operation schedules from those recommended by MOHURD to ASHRAE ($\Delta\theta$) increases electricity consumption between 9 and 15% from the base case scenario. Changing the electrification scenario has a higher impact for buildings in the North (Severe Cold and Cold climates) than changing any of the other two parameters. For example, when buildings go from self-providing heating by electric boilers to having their electricity provision met by gas or coal boilers ($\chi_1 \rightarrow \chi_2$) we see a 27 and 16% decrease in electricity consumption for buildings in the Severe Cold and Cold climate regions. On the other hand, buildings further south in the HSCW and HSWW climate regions only see a 10 and 6% decrease in yearly consumption from this transition. Providing the building's heating with more efficient electrified heating ($\chi_1 \rightarrow \chi_3$) has a smaller impact on electricity consumption than de-electrifying the heating load completely with consumption reductions between 4 to 18%.

2.8 Conclusion

In this Chapter we presented a model for an hourly commercial model at the climate region level in China for a given set of parameters in Section 2.5. The model parameters that define the commercial load are efficiency standards adoption (2020 vs 2025), operational schedules (China vs US), and heating electrification (no electrification, low-efficiency electrification, high-efficiency electrification). We found that our model predicts a range of building intensities consistent with literature. We also described that for a 2030 basecase scenario defined by a commercial sector with 2020 standards, Chinese operational schedules and low-efficiency electrification of heating the average commercial sector intensity is 138 $\frac{kWh}{m^2}$ 2.6. If we assume an average commercial building intensity of 170 $\frac{kWh}{m^2}$ as per [77], then, our basecase scenario has a reduction of 19% from the present intensity estimate. Finally, we examined the impacts of changing a parameter from basecase scenario. We found out that changing the operational schedules has the largest impact across all climate regions, but that changing heating electrification has a disproportionately large impact on the electricity consumption of buildings in Northern China. In the next chapter we will use the commercial model described here to develop an hourly load model at the climate region level.

Chapter 3

Electricity load forecast model for China

3.1 Introduction

In this chapter we develop a model to describe hourly load at the regional and national level in China using a parametrized model for the commercial sector at the climate region level described in Chapter 2. In order to build a model of the hourly load we first describe our assumptions in Section 3.2 which include national and provincial demand forecasts to 2030. We then describe our method to disaggregate the provincial demand data by time of the year and consumption sector (agricultural, commercial, industrial, and residential). We clearly define a portion of the commercial component load as a controllable load and provide a definition of a controllable regional and national hourly load model 3.2.6. Finally, we present the results of our model with an emphasis on understanding the descriptive statistics of load in 2030 in Section 3.3.

3.2 Assumptions

3.2.1 National and regional consumption, $C_{total,y}$ and $C_{region,y}$

Forecasting electricity consumption in China has been the subject of study among many researchers coming from a diverse set of angles [8]. Over the past 30 years, China has seen its electricity consumption rise in relative tandem with its economic output [20]. For some researchers, electricity consumption and economic output are intrinsically related and therefore formulate models to understand the future growth of the economy and the electricity sector in China [78, 79, 80].

In this work we use load trajectories from 2015 to 2030 at the national, climate region, and provincial levels. We assume that economic growth, and, therefore, electricity consumption continue to increase but with a decreasing growth rate. Between 2015 and 2020, we assume that electricity consumption at the national level grows

at 3.9% on average annually reaching 6878 TWh. Between 2020 and 2030, national consumption starts to significantly slow down, with an average yearly growth rate of 0.9%, achieving a relative plateau by 2030, as discussed in [19].

Nevertheless, as shown in Table 11, not all provinces or cities slow down at the same rate between 2015 and 2030. More developed cities, like Beijing and Shanghai, for example, have negative electricity consumption rates of -0.4 and -0.3%, respectively, depicting effects of both efficiency gains and overall decrease consumption. On the other hand, provinces with relatively low development indexes like Gansu, Tibet, and Xinjiang are expected to have only moderate decreases in growth rates from the 2015-2020 (3.3, 6.3, and 4.1% for Gansu, Tibet, and Xinjiang, respectively) to 2020-2030 (2.6, 3.2, and 4.1 % for the same provinces, respectively) periods.

At the climate region level, differences in consumption levels and rates can be observed. By 2030, the climate region with the highest consumption will be the Hot Summer Cold Winter (HSCW) region with over 3000 TWh of expected electricity consumption, equivalent to 40.7% of the total national consumption. This climate region spans over 12 cities and provinces, including Jiangsu province, Shanghai, and Zhejiang province. The second largest region is the Cold climate region spanning over 10 cities and provinces, including Beijing, Hebei and Shaanxi provinces. By 2030 the cold climate region is expected to consume over 2600 TWh, equivalent to 35.3% of the national total.

By 2030, we assume that China will consume just over 7500 TWh of electricity in 2030 if the commercial sector follows the baseline scenario as discussed in Chapter 2. We assume that further changes from the demand sector (outside of the modeled commercial sector), including efficiency gains or significant sectorial disruption do not occur. The impact of efficiency gains and other changes in the operation of the commercial sector on the total yearly demand by 2030 is demonstrated in Section 3.3 of this chapter.

To put China's national electricity consumption in 2030 into perspective, the US had a total consumption of approximately 3900 TWh in 2015. Assuming no further growth in electricity consumption, by 2030, China would consume about twice as much electricity than the US.

Climate	Province		Demand (TWh)		
			2015	2020	2030
Severe Cold					
	Heilongjiang		95	120	118
	Inner Mongolia		231	283	335
	Jilin		76	92	107
	Liaoning		226	282	314
	Qinghai		58	69	75
	Tibet		3	4	6
		Region	**689**	**851**	**955**
Cold					

Climate	Province		Demand (TWh) 2015	2020	2030
	Beijing		95	104	100
	Gansu		104	122	157
	Hebei		388	482	518
	Henan		328	408	420
	Ningxia		73	87	109
	Shaanxi		112	138	179
	Shandong		458	540	585
	Shanxi		229	276	285
	Tianjin		87	108	114
	Xinjiang		101	125	187
		Region	**1,975**	**2,390**	**2,653**
HSCW					
	Anhui		146	179	184
	Chongqing		84	109	132
	Fujian		181	219	237
	Guizhou		113	137	167
	Hubei		176	216	263
	Hunan		151	193	230
	Jiangsu		505	615	610
	Jiangxi		86	107	127
	Shanghai		163	196	190
	Sichuan		197	243	282
	Yunnan		135	161	183
	Zhejiang		375	450	451
		Region	**2,312**	**2,825**	**3,057**
HSWW					
	Guangdong		522	613	614
	Guangxi		143	169	196
	Hainan		24	31	36
		Region	**688**	**813**	**846**
China		**Total**	**5,665**	**6,878**	**7,506**

Table 11: Model demand in TWh, at the national, climate region, and provincial level for years 2015, 2020, and 2030

3.2.2 Daily demand share, $S_{total,d}$

Daily demand share of the total baseline consumption in a year, $C_{total,y}$, discussed in 3.2.1, was obtained from He et al work on renewable and load planning optimization

tools and scenarios [41]. The original model assigns a fraction of the total baseline consumption in a year to each month of the year. It then proceeds to divide the monthly consumption equally among the days in each month. The sum of the daily shares across the year equals 1. In this model, a modified version of the simple daily demand share model as utilized in [41] to build daily load profiles is proposed.

Instead of a single daily share throughout the month, two linear interpolations between three points, are used to describe the daily demand share in each day of the month. The middle of the month converges to the same daily demand share as proposed by the simplified model in [41]. The daily demand share of the first day of each month is the average of the daily demand share of the middle of the last and the current months. Similarly, the daily demand share of the last day of the month is defined as the average of the daily demand share of the middle of the current and the next months. From these simple points, linear interpolations are built for the demand share of each day in that month and for every month in a year. The sum of the daily shares across the year equals 1 for both the original and the modified daily share models.

In Figure 6, a comparison between the original daily share model (shown in gray) and the modified model (shown in black) is presented. Although other methods could have been used to smooth the transitions in daily demand shares between months, two linear interpolations for every month already decrease the inconsistencies in load estimates between the last hour of a month, and the first hour of the following month and create a more realistic baseline to study hour to hour ramping rates. A more accurate representation of load should most likely include a noise term in the interpolations. For future work we could analyze other ways to estimate daily demand shares using stochastic methods.

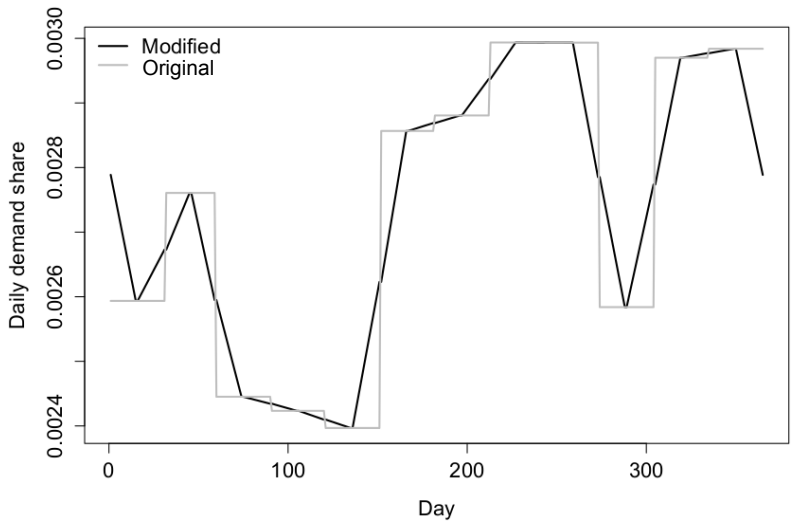

Figure 6: Daily demand share, S_{total}

For the remainder of this chapter we assume that the S_{total} is the same for all climate regions and for any given year, that is, on any given day d, the ratio between the total daily consumption and the regional yearly consumption is given by $S_{total,d}$.

3.2.3 Sectoral demand share, $\epsilon_{sector,y}$

The sectoral demand share is the proportion between the electricity consumption from different economic sectors (agriculture, commercial, industrial, and residential) at the national or regional level and the total or regional demand, respectively. We assume that the ratio of electricity consumed by a given sector in a given year is the same both at the national and climate region level.

In order to estimate the sectoral demand shares of the agricultural, commercial, industiral, and residential sectors we used Chinese Electricity Council statistics (CEC) for the last two decades [21]. The CEC releases yearly statistics on production and consumption of electricity that include breakdowns by energy source and economic sector, at the national level. Since breakdowns by economic sectors at the province or climate region level are not publicly available, in this work we assume that the national shares of electricity consumption by sector presented in this section apply at the climate region level.

Using available historical national electricity consumption data by sectors between 1990 and 2017, we built a linear regression model to estimate the sectoral demand share of the total national consumption to 2030 for the agriculture, commercial, industrial, and residential sectors. Statistical data collection bins by China's National Bureaus of Statistics do not cleanly coincide with our own defined sectors [20]. In our analysis we aggregated statistical industrial load data from the Industry and Construction categories. Residential, and agricultural loads are collected under the same categories as our defined sectors. Commercial sector load in this model is an aggregate of three statistical categories used by Chinese statistics: Transport-Storage-Post, Commercial and Other Commercial. The estimated sectoral demand shares using the linear regression model are presented in Table 12.

Year	Economic sector			
	Agriculture	Commercial	Industry	Residential
	$\epsilon_{ag,y}$	$\epsilon_{comm,y}$	$\epsilon_{ind,y}$	$\epsilon_{res,y}$
2010	0.023	0.107	0.748	0.122
2015	0.018	0.126	0.728	0.128
2020	0.016	0.145	0.699	0.140
2030	0.014	0.164	0.673	0.150

Table 12: Sectoral demand share of total electricity consumption in a given year

In 2015, 72% of the national electricity consumption was from industrial demand. Although the industrial share of total electricity consumption has been decreasing for

the last two decades, it is expected to continue to account for most of the electricity consumed in the country past 2030. As shown in Table 12, between 2010 and 2030, industrial load is expected to decrease its share of total electricity consumption from 74.8 to 67.3%. A similar decreasing trend is expected to occur for the agricultural sector where shares go from 2.3 to 1.4% of the national total.

On the other hand, both commercial and residential shares of the national total electricity consumption see an increasing trend between 2010 and 2030. Commercial and residential load shares increase from 10.7 to 16.4% and 12.2 to 15.0%

As the Chinese economy continues to grow and shift away from an industrial, export-oriented and towards a consumer-based economy the shares of industry and agriculture electricity consumption will continue to decrease and the shares of the commercial and residential sector electricity consumption from the total will continue to increase.

3.2.4 Non-Controllable load

In this work we model the hourly electricity demand from the agricultural, industrial, residential and a subset of the commercial sector, at the climate region level, with a simplified non-parametric model. In contrast to the commercial model described in Chapter 2, the hourly load from these sectors does not depend on any controllable parameter or variable and are non-physically based. For all these non-controllable models, an hourly load share curve is presented and compared.

Agricultural, Industrial, and Residential demand, $L_{\varsigma,r,y}$

The total electricity consumption from the agricultural, industrial and residential sectors, $C_{\varsigma,y}$, $\forall \varsigma \in \{ag, ind, res\}$, in a given year y, is described by Equation 3.2.1, where $C_{region,y}$ is the regional electricity consumption for a given region and $\epsilon_{\varsigma,y}$ is the sectorial share (as defined in Section 3.2.3) when $\varsigma \in \{ag, ind, res\}$ in year y, respectively.

$$C_{\varsigma,r,y} = C_{r,y} \cdot \epsilon_{\varsigma,y}, \forall \varsigma \in \{ag, ind, res\} \tag{3.2.1}$$

Typical hourly load shares of daily total consumption for the agricultural, industrial and residential sectors were obtained from Yao et al[51] and are shown in Figure 7. We assume that for the agricultural, industrial, and residential sectors the representative hourly share stays constant for any given day of the year and climate region.

The hourly load, $L_{\varsigma,y}(t)$ of sector $\varsigma \in \{ag, ind, res\}$, for a given year y, is defined in Equation 3.2.2.

$$L_{\varsigma,r,y}(t) = C_{\varsigma,r,y} \cdot [\mathbf{S}_{\varsigma} \circ \mathbf{S}_{total}] \tag{3.2.2}$$

where $C_{\varsigma,region,y}$ is the regional level consumption from a given sector, ς, in a given year y, $\circ$ represents the element-wise product,

$\mathbf{S}_\varsigma = \big(\underbrace{S_\varsigma \quad S_\varsigma \quad \cdots \quad S_\varsigma}_{365 \text{ elements}}\big)$, for a given sector $\varsigma \in \{ag, ind, res\}$, and

$\mathbf{S}_{total} = \big(\underbrace{S_{tot,d} \quad S_{tot,d} \quad \cdots \quad S_{tot,d}}_{24 \text{ elements}}\big)_{d=1}^{365}$

Note that the resulting vectors $\mathbf{S}_\varsigma$ and $\mathbf{S}_{total}$ have as many elements as hours in a year.

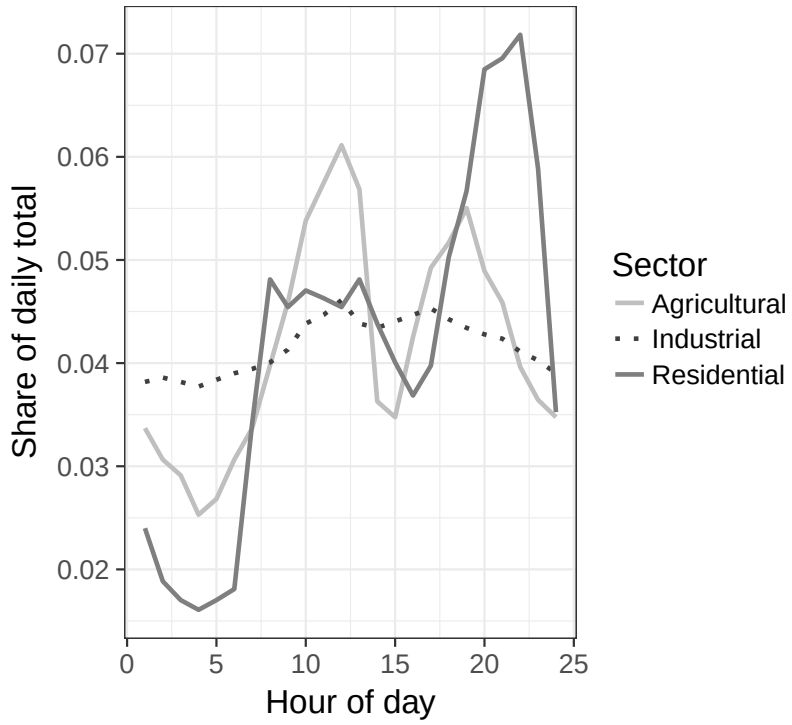

Figure 7: Agricultural S_{ag}, Industrial S_{ind}, and Residential S_{res} hourly shares of daily totals

The sum of the different sectorial hourly shares of daily totals shown in Figure 7 all equal 1 but are qualitatively very different. While the industrial daily load share curve is relatively flat, ranging 0.035 and 0.045 for any given hour, the residential load curve is expected to have a big peak at night time when people come home from work, around 0.07, and deep valley during the night hours when most people are asleep, around 0.015. These qualitative differences are important, because, as discussed in Section 3.2.3, the share of electricity consumed by the industrial sector is decreasing and the share from the residential sector is increasing. This qualitative shift in load composition will therefore rise to higher peaks, and lower lows in a typical day even if demand stays constant.

Non-Controllable Commercial load $L_{comm_{nc},r,y}$

The total electricity consumption from the non-controllable commercial sector, $C_{comm_{nc},y}$, in a given year y, is described by Equation 3.2.3, where $C_{region,y}$ is the climate region electricity consumption, $\epsilon_{comm,y}$ is the commercial sector share of the climate region consumption, and $\rho_{other,r,y}$ is the non-controllable component's share of the commercial sector yearly electricity consumption in a given region r, in year y, respectively.

$$C_{comm_{nc},region,y} = C_{region,y} \cdot \epsilon_{comm,y} \cdot \rho_{other,r,y} \tag{3.2.3}$$

Hourly load shares of daily total consumption for the non controllable commercial sectors for the four different climate regions were obtained from the estimated 2010 commercial sector model in Chapter 2 and follow the form shown in Equation 3.2.4.

$$S_{comm_{nc},r}(h) = \frac{\sum_{d=1}^{365} L_{comm_c,r,2010}((d-1)\cdot 24 + h)}{C_{comm_c,r,2010}} \tag{3.2.4}$$

where $\sum_{d=1}^{365} L_{comm_c,r,2010}((d-1)\cdot 24+h)$ is the sum of the commercial load in a given region, r, in 2010 for the hour $h \in 1-24$ of every day d of the year, and $C_{comm_c,r,2010}$ is the total consumption from the controllable component of the commercial sector in a given region in 2010.

The resulting hourly load shares of daily total consumption by the non controllable component of the commercial sector from the four different climate zones are shown in Figure 8. We assume that the non-controllable component of the commercial sectors hourly load share stays constant for any given day of the year within each climate region. When looking at the daily share of total electricity consumed in an specific season of the year we see a higher differentiation among our models. In Figure 9 we show the daily share of total electricity consumed in the winter season. As expected, the northernmost region in the country has the highest shares of electricity consumption for any given hour. As the model captures more southern buildings we see a decrease in the share of daily total for the Cold, HSCW, and HSWW climate regions, accordingly.

With a constructed set of hourly load shares from the non-controllable component of the commercial sector for every climate region, we can now find the hourly demand, $\bar{D}_{comm_{nc},region,y}(t)$, for the non-controllable component of the commercial sector for a given region and year y. This hourly demand is defined similarly to the hourly demand of the agricultural, industrial or residential sector and presented in Equation 3.2.5.

$$L_{comm_{nc},r,y}(t) = C_{comm_{nc},r,y} \cdot [\mathbf{S}_{comm_{nc},r} \circ \mathbf{S}_{total}] \tag{3.2.5}$$

where $C_{comm_{nc},region,y}$ is the regional level consumption from the non controllable component of the commercial in a given region, and year y, $\circ$ represents the element-wise product,

$$\mathbf{S}_{comm_{nc},region} = \big(\underbrace{S_{comm_{nc},region} \quad S_{comm_{nc},region} \quad \cdots \quad S_{comm_{nc},region}}_{\text{365 elements}}\big),$$

for a given climate region, and

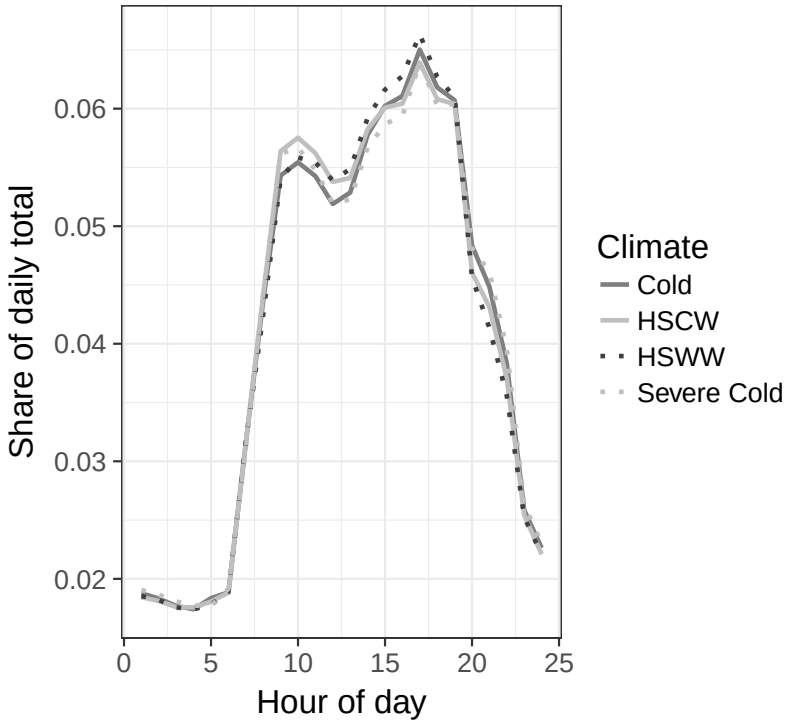

Figure 8: Hourly shares of daily total from the non-controlable commercial component of the commercial sector,n $S_{comm_{nc},r}$, for the four different climate regions in China

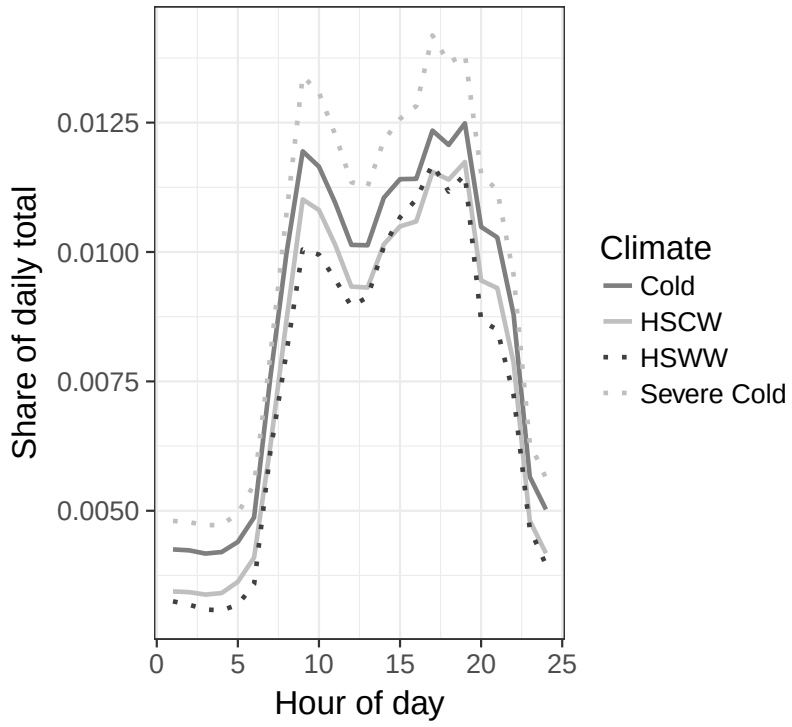

Figure 9: Hourly shares of daily total from the non-controlable commercial component of the commercial sector in the winter season, $S_{comm_{nc},r}$, for the four different climate regions in China

$$\mathbf{S}_{total} = \Big(\underbrace{S_{tot,d} \quad S_{tot,d} \quad \cdots \quad S_{tot,d}}_{\text{24 elements}}\Big)_{d=1}^{365}$$

As with the other non controllable loads previously presented, the length of the $\mathbf{S}_{comm_{nc},region}$ and $\mathbf{S}_{total}$ vectors equal the number of hours in a given year.

3.2.5 Controllable Commercial load, $L_{comm_c,r,y}$

Controllable commercial demand is modeled at the climate region level as the weighted average of the electricity demand from the six different individual controllable building models: offices with and without datacenters, retail buildings, hospitals, hotels, and schools and described at length in Chapter 2. The hourly controllable commmercial load for a region r and year y is described by Equation 2.5.7 in Chapter 2 and shown below.

$$L_{comm_c,r,y}(h) = \frac{\Gamma_{r,y}(h)}{\bar{i}_{baseline,r,y}} \cdot (1 - \rho_{other,r,y}) \cdot C_{r,y} \cdot \epsilon_{comm,y}$$

where $\Gamma_{r,y}(h)$ is the regional electricity density function as defined in Equation 2.5.6, $\bar{i}_{baseline,r,y}$ is the baseline average intensity, as defined in Equation 2.5.5, $\rho_{other,r,y}$ is the ratio between the yearly electricity consumption from building types not built from the individual models and the total commercial sector consumption in region r and year y. Parameters $C_{r,y}$ and $\epsilon_{comm,y}$ represent the total electricity consumption across all sectors, and the ratio of electricity consumption consumed by the commercial sector and the total electricity consumption across all sectors of the economy in region r and year y as described in Section 3.2.1.

It is useful to remind the reader that $L_{comm_c,r,y}$ is a function of the individual building models for the particular region and they in turn are a function of the efficiency standards, operational schedules, and heating electrification parameters chosen (ξ, θ, and χ). By extension, $L_{comm_c,r,y}$ is also a function of these three parameters as shown in Equation 3.2.6

$$L_{comm_c,r,y} = g(\xi, \theta, \chi) \tag{3.2.6}$$

3.2.6 Regional and national load, $L_{total,r,y}$, $L_{CH,y}$

The total hourly load for a given region and year, shown in Equation 3.2.7, is the sum of the load from the non-controllable agricultural, commercial, industrial and residential sectors, and the load from the controllable commercial sector.

$$L_{total,r,y} = \sum_{\varsigma \in S_{nc}} L_{\varsigma,r,y} + L_{comm_c,r,y} \tag{3.2.7}$$

where $\sum_{\varsigma \in S_{nc}} L_{\varsigma,r,y}$ is the sum of the load from all the non-controllable sectors included in set $S_{nc} = \{ag, comm_{nc}, ind, res\}$ and $L_{comm_c,r,y}$ is the load of the control-

lable commercial sector for region r, and year y, as defined in Sections 3.2.4 and 3.2.5 respectively.

If $L_{comm_c,r,y}$ is a function of the building parameters (ξ, θ, and χ) chosen, then $L_{total,r,y}$ is a also a function of these three parameters as shown in Equation 3.2.8.

$$L_{total,r,y} = \sum_{\varsigma \in S_{nc}} L_{\varsigma,r,y} + g(\xi, \theta, \chi) = h(\xi, \theta, \chi) \tag{3.2.8}$$

Summing Equation 3.2.8 over all climate regions in China, we can then obtain a national hourly load model as a function of the building parameters (ξ, θ, and χ) chosen, as shown in Equation 3.2.9.

$$L_{CH,y}(\xi, \theta, \chi) = \sum_{r \in CH} L_{total,r,y}(\xi, \theta, \chi) \tag{3.2.9}$$

3.3 Results

In this section we present the results of our simulated hourly load forecasts for the year 2030 across multiple set of parameters. We first provide a comparison between the estimated hourly loads in 2015 and the basecase scenario in 2030. We then present the descriptive statistics from all simulated scenarios across the three different parameters (ξ,θ,χ). We define six descriptive statistics as:

1. Total demand (TWh)
2. Load factor (unitless)
3. Peak load (GW)
4. Minimum hourly load (GW)
5. Maximum hour-to-hour up ramping rate (GW/h)
6. Maximum hour-to-hour down ramping rate (GW/h)

3.3.1 2015 vs 2030 basecase comparison

As we can see from Table 13 there is an increase across all descriptive statistics in our base case scenario load models for 2015 and 2030, $L_{CH}(\xi_1,\theta_1,\chi_1)$.

As mentioned earlier, total demand is expected to increase by almost 2,000 TWh, equivalent to a 32% increase from 2015. Load factor stays relatively constant increasing by less than 3% in the fifteen-year period. Peak load increases by over 250 GW while the lowest netload of the year increases by 130 GW, equivalent to a 29% increase for each.

	Statistics					
Year	Demand (TWh)	Load factor	Load (GW)		Ramping, ($\frac{GW}{h}$)	
			Peak	Min	↑, max	↓, max
2015	5662	0.75	862	439	89	-76
2030	7506	0.77	1115	568	160	-112
%Δ	32.6	2.6	29.3	29.5	80.5	46.8

Table 13: 2015 and basecase scenario 2030 load comparison across descriptive statistics. Percent change from 2015 load statistics

3.3.2 2030 load forecast across parameters

In Table 14 we show the descriptive statistics across the two standard adoption, two operational schedules, and three electrification of heating scenarios, for a total of twelve different load models developed in this work. As seen from the Demand columns, total yearly demand among our models varies between 7330 to 7630 TWh for the 2025 standards, Chinese schedules, and no electrification of heating commercial model scenario, and the 2020 standards, US schedules, and low-efficiency electrification scenarios, respectively. Load factors do not change dramatically with different parameters, staying within 0.76-0.77 across all parameters.

As shown under the Load, Peak column in Table 14, peak load ranges between 1,091 to 1,152 GW across all parameters, while lowest netload ranges between 560 to 580 GW. Maximum ramping up and down rates for the year for the base case 2030 scenario are 160 and 112 GW per hour. The range for maximum ramping up rates across all parameters is between 114 to 160 GW per hour, while the range for the maximum ramping down rates across all models is between 112 to 133 GW per hour.

Parameters			Statistics					
Standard	Schedule	Heating	Demand (TWh)	Load factor	Load (GW)		Ramping, ($\frac{GW}{h}$)	
ξ	θ	χ			Peak	Min	↑, max	↓, max
2020	CH	χ_1	7,506	0.77	1,115	568	160	-112
2020	CH	χ_2	7,357	0.76	1,099	561	122	-112
2020	CH	χ_3	7,407	0.77	1,100	564	122	-112
2020	US	χ_1	7,629	0.76	1,152	580	159	-133
2020	US	χ_2	7,439	0.76	1,115	573	117	-118
2020	US	χ_3	7,502	0.77	1,115	575	117	-118
2025	CH	χ_1	7,475	0.77	1,109	568	159	-112
2025	CH	χ_2	7,329	0.77	1,091	561	119	-112
2025	CH	χ_3	7,378	0.77	1,092	563	119	-112
2025	US	χ_1	7,596	0.76	1,146	578	160	-125
2025	US	χ_2	7,408	0.76	1,106	571	114	-117
2025	US	χ_3	7,471	0.77	1,107	574	114	-117

Table 14: Descriptive statistics for all load models developed across all parameters

3.4 Discussion

Statistic	Change in parameter			
	$\Delta\xi$	$\Delta\theta$	$\chi_1 \rightarrow \chi_2$	$\chi_1 \rightarrow \chi_2$
ΔDemand	-0.41	1.64	-1.99	-1.32
ΔLoad factor	0.13	-1.63	-0.62	-0.01
ΔPeak load	-0.54	3.32	-1.37	-1.31
ΔLoad, min	0.02	2.07	-1.14	-0.66
ΔRamping $\uparrow$, max	-0.41	-0.62	-23.64	-23.64
ΔRamping $\downarrow$, max	-0.28	19.21	0.19	0.03

Table 15: Percent change in load statistics from a variation in parameter

In general, as seen in Table 15, differences in efficiency standards as defined in Chapter 2.3.3 have a small effect on the descriptive statistics of load in 2030. A shift from 2020 to 2025 standards compliance by 2030 ($\Delta\xi$) only reduces electricity consumption by 0.41% from the basecase scenario ($L(\xi_1, \theta_1, \chi_1) \rightarrow L(\xi_2, \theta_1, \chi_1)$). The same shift decreases peak load by 0.54% and maximum ramping up and down, respectively, by 0.41 and 0.28%. In general, we see a small decrease on the descriptive statistics between improvements in efficiency.

On the other hand, the other two parameters (θ,χ) have a much larger impact on the electricity consumption in buildings and the national load in general. For example, changing the operational schedules from those recommended by MOHURD to ASHRAE ($\Delta\theta$), increases total system electricity consumption between by 1.64% from the base case scenario, decreases load factor by 1.63%. In addition, operating buildings like their American counterparts increases system peak load by 3.3% and lowest netload by 2.1%. While the maximum ramping up rate is only decreased by 0.6%, it increases the maximum ramping down by over 19%.

From performing a sensitivity analysis on the commercial sector in Chapter 2 we learned that changing the electrification scenario (χ) has a higher impact for buildings in the North (Severe Cold and Cold climates) than changing any of the other two parameters. In general, de-electrifying the heating load ($\chi_1 \rightarrow \chi_2$) has larger impacts than just increasing the efficiency of the heating provision ($\chi_1 \rightarrow \chi_3$). For example, when buildings go from self-providing heating by electric boilers to having their electricity provision met by gas or coal boilers ($\chi_1 \rightarrow \chi_2$) we see a 2% decrease in total electricity consumption at the national level. Both peak load and the lowest netload of the year decrease by 1.4 and 1.1%, respectively. This shift in heat provision decreases by 24% the maximum ramping up rate required in the system while increasing the maximum ramping down rate by only 0.2%.

Providing the building's heating with more efficient electrified heating ($\chi_1 \rightarrow \chi_3$) has a smaller impact on electricity consumption than de-electrifying the heating load completely with total system demand and peak load reductions of about 1.3%. The

maximum ramping up rate decreases by 24%, the same as when de-electrifying the heating load across all buildings in the commercial sector. All other descriptive statistics have the same direction but smaller magnitude in change as the de-electrification case ($\chi_1 \rightarrow \chi_2$).

3.5 Conclusion

In this Chapter we developed a model for an hourly load estimate of the Chinese demand in 2030. It is built on a parametrized commercial model with efficiency, operational schedules and electrification of heating as different parameters. The model allows us to understand how changes in the construction and operation of the commercial sector affect the total demand, peak load, and ramping rates of the system load. In contrast to other load forecasting tools it allows us to characterize ramping rates and the impact of the commercial sector on these rates. We found that expected electricity demand in China by 2030 will increase by 32% from its 2015 value. In addition, peak load is expected to increase about 29%. Ramping events will increase in number and magnitude with the maximum ramping up and down rates increasing by 80 and 46%, respectively between 2015 and 2030. We performed a sensitivity analysis and found that the commercial model parameters with the largest impact in overall system metrics are how buildings are operated (θ) and how heating load is met (χ).

We will use this load model in combination with hourly renewable production forecasts (Chapter 4) to formulate a netload scenario that allows us to understand the impact of renewable penetration on the constraints of the system (Chapter 5). Finally, making the commercial component of this load model controllable, will allow us to use it to estimate the impact of demand response from the commercial sector in the provision of system flexibility in a future system with significant penetration of renewables (Chapter 7).

Chapter 4

Solar PV and Wind Potential in China

4.1 Introduction

In this chapter we describe a model to estimate hourly renewable production from solar PV and wind by developing three different PV and wind capacity expansion scenarios to 2030. We first introduce the reader to the past and current growth in installed capacities for both renewable types studied here. We then present the current expansion plans to 2020 at the provincial level. Finally, using three different assumption for capacity expansion growth, we extrapolate the 2016-2020 growth rates to 2030 to formulate three different capacity scenarios. Using our capacity estimates and available hourly capacity factor data [40, 38] we compare the impact on demand from the three different scenarios.

In the last decade China has seen unparalleled growth in the installation of renewable energy capacity [8]. As seen in Table 16, between 2010 and 2016, China added renewable capacity at an average rate of 40% a year, increasing total installed renewable capacity from 29.8 to over 225 GW [21]. For the same time period, solar PV installed capacity has grown at an unprecedented rate of 168% a year reaching an installed capacity of over 77 GW in 2016. Similarly, installed wind capacity has grown at a rate of 30.8% a year reaching an installed capacity of over 148 GW in 2016. This sustained yearly growth in installed renewable capacity has made China the global leader on installed solar and wind capacities. By 2017, China surpassed the European Union in installed renewable capacity.

As seen in Table 17, the province with the most installed solar capacity in 2016 was Xinjiang where 8.6 GW of solar has been installed, accounting for over 11% of the total solar capacity. Gansu, Inner Mongolia, Ningxia, Qinghai, and Xinjiang autonomous regions together account for 33.9 GW or 43.8% of the total installed solar capacity. The province with the most installed wind capacity was Inner Mongolia where 25.6 GW has been installed, accounting for over 17% of the total wind capacity. As with

Renewable	2010	2016	Yearly Growth (%)
Solar	205.02	77,190	168
Wind	29,575	148,170	30.8
Total	29,780	225,360	40.1

Table 16: Solar and wind installed capacity in 2010 and 2016 in MW and yearly growth in this period in %.

solar, Gansu, Inner Mongolia, Ningxia, and Xinjiang autonomous regions together account for 65.5 GW or 44.0% of the total installed capacity. These provinces located in Northwest and Western China have relatively low populations and loads and are therefore net solar and wind electricity exporting regions.

4.2 Existing Plans to 2020

According to official documents from the Chinese Electricity Council (CEC)[21], China has goals of increasing its renewable capacity to almost 400 GW within the current Five-Year plan. The CEC has published goals for capacity installations to 2020 by province for solar PV and wind [9, 10].

4.2.1 Solar

As shown in Table 18, by 2020, expected installed solar capacity will almost double current levels, reaching over 130 GW. The fastest expected growth comes from provinces with relatively low installed capacity in 2016. For example, Heilongjiang, in Northeast China, is expected to grow at a 111% yearly rate adding over 3 GW of capacity in that period. Provinces that will see larger absolute increase in installed solar capacity include Hebei, Jiangsu, Shanxi and Zhejiang provinces with additional installed capacity of around 4 GW in each. The average yearly growth rate in solar installations between 2016-2020 at the national level is 14%

A number of cities and provinces including Beijing, Chongqing, Fujian, Gansu, Hainan, Ningxia, Tianjin, Tibet, Xinjiang, and to a lesser visible extent Inner Mongolia have reduced plans for expansion in installed capacity due to curtailment issues. Excluding these provinces from the calculation, the average yearly growth in installed solar capacity between 2016 and 2020 increases from 14 to 18%.

4.2.2 Wind

As shown in Table 19, between 2016 and 2020, the expected installed solar capacity will almost double reaching over 260 GW. The fastest expected growth comes from provinces with relatively low installed capacity in 2016. For example, Henan, in Central China, is expected to grow at a 88% yearly rate adding over 12 GW of capacity in that

Province	**Installed capacity (MW)**		
	Solar	**Wind**	**Total**
Anhui	3,450	1,770	5,220
Beijing	240	190	430
Chongqing	5	280	285
Fujian	270	2,140	2,410
Gansu	6,860	12,770	19,630
Guangdong	1,560	2,680	4,240
Guangxi	180	670	850
Guizhou	460	3,620	4,080
Hainan	340	310	650
Hebei	4,430	11,880	16,310
Heilongjiang	170	5,610	5,780
Henan	2,840	1,040	3,880
Hubei	1,870	2,010	3,880
Hunan	300	2,170	2,470
Inner Mongolia	6,370	25,570	31,940
Jiangsu	5,460	5,610	11,070
Jiangxi	2,280	1,080	3,360
Jilin	560	5,050	5,610
Liaoning	520	6,950	7,470
Ningxia	5,260	9,420	14,680
Qinghai	6,820	690	7,510
Shaanxi	3,340	2,490	5,830
Shandong	4,450	8,390	12,840
Shanghai	350	710	1,060
Shanxi	2,970	7,710	10,680
Sichuan	960	1,250	2,210
Tianjin	600	290	890
Tibet	330	10	340
Xinjiang	8,620	17,760	26,380
Yunnan	2,080	7,370	9,450
Zhejiang	3,380	1,190	4,570
National	**77,325**	**148,680**	**226,005**

Table 17: Solar and Wind installed capacity in 2016, by province, MW

Province	**2016**	**2020**	**Growth**
Anhui	3,450	5,850	14%
Beijing	240	240	0%
Chongqing	5	5	0%
Fujian	270	270	0%
Gansu	6,860	6,860	0%
Guangdong	1,560	4,460	30%
Guangxi	180	1,580	72%
Guizhou	460	1,660	38%
Hainan	340	340	0%
Hebei	4,430	9,030	19%
Heilongjiang	170	3,370	111%
Henan	2,840	5,240	17%
Hubei	1,870	3,470	17%
Hunan	300	1,900	59%
Inner Mongolia	6,370	10,370	13%
Jiangsu	5,460	9,660	15%
Jiangxi	2,280	3,680	13%
Jilin	560	2,260	42%
Liaoning	520	2,020	40%
Ningxia	5,260	5,260	0%
Qinghai	6,820	9,120	8%
Shaanxi	3,340	6,540	18%
Shandong	4,450	7,950	16%
Shanghai	350	350	0%
Shanxi	2,970	6,770	23%
Sichuan	960	2,560	28%
Tianjin	600	600	0%
Tibet	330	330	0%
Xinjiang	8,620	8,620	0%
Yunnan	2,080	4,080	18%
Zhejiang	3,380	7,380	22%
National	**77,325**	**131,825**	**14%**

Table 18: Provincial and national installed and planned solar capacity in 2016 and 2020, respectively, and yearly growth rate in MW and %, respectively

period. Provinces that will see larger absolute increase in installed solar capacity include Hebei, Henan, Shandong, Shanxi provinces with additional installed capacity of around 10 GW in each. The average yearly growth rate in wind installations between 2016-2020 at the national level is 15%

A number of provinces including Gansu, Heilongjiang, Inner Mongolia, Jilin, and Xinjiang, have reduced plans for expansion in installed capacity due to curtailment issues. Excluding these provinces from the national calculation, the average yearly growth in installed solar capacity between 2016 and 2020 increases from 15 to 24%.

4.2.3 Curtailment issues

Provinces with low or zero growth between 2016 and 2020 have had high curtailment rates or higher than average rates of capacity not connected to the grid in the last few years. Provinces with such problems were not included in plans for renewables capacity expansion to 2020 and are therefore not expected to see any growth in installed capacity until these curtailment and unconnected capacity rates are decreased.

As mentioned in section 4.2.1, in the case of solar installations, provinces and cities with very low growth include: Beijing, Chongqing, Fujian, Gansu, Hainan, Inner Mongolia, Ningxia, Tianjin, Tibet, and Xinjiang. Excluding these locations from the calculation, the average yearly growth for solar capacity between 2016 and 2020 is expected to increase from 14 to 18%. As mentioned in section 4.2.2, in the case of wind installations, provinces and cities with very small growth but with large potential include: Gansu, Heilongjiang, Inner Mongolia, Jilin, and Xinjiang. Excluding these locations the average yearly growth for solar between 2016 and 2020 would increase from 15 to 24%. These provinces with curtailment constraints between 2016 and 2020 are shown in Table 21.

Once the government alleviates the curtailment and low connection-to-grid issues, provinces with no expected additional capacity to 2020 might see increases in their expected capacity expansions. Forecasting renewable capacity growth to 2030 and beyond requires therefore at least two scenarios, one where curtailment issues are not resolved and continue to impair the provinces' growth opportunity, and another where the government decreases curtailment and increases connection to grid and therefore spur further capacity expansion in those provinces. Such scenarios will be presented in section 4.3.

4.3 Capacity Expansion Scenarios

In this section we describe the three different renewables capacity expansion scenarios in this work. We first start by introducing the primary component, yearly installation rate, for the construction of these renewable expansion scenarios in section 4.3.1. We then describe the applied limits on renewable capacity expansion in section 4.3.2 by presenting the physical potential of each renewable resource by province. Finally, we

Province	**2016**	**2020**	**Growth**
Anhui	1,770	6,270	37%
Beijing	190	390	20%
Chongqing	280	1,030	38%
Fujian	2,140	5,640	27%
Gansu	12,770	14,000	2%
Guangdong	2,680	8,830	35%
Guangxi	670	5,670	71%
Guizhou	3,620	6,010	14%
Hainan	310	660	21%
Hebei	11,880	23,270	18%
Heilongjiang	5,610	6,000	2%
Henan	1,040	13,040	88%
Hubei	2,010	9,530	48%
Hunan	2,170	9,790	46%
Inner Mongolia	25,570	27,000	1%
Jiangsu	5,610	9,310	14%
Jiangxi	1,080	5,810	52%
Jilin	5,050	5,050	0%
Liaoning	6,950	8,550	5%
Ningxia	9,420	9,420	0%
Qinghai	690	5,690	69%
Shaanxi	2,490	10,020	42%
Shandong	8,390	18,290	22%
Shanghai	710	1,010	9%
Shanxi	7,710	17,110	22%
Sichuan	1,250	1,950	12%
Tianjin	290	1,520	51%
Tibet	10	210	114%
Xinjiang	17,760	18,000	0%
Yunnan	7,370	9,320	6%
Zhejiang	1,190	3,990	35%
National	**148,680**	**262,380**	**15%**

Table 19: Provincial and national installed and planned wind capacity in 2016 and 2020, respectively, and yearly growth rate in MW and %, respectively

Renewable	City/Province
Solar	Beijing, Chongqing, Fujian, Gansu, Hainan, Inner Mongolia, Ningxia, Tianjin, Tibet, Xinjiang
Wind	Gansu, Heilongjiang, Inner Mongolia, Jilin, Xinjiang

Table 21: Cities and provinces with curtailment constraints between 2016 and 2020 development plans

present the hourly capacity factor data used to construct provincial average renewable electricity production profiles in section 4.3.3. We use these three building blocks to construct three different scenarios presented in sections 4.3.4, 4.3.5, and 4.3.6

4.3.1 Installation growth model

One way we estimate renewables installation growth between 2020 and 2030 is by extrapolating expected growth rates between 2016 and 2020 at the provincial level for both solar PV and wind. In order to provide a conservative growth estimate, we then divide these yearly growth rates by two, and apply it to each province between 2020 and 2030. As seen in Tables 18 and 19 national average yearly rates are 14 and 15%, and fluctuate between 0 and 111% and 0 and 114% for solar PV and wind respectively. The installation of renewables is therefore not uniform and provinces with very small installed capacities are expected to receive orders of magnitude increases in their installed capacities by 2020. As some of these yearly growth rates if maintained between 2020 and 2030 would give rise to improbably high capacities, constraints on the potential capacity for solar PV and wind at the province level needs to be discussed. In the next section we discuss what is the potential for expansion, based on physical and environmental constraints, for each province and how they were calculated.

4.3.2 Potential

He et al published two studies on the potential of capacity installations in China at the provincial level [38, 40]. The studies utilized 10-year hourly solar irradiation and wind speed data from 2001 to 2010 from 200 representative locations to develop provincial solar and wind availability profiles.

Solar PV potential

The study by He et al [40] found that China has a potential solar capacity from 4700 GW to 39300 GW, and the annual solar output could reach 6900 TWh to 70100 TWh. Resources are most concentrated in northwest provinces, topped by Gansu, Inner Mongolia, and Xinjiang. The challenge of solar development in China is integration of such resources rather than resource scarcity.

As shown in Table 22 China's national solar PV potential ranges from 4.7 and 39 TW. Current total capacity including coal, gas, hydro and nuclear barely surpasses 1 TW. The provinces with the most solar PV capacity potential are Gansu, Inner Mongolia, and Xinjiang with 297, 1,398, and 1,363 GW at the lower end, and 3,692, 13,599, and 12,343 GW at the higher end of the spectrum.

Wind potential

In his assessment study, He et al [38], found that China's annual wind generation could reach between 2000 TWh to 3500 TWh. Nationally this would correspond to an average capacity factor of 0.18. Reasons for why the capacity factor is this low are presented by [44]. The diurnal and seasonal variation shows spring and winter has better wind resources than in the summer and fall.

As shown in Table 23 China's national wind potential onshore ranges from 833 and 1,805 GW, and offshore potential is around 469 GW. The provinces with the most wind capacity potential are also Gansu, Inner Mongolia, and Xinjiang with 55, 291, and 285 GW at the lower end, and 121, 562, and 568 GW at the higher end of the spectrum for onshore. The provinces with most available offshore potential are Guangdong, Jiangsu, Liaoning, Shandong, and Zhejiang with 52, 107, 61, 77, and 54 GW, respectively.

4.3.3 Provincial capacity factors

Capacity factor data from the 200 representative sites, for 2001-2010, across the country for each renewable type was aggregated by province. At the province level, hourly data was averaged to produce a provincial capacity factor hourly time series for an average year. The mean and standard deviation of the resulting time series for each renewable type across all provinces are shown in Table 24.

Provinces with high capacity factors are deemed to be potentially rich in the resource if the environmental constraints allow it. For solar, Gansu, Inner Mongolia, Ningxia, Qinghai, Tibet and Yunnan all have average capacity factors above 0.2. For wind, Beijing, Fujian, Hainan, Hebei, Inner Mongolia, Jiangsu, Shandong, Shanghai, Shanxi and Zhejiang all have average capacity factors above 0.2.

4.3.4 Scenario R_a: 2020 goals

In Scenario R_a, our conservative scenario, we assume 2020 goals at every province are met, but that no further development occurs to 2030. This development pathway leads to a total solar PV and wind capacities of 132 and 262 GW, respectively. As shown in Table 25 the total installed renewables capacity adds up to 394.2 GW under R_a scenario.

Province	**Potential capacity (GW)**	
	Low	**High**
Anhui	8	34
Beijing	4	25
Chongqing	5	15
Fujian	32	280
Gansu	287	3,692
Guangdong	163	643
Guangxi	199	707
Guizhou	45	338
Hainan	91	205
Hebei	63	483
Heilongjiang	183	279
Henan	11	116
Hubei	10	70
Hunan	1	16
Inner Mongolia	1,398	13,599
Jiangsu	7	25.2
Jiangxi	56	265
Jilin	252	465
Liaoning	59	420
Ningxia	58	516
Qinghai	30	1,791
Shaanxi	91	1,106
Shandong	113	313
Shanghai	0.6	1.1
Shanxi	51	689
Sichuan	3	116
Tianjin	3	7
Tibet	1	21
Xinjiang	1,363	12,343
Yunnan	67	598
Zhejiang	13	120
National	**4,667.6**	**39,298.3**

Table 22: Low and High Solar PV installation potential, respectively, by province, GW

Province	Potential capacity (GW)		
	Low	High	Offshore
Anhui	3.31	9.03	0
Beijing	0.37	1.59	0
Chongqing	1.46	5.7	0
Fujian	2.84	12.2	28.05
Gansu	54.99	120.85	0
Guangdong	6.88	19.05	51.71
Guangxi	13.85	36.4	26.59
Guizhou	8.87	26.28	0
Hainan	2.28	5.04	10.36
Hebei	5.78	17.86	24.12
Heilongjiang	37.54	85.81	0
Henan	2.22	7	0
Hubei	4.98	15.71	0
Hunan	10.12	27.93	0
Inner Mongolia	291.55	562	0
Jiangsu	0.44	0.9	107.62
Jiangxi	8.67	22.48	0
Jilin	13.29	30.09	0
Liaoning	5.58	14.07	60.58
Ningxia	6.42	13.76	0
Qinghai	28.47	80.4	0
Shaanxi	13.55	35.06	0
Shandong	4.23	8.81	76.54
Shanghai	0.01	0.07	24.3
Shanxi	7.21	22.35	0
Sichuan	2.06	12.98	0
Tianjin	0.09	0.17	5.56
Tibet	0.1	0.83	0
Xinjiang	285.14	567.6	0
Yunnan	8.13	33.59	0
Zhejiang	2.22	9.44	53.84
National	**832.65**	**1,805.05**	**469.27**

Table 23: Low and High estimates for onshore wind, and offshore wind, installation potential, respectively, by province, GW

	Solar PV cf		**Wind cf**	
Province	μ	σ	μ	σ
Anhui	0.149	0.215	0.119	0.148
Beijing	0.181	0.241	0.253	0.251
Chongqing	0.126	0.198	0.182	0.202
Fujian	0.154	0.220	0.235	0.267
Gansu	0.206	0.252	0.143	0.147
Guangdong	0.153	0.209	0.192	0.191
Guangxi	0.148	0.203	0.171	0.195
Guizhou	0.162	0.221	0.157	0.200
Hainan	0.176	0.241	0.201	0.225
Hebei	0.180	0.234	0.204	0.234
Heilongjiang	0.178	0.228	0.184	0.190
Henan	0.150	0.214	0.085	0.118
Hubei	0.138	0.199	0.116	0.135
Hunan	0.134	0.199	0.123	0.133
Inner Mongolia	0.209	0.248	0.236	0.169
Jiangsu	0.153	0.217	0.204	0.241
Jiangxi	0.142	0.207	0.110	0.118
Jilin	0.174	0.233	0.147	0.166
Liaoning	0.172	0.230	0.191	0.228
Ningxia	0.204	0.265	0.112	0.151
Qinghai	0.262	0.301	0.109	0.132
Shaanxi	0.175	0.230	0.142	0.160
Shandong	0.164	0.226	0.204	0.234
Shanghai	0.151	0.228	0.233	0.257
Shanxi	0.189	0.249	0.248	0.251
Sichuan	0.167	0.208	0.103	0.109
Tianjin	0.168	0.231	0.116	0.170
Tibet	0.311	0.331	0.298	0.254
Xinjiang	0.183	0.227	0.176	0.168
Yunnan	0.215	0.265	0.185	0.188
Zhejiang	0.148	0.218	0.201	0.224

Table 24: Mean (μ) and standard deviation (σ) for hourly capacity factor data by province and renewable type

4.3.5 Scenario R_b: Historic growth, with curtailment

Scenario R_b represents an optimistic scenario; in it we assume solar and wind at the province level grow at a rate equal to half of the historic 2016-2020 period growth rate, as discussed in Section 4.3.1. This renewable installation scenario leads to installed capacities of solar PV and wind of 613 and 617 GW, respectively. As shown in Table 25, under scenario R_b, the total installed renewables capacity adds up to 1230 GW.

In this scenario we assume that provinces with offshore potential tap into it if their capacity under the growth scenario outlined in 4.3.1 surpasses that provinces onshore potential (high) as shown in Table 23. Installed solar PV capacity is assumed to be independent of wind installed capacity.

4.3.6 Scenario R_c: Historic growth, reduced curtailment

In Scenario R_c we assume a slightly more optimistic scenario where the capacity installation growth rates for all provinces, except the ones with curtailment issues, as shown in Table 21, are equal to that of Scenario R_b. After experiencing a hiatus in growth between 2016 and 2020, these provinces experience a growth rate equal to the national average rate without them, 18 and 24% for solar PV and wind respectively.

As shown in Table 25, this renewable installation scenario leads to installed capacities of solar PV and wind of 768 and 1122 GW, respectively. The total installed renewables capacity adds up to 1889 GW. In this scenario we still assume that provinces with offshore potential tap into it if their capacity under the growth scenario outlined in 4.3.1 surpasses that provinces onshore potential (high) as shown in Table 23.

Meeting 2020 goals without updating and surpassing them, as in Scenario R_a, would lead to an installation capacity of less than 400 GW. To provide a comparison, the US had approximately 130 GW of solar and wind capacity installed in 2017, while China had over 140 GW of just wind, by the end of 2016. Although not an insignificant amount compared to other industrialized nations, meeting 2020 goals in 2030 for renewable capacity expansion would provide around 8% of the total consumption of that year. Scenarios R_b and R_c would require a further 210 and 380% increase from 2020 goals (Scenario R_a) in the required installed capacity. In order to reduce the greenhouse emission in the power sector, a large ramp in capacity installed for both solar and wind is required. Both Scenarios R_b and R_c would meet expected expansion necessary to meet the COP21 goals [42].

4.4 Results: Renewable Production

The different renewable expansion scenarios (R_a,R_b, and R_c) map out to different futures in production and in reduction of green house gas emissions from the electricity sector. In Table 25 we can see the assumptions for capacity installed at the province level for each of the renewable scenarios outlined in Section 4.3.

Province	**Solar PV capacity (GW)**			**Wind capacity (GW)**		
	R_a	R_b	R_c	R_a	R_b	R_c
Anhui	5.9	11.6	11.6	6.3	9.0	9.0
Beijing	0.2	0.2	1.4	0.4	1.0	1.0
Chongqing	0.0	0.0	0.0	1.0	5.7	5.7
Fujian	0.3	0.3	1.6	5.6	20.4	20.4
Gansu	6.9	6.9	40.9	14.0	15.7	118.2
Guangdong	4.5	18.1	18.1	8.8	43.8	43.8
Guangxi	1.6	34.4	34.4	5.7	63.0	63.0
Guizhou	1.7	9.4	9.4	6.0	11.6	11.6
Hainan	0.3	0.3	2.0	0.7	1.8	1.8
Hebei	9.0	22.9	22.9	23.3	42.0	42.0
Heilongjiang	3.4	278.6	278.6	6.0	6.5	50.7
Henan	5.2	11.6	11.6	13.0	7.0	7.0
Hubei	3.5	7.7	7.7	9.5	15.7	15.7
Hunan	1.9	16.0	16.0	9.8	27.9	27.9
Inner Mongolia	10.4	19.4	61.8	27.0	28.9	228.0
Jiangsu	9.7	20.2	20.2	9.3	17.9	17.9
Jiangxi	3.7	6.8	6.8	5.8	22.5	22.5
Jilin	2.3	15.0	15.0	5.1	5.1	30.1
Liaoning	2.0	12.7	12.7	8.6	11.1	11.1
Ningxia	5.3	5.3	31.4	9.4	9.4	9.4
Qinghai	9.1	13.2	13.2	5.7	80.4	80.4
Shaanxi	6.5	15.7	15.7	10.0	35.1	35.1
Shandong	8.0	16.9	16.9	18.3	50.8	50.8
Shanghai	0.4	0.4	1.1	1.0	1.6	1.6
Shanxi	6.8	20.0	20.0	17.1	22.4	22.4
Sichuan	2.6	9.4	9.4	2.0	3.5	3.5
Tianjin	0.6	0.6	3.6	1.5	5.7	5.7
Tibet	0.3	0.3	2.0	0.2	0.8	0.8
Xinjiang	8.6	8.6	51.4	18.0	18.3	152.0
Yunnan	4.1	9.8	9.8	9.3	12.6	12.6
Zhejiang	7.4	20.5	20.5	4.0	20.3	20.3
National	**131.8**	**612.8**	**767.8**	**262.4**	**617.3**	**1122**

Table 25: Solar PV and wind capacity installations for the three different 2030 scenarios, by province, GW

Using the provincial average hourly capacity factor data mentioned in Section 4.3.3 and the renewables installation estimates for the different renewable scenarios shown in Table 25 we can calculate hourly solar PV and wind production time series as a function of the renewable scenario. Solar PV production as a function of renewable scenario ($RP_{solar,p}(R_i)$) at province p is defined in Equation 4.4.1

$$RP_{solar,p}(R_i) = \varphi_{solar,p} \cdot K_{solar,p}(R_i) \tag{4.4.1}$$

where $\varphi_{solar,p}$ and $K_{solar,p}(R_i)$ are the provincial average hourly solar PV capacity factor for every hour of the year, and the solar capacity installed in province p under renewable scenario R_i.

Depending on the province's location, provincial wind installation might be located on or offshore. Therefore, hourly wind production in province p under renewable scenario R_i is defined in Equation 4.4.2

$$RP_{wind,p}(R_i) = \varphi_{wind,on,p} \cdot K_{wind,on,p}(R_i) + \varphi_{wind,off,p} \cdot K_{wind,off,p}(R_i) \tag{4.4.2}$$

where $\varphi_{wind,on,p}$ and $K_{wind,on,p}(R_i)$ are the provincial average hourly onshore wind capacity factor for every hour of the year, and the onshore wind capacity installed in province p under renewable scenario R_i. Similarly, $\varphi_{wind,off,p}$ and $K_{wind,off,p}(R_i)$ are the provincial average hourly offshore wind capacity factor for every hour of the year, and the offshore wind capacity installed in province p under renewable scenario R_i

Combining Equations 4.4.1 and 4.4.2 we obtained a generalized model for the hourly renewable production in province p under renewable scenario R_i represented in Equation 4.4.3.

$$RP_p(R_i) = RP_{solar,p}(R_i) + RP_{wind,p}(R_i) \tag{4.4.3}$$

By summing across all provinces in China, we can obtain a national hourly renewable production under renewable scenario R_i as shown in Equation 4.4.4

$$RP_{CH}(R_i) = \sum_{p \in CH} RP_p(R_i) \tag{4.4.4}$$

Table 26 shows the expected solar PV, wind, and total capacity installed by 2030 under the three different renewable scenarios described in this chapter. In addition, the total yearly renewable production as calculated by Equation 4.4.4 is seen on the right most column.

Under Scenario R_a renewables would provide about 616 TWh of electricity, equivalent to 8% of the total electricity consumption in the country (7506 TWh) for the base case load scenario scenario (see 3.2.1). Assuming no further curtailment, scenario R_b would produce 1230 TWh of renewable electricity, equivalent to about 25% of the total electricity consumption in 2030. Finally under renewable scenario R_c, and assuming no further curtailment, we calculate a yearly renewables production in 2030 of 2971

Scenario	Solar PV (GW)	Wind (GW)	Total (GW)	Production (TWh)
R_a: 2020 goals	131.8	262.4	394.2	615.9
R_b: Growth, with curtailment	612.8	617.3	1230	1852
R_c: Growth, reduced curtailment	767.8	1122	1889	2971

Table 26: Installed renewables capacity and total yearly electricity production in 2030 under different scenarios

TWh. In this scenario, renewables would provide about 40% of the total electricity consumption by 2030.

4.5 Conclusion

In this chapter we presented the historical growth of solar PV and wind installed capacity in China. In addition we presented the expected capacity expansion for each solar PV and wind to 2020. We used the growth rates between 2016 and 2020 to formulate growth scenarios between 2020 and 2030 at the provincial level. We assumed that growth would fall within the two most extreme renewable scenarios developed: a future with no added capacity beyond 2020 goals (R_a), and a future with increased investment in renewable capacity R_c reaching a total of 1889 GW renewable capacity installed. In a R_a future, and assuming a total electricity demand of 7500 TWh in 2030, solar PV and wind could account for around 8% of total generation. In the most optimistic scenario, solar PV and wind would account for just over 40% of total generation. Other researchers have estimated that wind could provide about 26% of electricity demand in 2030 [3]. As more renewable capacity gets added to the grid, challenges for the integration of renewable become more prominent. The effects of integrating large amounts of renewable electricity into the system under different renewable scenarios will be discussed in detail in Chapter 5.

Chapter 5

Electricity netload forecast model for China

5.1 Introduction

The increasing penetration of intermittent renewables into the Chinese electricity system will exacerbate problems that are already causing solar PV and wind installations to have relatively low capacity factors and high curtailment rates [81, 44]. Increasing penetration of renewable will have an impact on all system load characteristics from peak load, to ramping rates. Understanding these impacts is a key component in assessing the required capacity or the flexibility requirements from increased ramping rates needed by 2030 [37, 45, 82].

In this chapter we will develop an hourly netload model for the Chinese electricity system as a function of the parameters defining the commercial sector, and the renewable penetration scenario expected between 2020 and 2030. After introducing the model, we present the results from our model by providing key statistics in the forecasted netload under different scenarios. Finally, we analyze these results with emphasis on understanding the increase flexibility requirements that need to be met across different efficiency and renewable penetration scenarios.

5.2 Model Description

In Chapter 3, an hourly load model as a function of the efficiency standards, operational schedules, and heating electrification modes (ξ,θ, and χ, respectively) for the commercial sector was presented and used to forecast load and to assess load characteristics in 2030. In this chapter, we combine the results derived by the model in Chapter 3 and the renewable penetration and production scenarios presented in Chapter 4 to produce a model for Chinese netload in 2030.

The netload of the system at any hour of the year is defined as the difference between the load and the renewable production at that location and time. Since the

hourly load (L_{CH}) is a function of the efficiency standards, operational schedules, and heating electrification modes (ξ,θ, and χ, respectively) and the hourly national renewable production RP_{CH} is a function of the renewable penetration scenario (R_i), then it follows that the the hourly netload at the national level would be a function of ξ,θ, χ, and R_i as shown in Equation 5.2.1.

$$NL_{CH}(\xi, \theta, \chi, R_i) = L_{CH}(\xi, \theta, \chi) - RP_{CH}(R_i) \tag{5.2.1}$$

where NL_{CH}, L_{CH}, and RP_{CH} are the national hourly netload, load, and renewable production, respectively, and the parameters ξ, θ, χ, and R_i represent the global parameters: efficiency standards, operation schedules, heating electrification, and renewable penetration, respectively. Table 27 describe the different values for the global parameters in the netload model. For a more detailed description of these parameters see Chapters 2 and 4.

Parameter	Value: Description
ξ, Efficiency standards	ξ_1: Buildings follow 2020 standards in 2030 ξ_2: Buildings follow 2025 standards in 2030
θ, Operation schedules	θ_1: Buildings follow Chinese operational schedules guidelines θ_2: Buildings follow US operational schedules guidelines
χ, Heating electrification	χ_1: Heating is provided by low efficiency electric boilers χ_2: Heating is provided by gas or coal boilers χ_3: Heating is provided by high efficiency electric heat pumps
R_i, Renewable penetration	R_a: Renewable capacity stays constant after 2020 (installed capacity = 394 GW) R_b: Capacity continues to grow to 2030, high potential provinces have limited additional capacity installations (1230 GW) R_c: Capacity continues to grow to 2030 for all provinces (1890 GW)

Table 27: Global parameters for the national hourly netload model

In the next Section 5.3 we will discuss the output of the netload model under a variety of global parameters. In particular, we will compare models from the base case scenario as defined by a hourly netload output of $NL_{CH}(\xi_1, \theta_1, \chi_1, R_i)$ across different renewable scenarios. In Section 5.4 we will analyze the impact emissions, and load from renewable pathways, and the effect of global load parameters on the netload hourly output.

5.3 Results

In this section we present several key statistics that show the impact of introducing renewables into the Chinese grid for the base case load scenario defined by the output of the function $L(\xi_1, \theta_1, \chi_1)$.

5.3.1 Netload statistics

In Table 28 we show seven different netload statistics across the three renewable scenarios.

Renewable	Statistics						
	Demand_{NL} (TWh)	Excess_{RP} (TWh)	Load factor	Netload (GW)		Ramping, $(\frac{GW}{h})$	
				Max	Min	Max	Min
R_a	6,890	-	0.73	1,082	458	159	-112
R_b	5,559	-	0.60	1,065	90	215	-121
R_c	4,443	3.2	0.50	1,023	-150	242	-144

Table 28: Netload statistics for the base case load scenario $L(\xi_1, \theta_1, \chi_1)$ for the three different renewable penetration scenarios.

Demand_{NL} is defined as the sum of the hourly netload across all hours when netload is positive. Excess_{RP} is defined as the sum of the renewable production across all hours of the year when $RP > L$.

As Table 28 shows, netload under scenario R_a, $NL(\xi_1, \theta_1, \chi_1, R_a)$, has a total demand not met by renewables of about 6,900 TWh. The load factor of this yearly netload is 0.73. The maximum peak load reaches 1080 GW, while the lowest drops to 460 GW. The highest ramping up rate between any two hours of the year is about 160 $\frac{GW}{h}$, while the highest ramping down rate is -112 $\frac{GW}{h}$. As renewable capacity increases, so would the renewable production. Therefore, we can see in Table 28 that the load not met by renewables drops to about 5,500 TWh under renewable scenario R_b. Furthermore, the load factor sees a reduction to 0.6. Peak netload does not change by as much but lowest netload decreases to about 90 GW. Both ramping up and down rates increase in their magnitude reaching 215, and -121 $\frac{GW}{h}$. Under our most aggressive renewable penetration scenario, R_c, we continue to see decreases in the load not met by renewables down to about 4,500 TWh. With total installed capacities in the country surpassing 760, and 1,100 GW of solar PV and wind, respectively, some hours of the year see more renewable production than actual load. In contrast with the other two renewable scenarios, under R_c we see renewable excess production of about 3 TWh. Since, as with the other two renewable scenarios, the peak netload does not change dramatically, while the lowest netload drops below zero and down to -150 GW, the load factor sees a further decrease to 0.50. Ramping continues the trend up as ramping up and down rates increase to 240 and -140 $\frac{GW}{h}$ at the extreme.

5.3.2 Statistics variation and renewable scenarios

Overall, we see a significant change in load not met by renewables, load factor, minimum netload and highest ramping up rates of the year as penetration of renewables increases in the Chinese grid. Table 29 shows the percent change in key load characteristics between the original load defined by $L(\xi_1, \theta_1, \chi_1)$ and the netload associated with the three different renewable scenarios.

Renewable	Statistics					
	ΔDemand$_{NL}$	ΔLoad factor	ΔNetload		ΔRamping	
			Max	Min	Max	Min
R_a	-8.2	-5.5	-2.9	-19.4	-0.6	0.5
R_b	-25.9	-22.5	-4.4	-84.1	34.5	7.8
R_c	-40.8	-35.6	-8.2	-126.4	51.0	28.5

Table 29: Netload statistics change from base case load $L(\xi_1, \theta_1, \chi_1)$, for the three different renewable penetration scenarios, in percentage terms

With renewable installed capacity to levels described by the renewable scenario R_a load demand, ΔDemand$_{NL}$, falls by about 8% while load factor decreases by about 5.5%. While netload maximum and minimum drop by about 3 and 19% respectively. Ramping rates stay relatively stable when we compare the load and netload associated with renewable scenario R_a.

As the installed capacity increases to levels described in renewable scenario R_b total demand not met by renewables decreases to almost -26%, both peak and lowest netload decrease by 4.4 and 84 % respectively. Load factor sees a more dramatic decrease than with the renewable scenario R_a, decreasing 22.5 percent. On the other hand, ramping up and down rates, both, increase by 34 and 8% respectively when compared to rates in the base case load.

Finally, as installation capacities reach those of renewable scenario R_c demand not met by renewables and load factor both fall by 40 and 36 % respectively. Peak and lowest netload also fall by 8 and 126% respectively. We see decrease larger than 100% in lowest netload in the year because with almost 2,000 GW of combined solar and wind capacity installed, there are hours of the year that have renewable production that exceeds the base case load. On the other hand, just like under scenario R_b, both maximum ramping up and down rates increase by 51 and 29 % respectively. Ramping down sees a significant increase in particular.

5.3.3 Average daily netload curves

From the netload statistics in Table 28 is not possible to see what drives the sharp decrease in load factor as the renewables installed capacity increases. One way to understand both the decrease in load factor and the increase in ramping rates is by

plotting what the average daily load looks like as renewable penetration increases against the basecase load scenario.

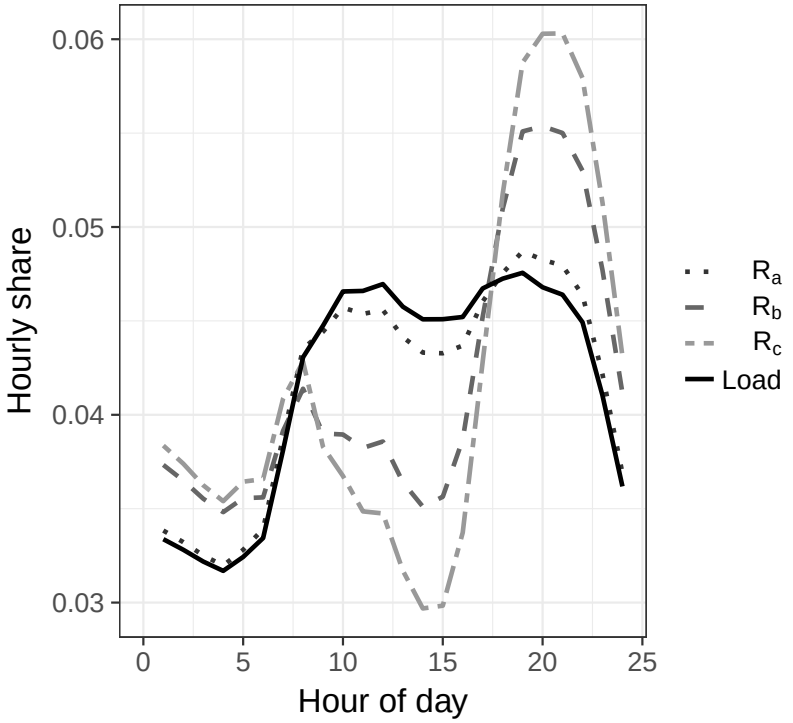

Figure 10: Hourly shares of yearly national total case case load and netload for the three renewable penetration scenarios

Figure 10 shows a comparison of the average hourly share between the base case load, shown in a black solid line, and the three different netload under different renewable scenarios, shown in dashed and dotted gray lines. As the installed renewable capacity increases, we see that there is an increasingly large dip in netload between 10 am and 3 pm in comparison with the original base case load. In the R_c renewable case, on average, the hours between 10 am and 3 pm consume less electricity than the early hours of the day when load is at a minimum. This implies that large amounts of renewables produce electricity at around these times. By increasing the relative distance between the average daily peak and the average load of the day, the load factor starts to decrease as the installed renewable capacity increases. On the other hand, the evening peak of load not met by renewables moves later in the day as the production from solar decreases. As we can see from Figure 10, on average, this change increases the need for ramping up flexibility between 3 and 8 pm. By the same process, ramping down rates, on average, increase when solar production ramps up around 8 am.

5.3.4 Netload duration curves

Another way to understand the effects of renewable integration into the grid is by visualizing the effects on the load duration curve associated with different netload scenarios. Figure 11 shows a snapshot of the sorted lowest and highest 100 load hours of 2030 for the original base case load scenario and the associated netload from the three different renewable installed capacity scenarios.

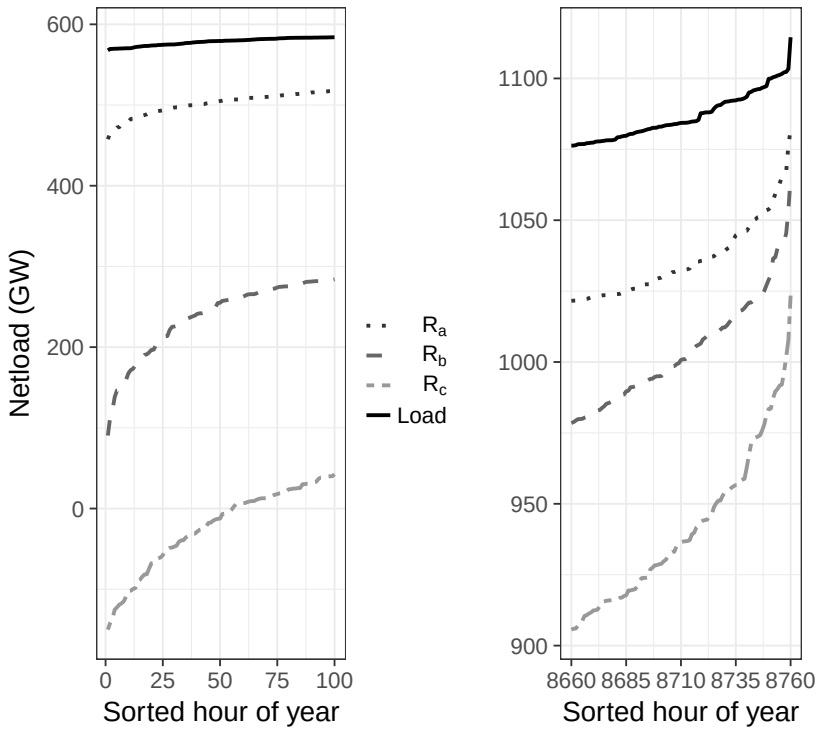

Figure 11: Load duration curve details on the lowest and highest 1% of hours in the year of base case load and netload for the three renewable penetration scenarios in 2030.

On the left panel of Figure 11 we show the lowest 100 hours of netload in 2030 under different renewable scenarios. With hour 1 as the lowest of the year, we can see how the increasing installed renewable capacity pushes the lowest netload hours from just below 600 GW to below 500, 100, and below zero GW for renewable penetration scenarios R_a, R_b, and R_c, respectively. When compared to the base case load scenario, all netload scenarios show a greater disparity between the lowest netload hour (hour = 1) than the hundredth lowest hour with only about fifty hours of negative netload for the most aggressive renewable scenario (R_c).

On the right panel of Figure 11 we show the highest 100 hours of netload in 2030 under different renewable scenarios. With hour 8760 as the highest of the year, we can see how the increasing installed renewable capacity decreases the highest netload

hours from just above 1,100 GW to about 1,025 GW under R_c renewable scenario. In contrast with the lowest hour of the year, renewable production does not have as great an impact on decreasing system peak load. While the maximum difference at the peak load hour between load and netload scenarios is about 90 GW, the maximum difference between the lowest load and netload hour is over 700 GW.

5.3.5 Ramping duration curves

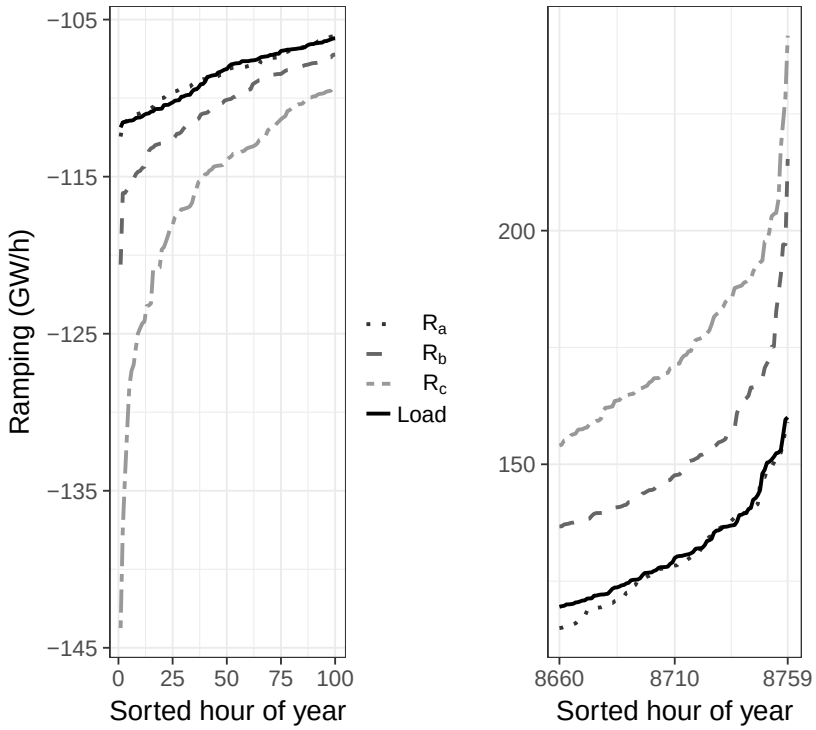

Figure 12: Load duration-type curve details on the lowest and highest 1% of hours in the year of base case load and netload ramping for the three renewable penetration scenarios in 2030.

Increasing renewable production also lead to increasing rates in the ramping up and down rates on an hour to hour basis. Figure 12 shows the sorted ramping hours for the base case load scenario and the netload for the three different renewable scenarios.

On the left panel we can see a comparison among the hundred largest hour-to-hour ramping down rates for the load and netload scenarios. Hour 1 shows the highest down ramping rate in the system. The impact of the R_a renewable scenario on ramping in comparison to the base case load scenario seems negligible in comparison to the impact from the other two renewable scenarios. With renewable scenario R_b the highest down ramping rate increases by about 10 GW per hour, while with the most aggressive scenario R_c, the new largest down ramping rate is almost 35 GW per hour larger. In

addition, the hours when down ramping is larger (more negative) for netload scenarios R_b and R_c than the largest down ramping of the original base case load scenario is 25 and 75 hours of the year respectively. What this translates to is to a system that has larger swings, and where larger swings are more recurrent.

On the right panel of Figure 12 we can see the comparison among the hundred largest hour-to-hour ramping up rates for the load and netload scenarios. Hour 8759 shows the highest ramping up rate in the system. As with the down ramping rates, the impact of the R_a renewable scenario on ramping in comparison to the base case load scenario seems negligible in comparison to the impact from the other two renewable scenarios. With renewable scenario R_b, the highest up ramping rate increases by over 50 GW per hour, while with the most aggressive scenario R_c, the new largest down ramping rate is almost 80 GW per hour larger. In addition, the hours when up ramping is larger for netload scenarios R_b and R_c than the largest up ramping of the original base case load scenario is about 25 and 80 hours of the year respectively.

With increasing installed renewable capacity in the system, there are larger hour-to-hour up and down netload swings, and the occurrance of these swings increases as well.

5.3.6 Impact of renewables on extreme case days

In this section we compare four 24-hour periods of the base case load and the netload associated with the three different renewable scenarios. Each 24-hour period is centered around the hour of highest and lowest netload, and highest up and down ramping for the most aggressive renewable penetration scenario. The goal of this section is to provide a visualization of the impact of renewable production on the day around the extreme netload and ramping hours of the system.

The left panel of Figure 13 shows the load and netload scenarios of the 24 hour period around 4 pm in April 25th, 2030, when netload is lowest in a system with base case load and installed renewable capacities described by renewable scenario R_c. By taking the difference between base case load, represented by the solid black line, and the dashed and dotted lines representing the netload with different renewable scenarios we can calculate the renewable electricity production at a given hour. At 4 pm on that day, renewable production almost reaches 1 TWh exceeding the required load and therefore going negative for the renewable scenario R_c. For this scenario, renewable production exceeds load between 11 am and 6 pm. With less installed capacity, there is no overproduction from renewables. Nevertheless, under renewable scenario R_b the daily load shape still retains its overall morphed shape with the lowest netload (around 250 GW) occuring at around 4 pm, and rising to approximately 600 GW around 10 pm. Under these two scenarios, ramping between 4 and 10 pm is about 400 and 550 GW over that period for the R_b and R_c cases respectively.

The right panel of Figure 13 shows the load and netload scenarios of the 24 hour period around 8 pm of August 28th, 2030, when netload is at its highest point in a system with base case load and installed renewable capacities described by renewable

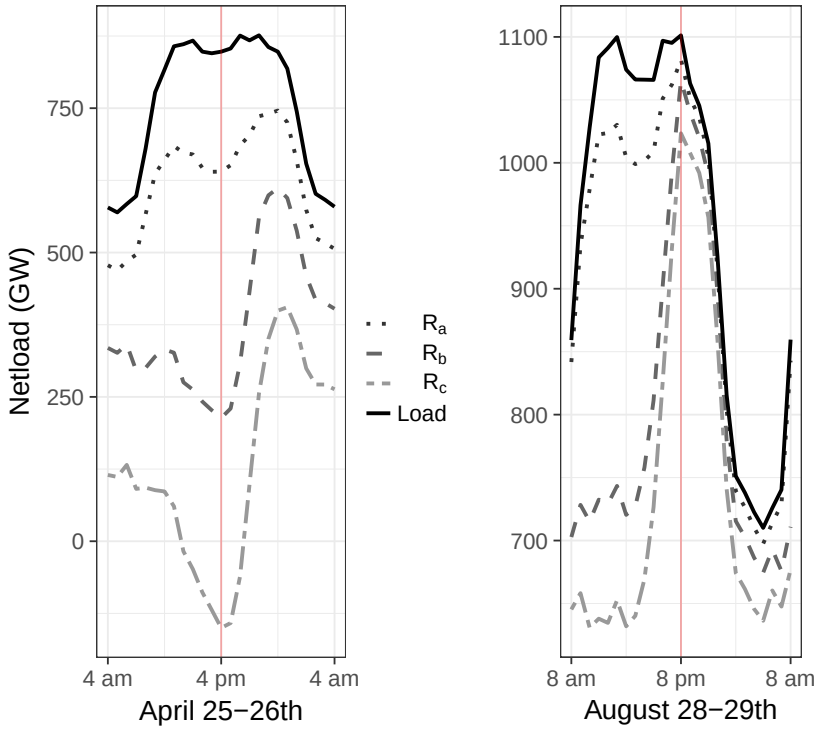

Figure 13: Renewable production impact on the 24 hours around the lowest and highest netload hour for the netload model $NL(\xi_1, \theta_1, \chi_1, R_c)$ for load and netload across the three renewable penetration scenarios.

scenario R_c. At 8 pm on that day, renewable production is less than 100 GWh for the most aggressive renewable installation scenario, R_c, and less than 50 GWh for the other two scenarios. Since at that time, solar production will probably be close to zero, having a small renewables production means that wind production around 8 pm is low across the country, or that the provinces with the biggest installation capacities have very low production. Although the renewable production before 8 pm on that day seems to be significant for scenarios R_b and R_c, renewable production has little impact on the hour of the peak load. Due to the decrease in production from solar after 2 pm, and the lack of production from wind, we see ramping rates between 2 and 8 pm increase to over 300 and 500 GW in that six hour window for the R_b and R_c renewable scenario cases, respectively.

We can do a similar analysis for the 24 hour periods around the highest down and up ramping hours of the year. The left panel of Figure 14 shows the load and netload scenarios of the 24 hour period around 8 am in November 24th, 2030, when hour-to-hour ramping down is highest in a system with base case load and installed renewable capacities described by renewable scenario R_c. This rapid decrease in netload coincides with the beginning of the diurnal cycle of solar production for that day. Between 8 and 9 am of that day, renewables production increases faster than load by 144 GW. Such a large decrease in netload surpasses the ramping maximum of 112 GW per hour decrease in the original base case load scenario (not shown). Assuming that system operators are ready to meet a 112 GW capacity shed in the system with no intermittent renewables, there is still a 32 GW decrease in that that needs to be met across the system if renewables penetration reaches the levels described in renewable scenario R_c. As the installed capacity decreases, the required hour-to-hour ramping down rate at that hour decreases to less than 100 GW for the less aggressive R_b scenario. For a moderate renewable penetration scenario as described by R_a netload is not as affected at that hour and follows the upward trend of the original base case load.

The right panel of Figure 14 shows the load and netload scenarios of the 24 hour period around 6 pm in March 24th, 2030, when hour-to-hour ramping up is highest in a system with base case load and installed renewable capacities described by renewable scenario R_c. This rapid increase in netload coincides with the end of the diurnal cycle of solar production for that day. Between 6 and 7 pm of that day, renewables production decreases while load increases creating a hour-to-hour ramping of approximately 215 and 240 GW in that period. Such a large increase in netload surpasses the ramping maximum of 160 GW per hour increase in the original base case load scenario (not shown). Assuming that system operators are ready to meet a 160 GW capacity addition in a given hour in the system with no intermittent renewables, there is still a 55 and 80 GW increase that needs to be met across the system if renewables penetration reaches the levels described in renewable scenarios R_b and R_c respectively. As the installed capacity decreases, the required hour-to-hour ramping up at that hour decreases.

The maximum ramping up and down rates in the system occur on the edges of the diurnal solar production cycles and are therefore a new feature of a system with high penetration of solar PV, and to a lesser extent, wind capacity.

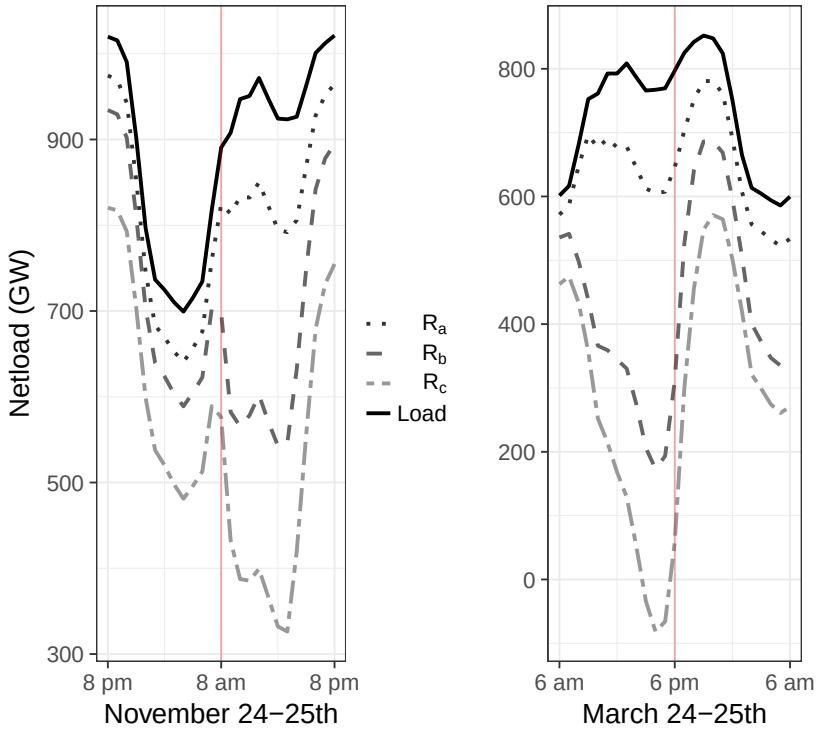

Figure 14: Renewable production impact on the 24 hours around the lowest and highest netload ramping hour for the netload model $NL(\xi_1, \theta_1, \chi_1, R_c)$ for load and netload across the three renewable penetration scenarios.

5.4 Discussion

5.4.1 Increased flexibility requirements

As we saw in Table 29, the introduction of intermittent renewables into the Chinese grid according to the scenarios discussed in Chapter 4 has an impact on the effective peak and lowest load, as well as on the highest hour-to-hour up and down ramping rates in the system. Assuming that the system planners and operators have the capacity to provide peak load, and ramping up to the requirements of the base case load scenario, then the introduction of renewables facilitates or adds challenges to the effective operation of the system, depending on what metric we focus on.

Decreasing netload for the system

Across all renewable scenarios, meeting peak load is facilitated by the introduction of renewable capacity. At the most conservative end, keeping 2020 renewable capacities constant to 2030 would decrease effective peak load by about 3%. As the penetration of renewables increases, the effective peak load decreases by 4.4 and 8.2% for the R_b and R_c scenarios respectively. Despite the reduction in effective peak load, load factor decreases, as intermittent renewable production increases, by 5.5, 22.5 and 35.6% for the R_a, R_b, and R_c, respectively, when compared to the load factor of the base case load. This decrease in load factor imply that the overall average load is reduced more than the peak load.

When we add the effects of renewable production on the minimum netload we start to see that the impact from the addition of renewables on the operation of the system is more dramatic on the lower netload hours. As renewable production increases, the minimum load not met by renewables decreases dramatically. As the minimum netload requirement falls from 460 to 90 GW for the R_a and R_b scenarios respectively system operators already have a significantly different system operating conditions. With a difference between peak and minimum netload increasing for these two renewable scenarios from 600 to almost 1,000 GW, the ability to provide a minimum stable production baseline for long term contracts or for slow ramping units decreases significantly. What is more, if the renewable penetration reaches the installed capacities outlined in scenario R_c, the system might see some hours when renewable production exceeds load. Three ways on how to handle this overproduction exist for such hours. First, the renewable excess production will be curtailed. This entails losses and uncertainty to the renewable providers. Second, the excess production could be used in some ways by either shifting load to those hours, and/or by storing massive amounts of electricity in batteries. Finally, the third option system operators might have during such windows of high renewable production at the national level is to export across national boundaries to neighboring countries. At the hour of minimum netload for the R_c renewable scenario, all three options might be required, as overcapacity is equivalent to 150 GW, the size of a small neighboring country's electricity system.

Increasing ramps for the system

Hour to hour load changes increase as the installed capacity of renewable increases. For a system with a renewable capacity described by scenario R_a ramping requirements do not change significantly. Nevertheless, as capacity increases to levels described in scenarios R_b and R_c the highest hour-to-hour ramping up and down increases. As shown in Section 5.3.6 with high penetration of solar PV and wind the diurnal cycle of solar and wind become more important in changing the shape of load not met by renewables. As found in other research[83]], the number and intensity of ramping events increased as the renewables penetration increases.

Specifically in our model, a large drop in netload (coincident with increasing PV production) followed by a large increase in netload when solar production decreases increases the system ramping requirements on an almost daily basis. Furthermore, the highest ramping up rates with scenarios R_b and R_c increase by 35 and 51 % when compared to the rates required to meet load every hour. Similarly, the highest ramping down rates increase by 8 and 29 % with renewable scenarios R_b and R_c respectively. A 30-50% on an already large (160 GW per hour) ramping up rate amounts to bringing hundreds of gigawatt-sized power plants an hour. Conversely, an 8 to 29 % increase on top of a 110 GW per hour ramping down rate means shutting down tens of gigawatt-sized power plants an hour.

Figure 15 shows the maximum, and top 0.1 and 1% of up and down ramps in 2030 for the netload models $NL(\xi_1, \theta_1, \chi_1, R_{a-c})$ as a proportion of the average load. The expected increase in ramping as penetration of renewable increase in China is similar to that of other countries around the world as presented in [84]. In Figure 15 our data for the netload models $NL(\xi_1, \theta_1, \chi_1, R_{a-c})$ is shown in dots, while the estimated relationship between ramping rates and penetration for other renewable scenarios is shown as the trendlines. It's important to note that given the limits in the number of our renewable scenarios, the trendlines appear linear, while the ones in [84] do not.

As seen in Figure 15, as renewable penetration increases, the up ramping rates increase faster than the down ramping rates. In order to integrate larger amounts of renewables, efforts to provide up ramping flexibility will be key.

5.4.2 Effect of renewable path

If we assume that a national plan points towards a renewable future that resembles the R_b renewables scenario what are the consequences of changing pathways towards a less or more aggressive renewable penetration scenario? By comparing total demand, load factor, max and minimum netload, and highest up and down ramping rates between R_a, R_c and R_b scenarios we can estimate the changing system operation challenges faced by operators under different renewable scenarios.

If the political will to build a system with higher penetration of renewables waned after reaching the 2020 capacity goals described in 4.2 then operating the system would require to prepare for a 1.6% increase in peak load, but a 400% increase in minimum

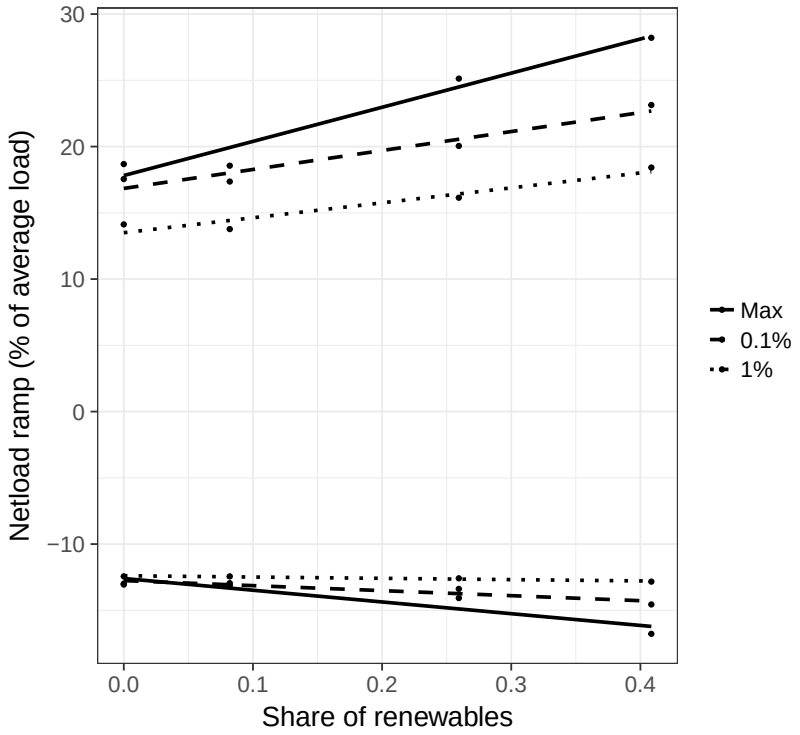

Figure 15: Extreme hourly ramps in netload with increasing renewables penetration level in China. Maximum ramp values as well as positive and negative ramps presenting 0.1% and 1% of exceedence level are shown.

Statistic	Renewable scenario comparison	
	$R_b \rightarrow R_a$	$R_b \rightarrow R_c$
ΔDemand$_{NL}$	24	-20
ΔLoad factor	22	-17
ΔNetload, max	1.6	-3.9
ΔNetload, min	406	-266
ΔRamping, up	-26	12
ΔRamping, down	-7	19

Table 30: Netload statistics comparison between renewable scenario R_b and the other two renewable scenarios, holding base case load constant, in percentage terms

netload. This in turn would improve the load factor by 22%. Maximum ramping requirements would experience decreases of 26 and 7% for up and down hour-to-hour load changes, making it that much easier to maintain balance in demand and supply. The cost of operating a system with these relaxed constraints is a total increase of 24% (about 1,300 TWh) in electricity demand that needs to be met by other sources. The impact on emissions of such a scenario depends on the assumed carbon intensity of electricity from other sources in 2030 but it's likely to be significant.

A more ambitious shift towards renewable electricity as the foundation of the Chinese grid modeled as a shift from scenario R_b to R_c would reduce the electricity demand that needs to be met by other sources by 20%. Less electricity demand unmet means lower total emissions from the power system overall. Nevertheless, this decrease in potentially carbon-intensive electricity demand comes with overall higher operational constraints. Although peak netload decreases by about 4%, hours when renewable production exceeds load start occurring and the overall decrease in minimum netload reaches 266%. Furthermore, as discussed in Section 5.4.1, the diurnal cycle of renewable production on scale starts increase ramping up and down rates by 12 and 19% respectively.

From these comparisons it's reasonable to conclude that increasing renewable participation in the system effectively requires not only improved capabilities of ramping provision, but demand response, storage or efficient ways to export electricity at times of high production. These decision are especially important when deciding on the market design of ramping products or how to improve flexibility from thermal plants [83, 85]. In Chapter 6 we present a working model for regulation provision using demand management at the building level. In Chapter 7 we will present a case of the potential impact of demand response in alleviating these increased flexibility constraints.

Impact on emissions and operation costs

From a carbon mitigation perspective, reducing netload ideally reduces the need to build and operate thermal power plants. Ideally, the introduction of renewables would displace production from inefficient thermal plants. Without better knowledge of the specific generation portfolio expected in 2030 we estimate that reduced needed production will come mostly from coal power plants.

Using a 2010 study by the National Energy Technology Laboratory (NETL) [1] which estimated costs and performance for different fossil energy plants we can provide an estimate for the carbon emissions and financial savings for the netload reduction across the three renewable scenarios using the emissions and cost of electricity (COE) per megawatt-hour in Table 31.

If we assume that the displaced thermal production is composed of 90% pulverized coal (PC) supercritical boilers, and 10% natural gas combined cycle (NGCC) plants we can then estimate the system savings in terms of both carbon and dollars, for a given renewable penetration scenario.

Under the given assumptions, a future installed capacity outlined by renewable

Power plant type	CO_2 emissions (tons per MWh)	COE ($ per MWh)
IGCC	0.78	76.3
PC, Supercritical	0.80	58.9
NGCC	0.37	58.9

Table 31: Power plant CO_2 emissions and COE data

Renewable Scenario	Emission savings (GTons C)	Cost savings (billions of $)
Meeting 2020 goals, R_a	0.5	36.3
Historic growth, key provinces curtailed, R_b	1.5	115
Historic growth, reduced curtailment, R_c	2.3	180

Table 32: Associated carbon emisssions and cost savings for the three different renewable scenarios

scenario R_a would reduce emissions in 2030 by 0.5 gigatons of carbon and system costs of 36.3 billion dollars. As renewable generation increases, emissions and cost savings increase. Carbon emission savings increase to 1.5 and 2.3 gigatons of carbon for a renewable installed capacity outlined by renewables scenarios R_b and R_c, respectively. Operation and maintenance savings increase to 115 and 180 billion dollars for those two renewable scenarios, respectively. Assuming an optimistic carbon emission rate of 12 gigatons of carbon in 2030, then under the three renewable scenarios, carbon emissions could be reduced by 4, 12.5 and 19.2%.

If renewable integration was not given priority in system operation, or if the displaced thermal plants differed significantly from our stated assumptions, total emission and cost savings would also differ accordingly.

Negative load

In hours of very low netload, or at the extreme, hours when renewable production surpasses load, under current system flexibility circumstances, renewable production most likely will be curtailed [86]. The discussion about the benefits of raising the minimum netload in order to increase the role renewables play on the provision of electricity, should include a more nuanced analysis on who benefits and who loses when the minimum is increased.

From the point of view of renewable electricity suppliers, increasing the lowest netload of the system might reduce the need to have flexible provision for baseload hours, by effectively increasing the power that can be met from baseload (usually less flexible but cheaper) power plants. The second way that increasing the netload of the system with demand response facilitates the integration of renewables is by reducing the need for high capacity storage in hours of over production.

Nevertheless, the benefits and costs of a higher baseload capacity depend on the power plants meeting such capacity. If baseload is met with power production from coal power plants, then the impact on emissions by letting more coal plants operate is significant. If in 2030 the system baseload is met with a combination of nuclear and hydro then there is no significant impact on emissions.

5.4.3 Effect of parameters

As discussed in Chapter 3, the hourly load model is a function of three global parameters that affect the simulated commercial model 2. In this section we study the effect of changes in parameters on the system netload compared against renewable scenario R_b. In Table 33 we show the effect of changing a parameter at a time across the three parameters (efficiency standards adoption, operating schedule selection, and heating electrification, ξ, θ, and χ, respectively) on the different netload statistics for the base case load scenario $L(\xi_1, \theta_1, \chi_1)$. Parameters and their respective values are described in Table 27 of this chapter.

Statistic	Change in parameter			
	$\Delta\xi$	$\Delta\theta$	$\chi_1 \to \chi_2$	$\chi_1 \to \chi_3$
ΔDemand$_{NL}$	-0.6	2.2	-2.7	-1.8
ΔLoad factor	0.2	-0.5	-2.5	-1.7
ΔNetload, peak	-0.8	2.7	-0.2	-0.1
ΔNetload, min	-1.8	26.0	-13.1	-8.7
ΔRamping $\uparrow$, max	-0.1	-4.8	0.3	0.2
ΔRamping $\downarrow$, max	-0.8	16.4	-1.9	-2.9

Table 33: Netload statistics effect of change in load parameters, holding renewable scenario R_b constant, in percentage terms

Improving the efficiency standards of the commercial sector $\xi_1 \to \xi_2$ has a small effect on the overall characteristics of the netload under scenario R_b. As it is expected, improving efficiency reduces the total demand not met by renewables by 0.6% and improves load factor by 0.2%. Peak netload, and ramping rates are decreased by less than 1% each as the commercial sector becomes more efficient. Minimum netload decreases by almost 2% as efficiency gains reduce overall commercial sector consumption.

Operating the buildings as recommended by the prototype US buildings $\theta_1 \to \theta_2$ has a larger effect on netload than changing efficiency standards in our model. Total demand increases by 2.2% while load factor decreases by 0.5%. Both peak and minimum netload increase by 2.7 and 26% respectively. The highest ramping up rate see a decrease of almost 5% while the highest ramping down rate increases by over 16%

Finally, if heating in the commercial building is de-electrified from a high-efficiency electric boiler to a equally high-efficiency gas boiler we see decreases in total electricity consumed, load factor, peak and minimum netload of 2.7, 2.5, 0.2 and 13.1%

respectively. Highest ramping rates up are increased by 0.3%, while ramping down is decreased by 1.9%. If heating provision in commercial buildings stay electric but becomes significantly more efficient, then the changes when compared to the load case scenario become smaller with total demand, load factor, maximum and minimun net-load decreasing by 1.8, 1.7, 0.1, and 8.7% respectively. Maximum ramping down rate decreases by 2.9%, which is a larger decrease than under the no electrification scenario.

5.5 Conclusion

China has ambitious goals for the role of solar and wind renewable generation in their grid. The introduction of renewables into the Chinese grid provides important opportunities for carbon emission and cost savings but also poses significant impacts on system operation. In particular, we studied the impacts on four netload cases: high and low netload, and down and up ramping hours. We found that peak netload is reduced by a small margin, while netload at the lowest hours is significantly decreased as renewable penetration increases. Both down and up ramping rates are increased in systems with large penetration of renewables (shown by renewable scenarios R_b, and R_c) but not changed significantly under less aggressive penetration scenarios (R_a). Large increases in renewable shares in the Chinese electricity system will require increase focus on flexibility provision in planning and operation. In the following Chapters we build a case for the provision of such flexibility by managing demand of existing infrastructure. In Chapter 6 we develop and test a building control model to provide regulation-like services to the grid. In Chapter 7 we present a study on the impacts of managing load at the commercial sector level in China to provide system flexibility under different commercial model parameter and renewable penetration scenarios.

Chapter 6

A case for building-level demand response for regulation provision

6.1 Introduction

With increasing penetration of renewable electricity into the grid, supply forecast error and flexibility requirements are growing rapidly[81, 87]. In the United States, short-term forecast error is currently managed by using ancillary services, such as regulation, and sub-hourly generator dispatch. Fast-ramping conventional power plants, such as gas turbines, currently dominate the provision of ancillary services. Nevertheless, development of communication and control strategies is creating opportunities for electric loads to participate in demand side management programs to help balance the grid [13, 51]. Aggregations of electric loads can offset forecast error by shifting the timing of electricity use relative to an uncontrolled baseline[88]. Similarly, controlling a HVAC system in a building can provide ancillary services[89].

DR control strategies should be designed to avoid impacting mechanical wear or equipment warranties. Interviews with application engineers with major chiller and fan manufacturers have indicated that frequent adjustment of chiller and fan capacity should have no negative effect upon variable speed equipment[54]. In contrast, their primary concern is control stability. Nevertheless full variable speed cooling systems are currently mostly limited to large chiller and air-handling unit systems. Multi-stage direct expansion units (currently common) could be negatively affected by excessive cycling, since they would actually turn compressors on and off without regard for their current state.

This chapter investigates whether air-based cooling systems with continuously controllable cooling output can be used effectively to balance positive and negative forecast errors in power systems (either in load or renewable generation capacity) using a model predictive control approach. Previous research has been done on MPC systems in buildings [90, 91], but they have mostly focused on improving building efficiency. The specific question to be answered is whether cooling system power can be managed

to provide high quality power signal tracking without loss in comfort for occupants. The building and HVAC models are described in the following section. Then, the linear system model developed to test system performance under control is presented and the power tracking and thermal comfort performance for the different target signals are studied and analyzed. Finally the last two sections provide an analysis for climate applicability in the United States and concluding remarks respectively.

6.2 Model Description

A simplified building and HVAC system model incorporating first and second order transfer functions to approximate VAV system dynamics, based on a previous methodology by Underwood [92], was developed. Several simplifying assumptions are made. First, internal and external loads are constant during the simulation time frame. Second, time dependent model variables, such as temperature and airflow rates, depict deviations from an baseline value and not the absolute values of such state. Third, the non-linear relationship between room airflow and temperature is reduced to a first-order approximation. Fourth, room temperatures are perfectly uniform throughout the rooms. Fifth, cooling demand is only a function of sensible load, and coil dynamic behavior uses an average of wet and dry conditions. Finally, each of the rooms is in cooling mode upon disturbance and room reheat is ignored as the heat source is usually not electricity.

Working under these assumptions, models for the building walls, rooms, and cooling and fan systems are presented in the following section.

6.2.1 Wall Model

Each external wall is modeled using three layers: gypsum, insulation and brick.The three materials are characterized by their respective layer and thermal properties described in Table 34. The heat transfer through the first layer of the walls, gypsum, is depicted in Fig. 16 below with a two layer model of each wall component.

Performing an energy balance on the system represented in Fig. 16, the deviation in the gypsum layer temperature can be described by the coupled differential Eq. (6.2.1) and (6.2.2) below.

$$l_g \rho_g c_{p,g} \frac{d\theta_g}{dt} = u_{g,i}(\theta_r - \theta_g) - u_g(\theta_g - \theta_{g,o}) \tag{6.2.1}$$

$$l_g \rho_g c_{p,g} \frac{d\theta_{g,o}}{dt} = u_g(\theta_g - \theta_{g,o}) - u_{g,o}(\theta_{g,o} - \theta_{ins}) \tag{6.2.2}$$

where all parameters are defined in Table 34 above.

Taking the Laplace transform of Eq. (6.2.1) and (6.2.2), combining them and rearranging variables, the following transfer function for the temperature deviation

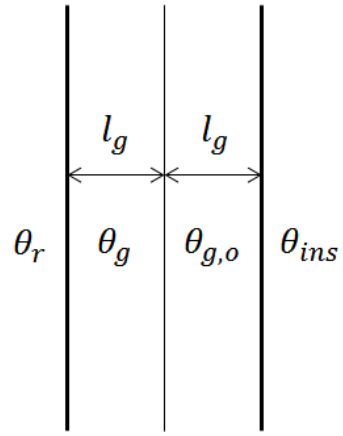

Figure 16: Two later wall model diagram

on the first layer, as a function of the temperature deviations in the room, and the temperature deviations in the insulation layer is obtained:

$$\theta_g(s) = \frac{A_g s + B_g}{C_g s^2 + D_g s + E_g}\theta_r(s) + \frac{F_g}{C_g s^2 + D_g s + E_g}\theta_{ins}(s) \tag{6.2.3}$$

where

$$A_g = l_g \rho_g c_{p,g} u_{g,i} \qquad B_g = u_g u_{g,i} + u_{g,o} u_{g,i}$$
$$C_g = (l_g \rho_g c_{p,g})^2 \qquad D_g = l_g \rho_g c_{p,g}(2u_g + u_{g,i} + u_{g,o})$$
$$E_g = u_g u_{g,i} + u_{g,o} u_{g,i} + u_g u_{g,o} \qquad F_g = u_g u_{g,o}$$

Performing the same procedure on the insulation and brick wall layers, the transfer functions depicting temperature deviations of those layers are as follows:

$$\theta_{ins}(s) = \frac{A_{ins} s + B_{ins}}{C_{ins} s^2 + D_{ins} s + E_{ins}}\theta_g(s) + \frac{F_{ins}}{C_{ins} s^2 + D_{ins} s + E_{ins}}\theta_{br}(s) \tag{6.2.4}$$

$$\theta_{br}(s) = \frac{A_{br} s + B_{br}}{C_{br} s^2 + D_{br} s + E_{br}}\theta_{ins}(s) + \frac{F_{br}}{C_{br} s^2 + D_{br} s + E_{br}}\theta_{oa}(s) \tag{6.2.5}$$

The transfer function coefficients in Eq. (6.2.4) and (6.2.5), above, are defined similarly to the coefficients in Eq. (6.2.3), but using their respective layer material thermal properties, as defined in Table 34.

6.2.2 Room Model

Four identical rooms are modeled as if they were uniform thermal masses with a VAV box supplying chilled air to each. Each room is differentiated from each other by a

Parameter	Gypsum	Insulation	Brick	Units
	$m=g$	$m=ins$	$m=br$	
l_m	0.016	0.05	0.11	m
ρ_m	595	30	1700	kg/m^3
$c_{p,m}$	1.1	1.0	0.8	kJ/kg·K
$u_{m,i}$	8.31	21.4	1.4	W/m·K
u_m	21.4	1.4	15	W/m·K
$u_{m,o}$	21.4	8.33	8.33	W/m·K

Table 34: Wall model parameters

different supply air flow rate needed to maintain steady state in the room without changes in load. Each VAV terminal box is connected to the air supply system that ultimately leads to the cooling unit. The only thermal mass in the room is assumed to be that of the air. For this reason, the model would overestimate the temperature deviations that would occur from a given disturbance. Finally, since the interior of the building is pressurized, no infiltration occurs.

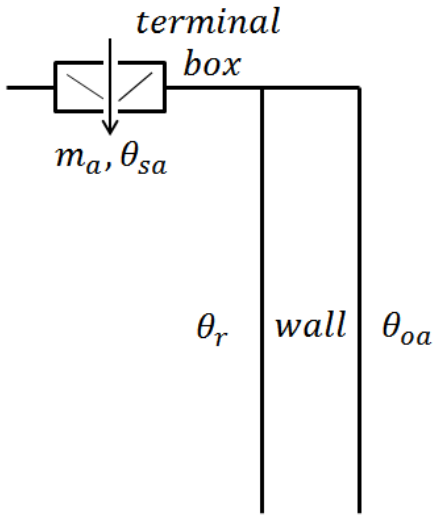

Figure 17: Side view diagram of a room

Figure 17 depicts a cross view of a room with the left depicting the inside of the building, and the right depicting the outside conditions with the middle wall separating the two different thermal masses. The temperature deviation upon a disturbance in room i, can be derived from the simplified differential Eq. (6.2.6) below

Parameter	Value	Units
V_r	240	m^3
ρ	1.2	kg/m^3
c_{pa}	1.0	kJ/kg-K
ΣUA	0.2	W/K
$\theta_{sa,ss}$	12.7	C°
$\theta_{r,ss}$	23.8	C°
$m_{a,1,ss}$	0.32	m^3/s
$m_{a,2,ss}$	0.36	m^3/s
$m_{a,3,ss}$	0.41	m^3/s
$m_{a,4,ss}$	0.43	m^3/s

Table 35: Room model parameters

$$V_r \rho c_{pa} \frac{d\theta_{r,i}}{dt} = q_{plant,i} - \Sigma(UA)(\theta_{r,i} - \theta_{g,i}) \tag{6.2.6}$$

where all parameters are defined in Table 35 and $q_{plant,i}$, defined in Eq. (6.2.7) below, is the linear approximation in cooling load deviation supplied by the VAV box in the room.

$$q_{plant,i} \approx c_{pa}(\theta_{sa,ss} - \theta_{r,ss}) m_{a,i} + m_{a,i,ss} c_{pa} (\theta_{sa} - \theta_{r,i}) \tag{6.2.7}$$

Substituting Eq. (6.2.7) into Eq. (6.2.6), rearranging variables, and expressing in the Laplace domain, a transfer function (6.2.8) that relates $\theta_{r,i}$ to $m_{a,i}$, θ_{sa} and $\theta_{g,i}$ in room i is obtained.

$$\theta_{r,i}(s) = \frac{G_{m_a,i}}{(\tau_{r,i}s + 1)} m_{a,i}(s) + \frac{G_{\theta_{sa,i}}}{(\tau_{r,i}s + 1)} \theta_{sa}(s) + \frac{G_{\theta_{g,i}}}{(\tau_{r,i}s + 1)} \theta_g(s) \tag{6.2.8}$$

where

$$\tau_{r,i} = \frac{V_r \rho c_{pa}}{m_{a,ss,i} c_{pa} + \Sigma(UA)} \qquad G_{m_a,i} = \frac{c_{pa}(\theta_{sa,ss} - \theta_{r,ss})}{m_{a,ss,i} c_{pa} + \Sigma(UA)}$$

$$G_{\theta_{sa},i} = \frac{m_{a,ss,i} c_{pa}}{m_{a,ss,i} c_{pa} + \Sigma(UA)} \qquad G_{\theta_g,i} = \frac{\Sigma UA}{m_{a,ss,i} c_{pa} + \Sigma(UA)}$$

Combining transfer functions [6.2.3-6.2.5], describing wall heat transfers, with Eq. (6.2.8) describing room temperature into a block diagram, a block diagram for the coupled wall-room system in Fig. 18 below is obtained.

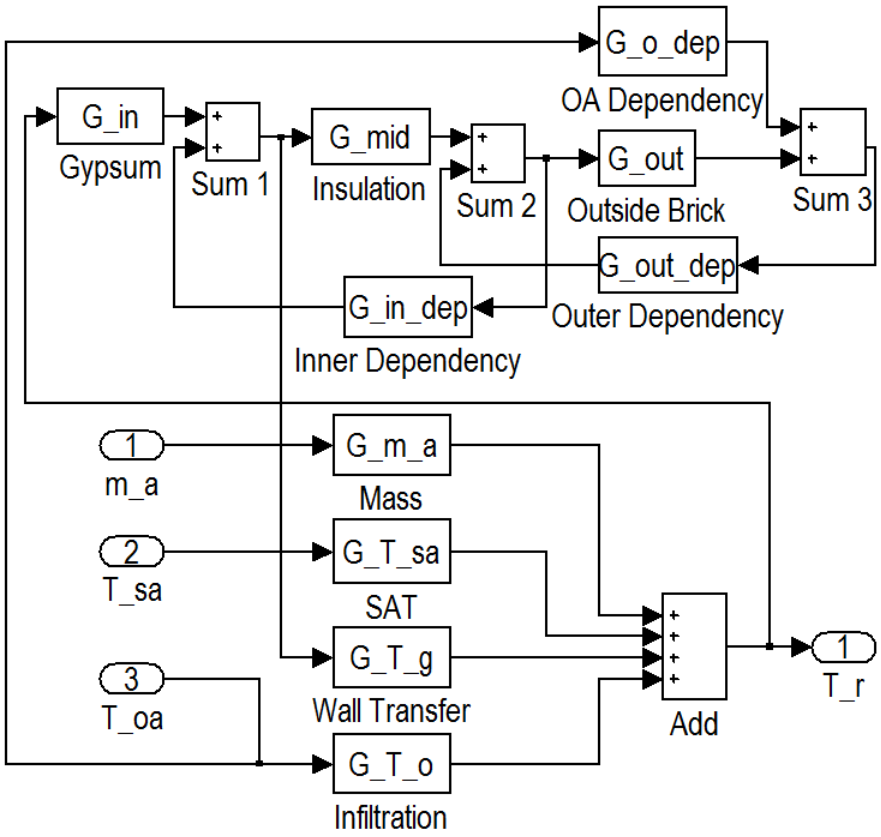

Figure 18: Block diagram for the coupled wall - air mass model

6.2.3 VAV Terminal Box Model

The VAV terminal box modulates airflow into each room via an air valve. A PI controller measures and controls airflow with K = -0.19 and I = -2.4x10^{-4}. The gains are optimized in Simulink. The PI controller uses the difference between the desired room temperature, T_{set}, and the actual room temperature, T_r, as the input signal. The control signal modifies the airflow, m_a required to correct for difference in temperatures by adjusting the valve position. We assume that from 18% to 68% open the airflow response to valve position is linear and constrained to not exceed the maximum or minimum flow rates and that it takes between 45 and 90 seconds, with constant speed, for the valve to change from fully closed to fully open, or vice versa [93, 94]. While the air valve reacts rather quickly to signal changes, thermostats usually lag by several minutes. The thermostat is approximated with a first order time lag with time constant of 2 minutes. Fig. 19 below, depicts the block diagram for the terminal box model. The 'Room' block in Fig. 19 represents the coupled wall-room model in Fig.18.

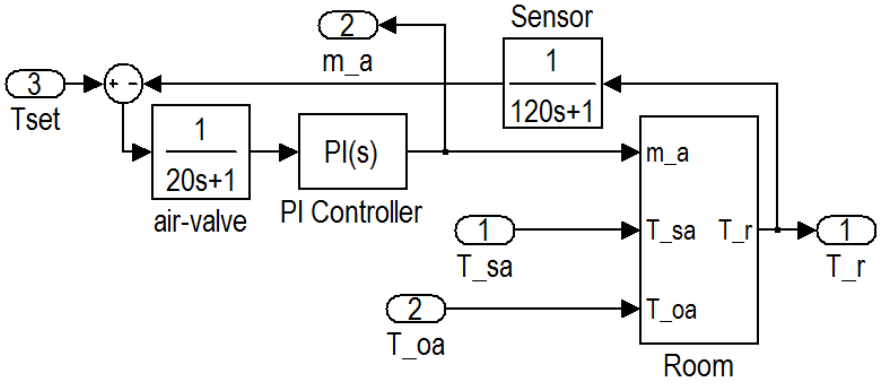

Figure 19: Block diagram for the terminal box model

6.2.4 Fan Model

The building's fan system is modeled by adding the deviations in air flow rate in each of the rooms, as in Eq. (6.2.9) and applying a first order lag with a 30-second time constant[95]. The block diagram for the building fan system is shown in Fig. 20 below.

$$m_{a,net} = \sum_{i=1}^{4} m_{a,i} \tag{6.2.9}$$

The net change in air flow rate, $m_{a,net}$, determines the change in fan power in the model. Fan power is nonlinearly related to change in airflow, however, in the model it is approximated with a piecewise affine function of $m_{a,net}$ estimated about the baseline operating point shown in Eq. (6.2.10) below.

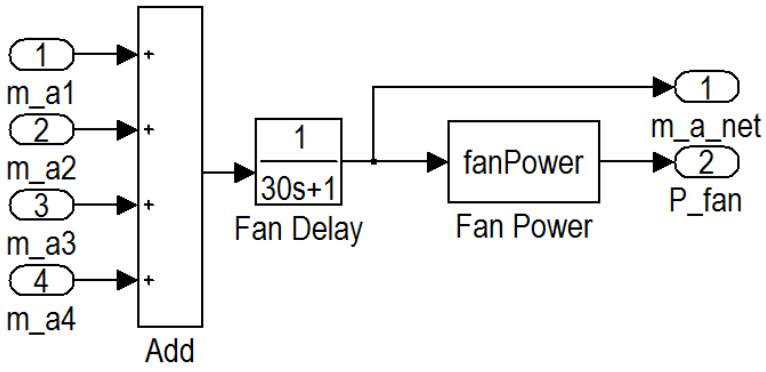

Figure 20: Block diagram for the fan model

Symbol	Value	Units
$P_{fan,max}$	3.2	kW
$P_{fan,ss}$	2.1	kW
$m_{a,max}$	1.85	kg/s
$m_{a,ss}$	1.54	kg/s

Table 36: Fan model parameters

$$P_{fan} = \begin{cases} 2.3m_{a,net} - 0.06 & \text{if } m_{a,net} \leq -0.1 \\ 3m_{a,net} + 0.01 & \text{if } -0.1 < m_{a,net} \leq 0.1 \\ 3.8m_{a,net} - 0.07 & \text{if } m_{a,net} > 0.1 \end{cases} \tag{6.2.10}$$

The MPC algorithm, explained in the next section, will use the affine power calculation, in Eq. (6.2.10), to optimize the system and to control the power consumption of the building, but in order to more rigorously assess the efficacy of the controller, the tracking error is measured against the non-linear power calculation (from[96]) of Eq. (6.2.11) below.

$$P_{fan,nl} = P_{fan,max}\left(m_{a,f}^3 - 0.46m_{a,f}^2 + 0.38m_{a,f} + 0.07\right) - P_{fan,ss} \tag{6.2.11}$$

where

$$m_{a,f} = \frac{m_{a,net} + m_{a,ss}}{m_{a,max}} \tag{6.2.12}$$

and the coefficients for steady state and maximum fan power are defined in Table 36.

Symbol	Value	Units
C_s	30	kW
$P_{cool,max}$	6.99	kW
$P_{cool,ss}$	5.63	kW
c_{pw}	4.18	J/g·K
$m_{w,max}$	0.97	kg/s
$m_{w,ss}$	0.81	kg/s
τ_c	200	s

Table 37: Cooling model parameters

6.2.5 Cooling Model

In the model, there are four main interactions that affect the air temperature supplied by the cooling unit, θ_{sa}: m_w, $m_{a,net}$, fan heat, and $OA_{\%}$.

Based on previous work by Underwood [92], a PI controller, a temperature sensor, and a cooling coil are modeled to estimate the interaction between θ_{sa} and m_w. For the PI controller, the gains K =-1.0, and I = -1.0x10^{-3} were chosen by the Simulink PI controller optimizer. We model the temperature sensor with a 20-second first order characteristic time[93, 94]. The time constant representing the response in supply temperature from a change in water flow, τ_c is assumed to be 200 seconds [95]. The air temperature change on the coil outlet takes the following form:

$$\theta_c(s) = \frac{C_s m_w(s)}{m_{w,ss} c_{pw}(\tau_c s + 1)} \tag{6.2.13}$$

The characteristic rates and constants defining the cooling system are presented in Table 37.

In order to capture the interactions between θ_{sa} and $m_{a,net}$, a transfer function with gain and time constant of 6.5 and two seconds respectively is defined. θ_{sa} is affected by the fan in proportion to fan power consumption and the air flow through it, $m_{a,net}$. Finally, $OA_{\%}$ affects θ_{sa} proportionally. The outdoor air is assumed to be 5 °C above the return air temperature in the system. All the interactions are added to provide the resulting θ_{sa} as depicted in the block diagrams in Fig. 21 below.

While θ_{sa} is a function of several variables, the model assumes that cooling power is described by a piecewise affine function of m_w, as shown in Eq. (6.2.14) below. As with fan power, the MPC algorithm will use the affine version of the cooling power calculation to optimize the system and to control the power consumption of the building.

$$P_{cool} = \begin{cases} 7.5 m_w - 0.034 & \text{if } m_w \leq 0 \\ 8.5 m_w - 0.034 & \text{if } m_w > 0 \end{cases} \tag{6.2.14}$$

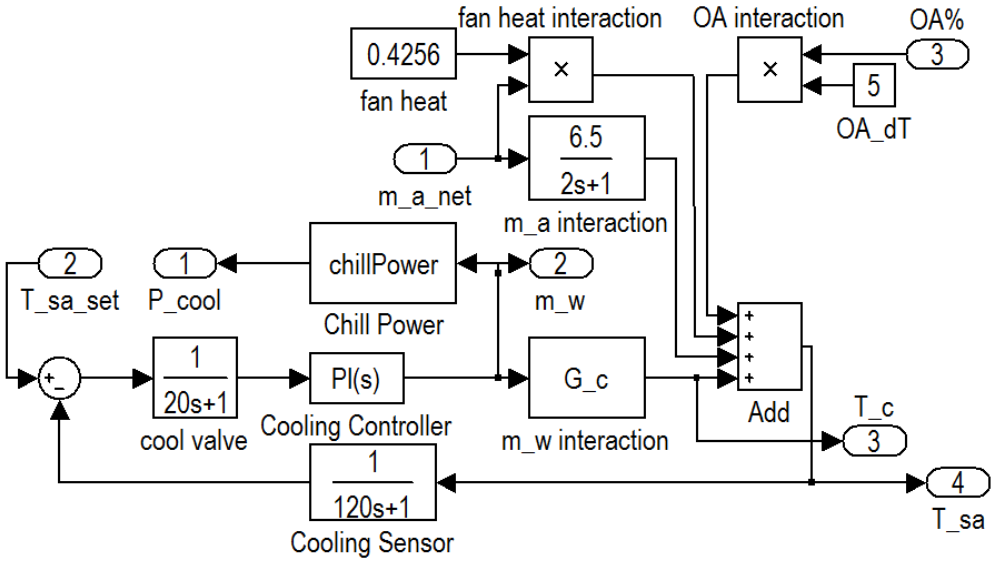

Figure 21: Block diagram for cooling model

A quadratic approximation for cooling power, shown in Eq. (6.2.15) (from[96]) is used for comparison and error measurement.

$$P_{cool,nl} = P_{cool,max}\left(0.22m_{w,f}^2 + 0.73m_{w,f} + 0.04\right) - P_{cool,ss} \tag{6.2.15}$$

where coefficients for steady state and maximum cooling power are defined in Table 37 and

$$m_{w,f} = \frac{m_w + m_{w,ss}}{m_{w,max}} \tag{6.2.16}$$

6.3 System Simulation

The model links the inputs and outputs that define the individual components described in the previous sections, and illustrated in Figs. [18-21], into a building wide system. Figure 22 illustrates how the cooling loop, the thermal zones, and the fan interact with each other in a Simulink model. In addition, it shows the input variables that to manipulate the system: four temperature setpoints describing each of the the four rooms thermostats, the cooling supply air temperature setpoint, and the percentage of outside air in the air supply.

In order to test the ability of a building to provide ancillary services, and in specific follow a target signal for power deviation, the main output of concern is system power consumption defined in Eq. (6.3.1) below.

$$P_{model} = P_{fan} + P_{cool} \tag{6.3.1}$$

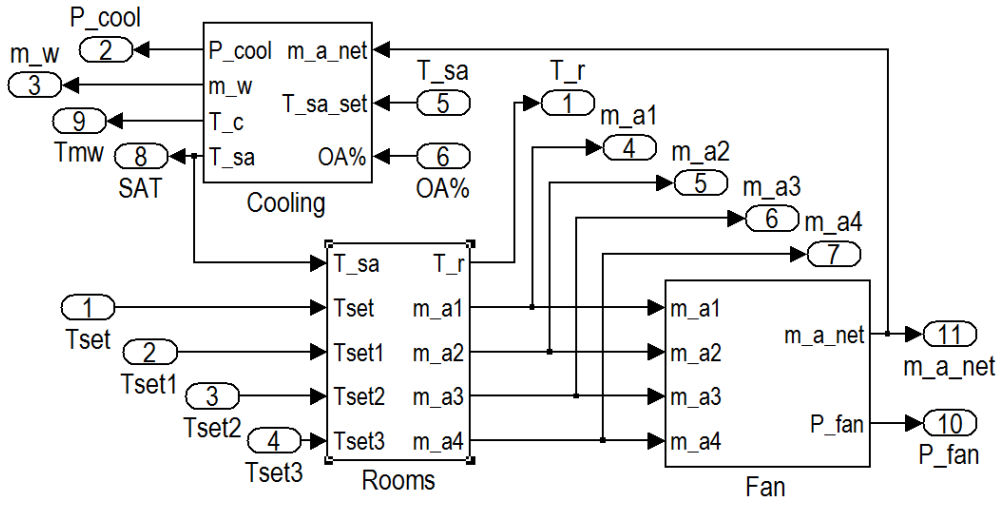

Figure 22: Block diagram for building's HVAC system

6.3.1 MPC Algorithm

A supervisory MPC algorithm to control system power by manipulating the control inputs on the combined model was implemented on MATLAB. The controller uses a state space linear model provided by the *dlinmod* command with a one-minute time step to discretize the combined block diagram system shown in Fig. 22. The linear time invariant state space model that describes the system takes the following form:

$$x_{k+1} = Ax_k + Bu_k \tag{6.3.2}$$

where $A \in \Re^{78x78}$ and $B \in \Re^{78x6}$ are built by the *dlinmod* MATLAB command.

The MPC controller decides the optimal set of inputs that minimize both tracking error between model power and target power deviations, defined in Eq. (6.3.3), and room temperature deviations.

$$\epsilon = P_{model} - P_{target} \tag{6.3.3}$$

The objective function is described in Eq. (6.3.4) below over the whole control horizon, N steps ahead. The superscript T refers to the transpose of the vector. In this implementation, the control horizon, N, equals five minutes. Increasing N results in better performance, but it assumes receiving a target signal at higher frequency, which might might not be feasible in a real implementation.

$$F = \phi_\epsilon \sum_{k=1}^{N} |\epsilon_{t+k}|_2^2 + \phi_\theta \sum_{k=1}^{N} |\theta_{t+k}|_2^2 \tag{6.3.4}$$

subject to

$$
\begin{aligned}
x_{k+1} = Ax_k + Bu_k, \text{ for } k = 1, ..., N \\
-1\,^\circ\text{C} \leq \theta < 1\,^\circ\text{C} \\
-2\,^\circ\text{C} \leq \theta_{sa} < 5\,^\circ\text{C} \\
0.068 - m_{a,i,ss} \leq m_{a,i} < 0.453 - m_{a,i,ss}, \forall i \\
0.3m_{w,k-1} - m_{w,ss} \leq m_w < m_{w,k-1} - m_{w,ss} \\
-10\% \leq OA_{\%} < 10\%
\end{aligned}
$$

Both ϵ and θ are functions of the optimization variable u_k. The subscript notation $t+k$ refers to a time k timesteps beyond timestep t given that t is the beginning of the optimization time horizon. The MPC controller will choose a set of u_k for $k = 1, ..., N$ that optimizes the cost function at each time step in the horizon. The controller only acts on the first of these input vectors updating the state of the system. It then sets up to find the optimal inputs for the next N steps.

For plants with full variable speed control, the control strategy outlined here, could be implemented using existing building energy management control system (EMCS) equipment with some parallel computing. The MPC would run in parallel locally or on the cloud, as long as the calculation runtime is shorter than the MPC step time, and then submit control setpoints to the building's EMCS for implementation.

6.4 Model Testing

The purpose of the model is to test the controllability of a building's power consumption through the implemented MPC algorithm. Controllability is tested against two different sets of power signals to be followed. The signals communicate the deviation from baseline power consumption as a percentage of the power rating of the system. The signals were chosen because they resemble actual signals used by system operators and can be applied to systems of different sizes and, therefore, potentials. For this system, the power rating = $P_{cool,max} + P_{fan,max}$

6.4.1 Zero Mean Target

The first set of random target signals tests the ability of the system to provide continuous DR to the grid that resemble load following and regulation services. The set is characterized by a zero mean trajectory within the limits on the maximum allowable deviations in power, given in percent. The limits are symmetrical, that is, the value of the maximum possible positive deviation is equal to the maximum possible negative deviation. The set of target signals studied have 10, 15, 20 and 25% limits respectively. Every five minutes a new random target power deviation within the ±limit range is set. The power trajectory ramps down or up linearly from every subsequent target point to the next.

6.4.2 Step Target

The second set of target signals tests the ability of the system to provide a sustained power deviation from baseline, resembling a traditional DR signal such as those in load shifting or load curtailing programs. The target is a step percentage change from base power consumption, held for fifty minutes. It takes five minutes to ramp up from baseline to the target and five minutes to ramp down to zero, back to baseline consumption. The ramping time was chosen arbitrarily, but longer ramping times would smooth out the effects caused by the required input signals.

6.5 Results and Discussion

Performance with Zero Mean Targets

For the set of zero mean target signals, a hundred runs with random, zero mean, target trajectories were simulated. The performance error is defined, in Eq. (6.5.1), as the difference between the target deviation and the system's power deviation, as a percentage of total power rating.

$$\epsilon_{\%} = \frac{P_{actual} - P_{target}}{P_{fan,max} + P_{cool,max}} x100\% \tag{6.5.1}$$

where

$$P_{actual} = P_{fan,nl} + P_{cool,nl} \tag{6.5.2}$$

The system power is calculated in Eq. (6.5.2) using the non-linear functions for fan and cooling loads as defined in Eq. (6.2.11) and (6.2.15) respectively. A sample of the results tracking a target signal is provided in Fig. 23 below.

Figure 24 shows the median and variability of $\epsilon_{\%}$ across different target ranges on each of the four types of runs with different defined limits. Each plot presents the resulting $\epsilon_{\%}$ from the one hundred target signals within their respective limit, as a function of the range the target requested fell in for each run.

The top and down row plots in Fig. 24 show the results for the one hundred runs with target signals within the $\pm 10\%$ and $\pm 15\%$ and $\pm 20\%$ and $\pm 25\%$ limits from left to right, respectively. The mean $\epsilon_{\%}$ is depicted by the bold black line, with the 95% confidence interval shaded.

There are several main takeaways from these results. First, $\epsilon_{\%}$ has a small positive bias, that is, it is on average above the requested target signal. Second, taking this bias into account, $\epsilon_{\%}$ is the smallest for requests that fall in the $5\% - 10\%$ range across all different limits. Third, variability in $\epsilon_{\%}$ generally increases with increasing values of requests, that is, expected variability in $\epsilon_{\%}$ is smaller for the $5\% - 10\%$ target range than for the $10\% - 15\%$. Finally, variability in $\epsilon_{\%}$ generally increases as the limits of the target signal increases. This last point is important as it implies that participants

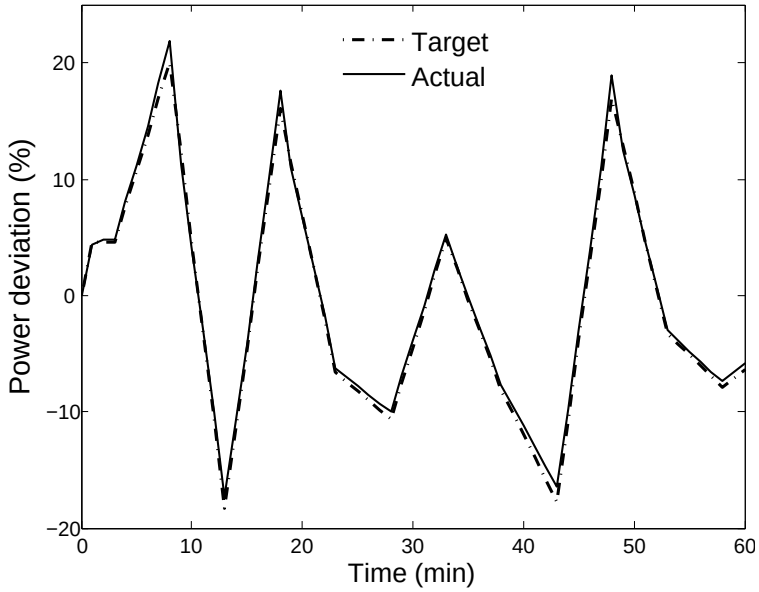

Figure 23: Tracking results for a single zero mean target trajectory within ±20% limits

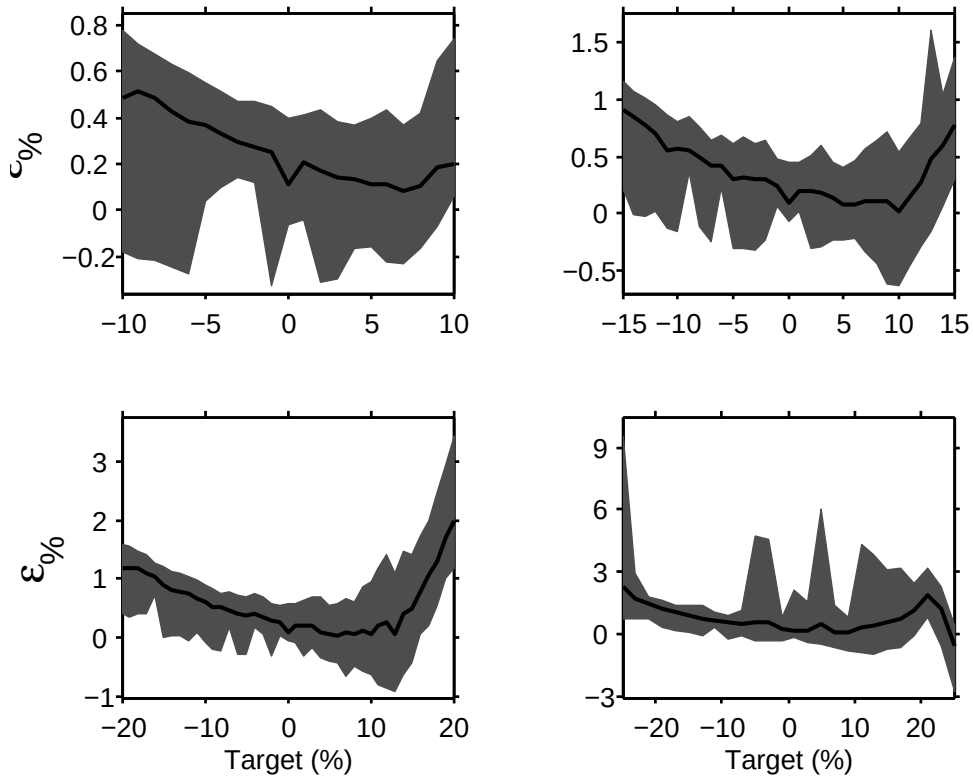

Figure 24: Error as a function of target range for all runs.

in DR programs with a higher tolerance for power deviations will, all else staying the same, provide a response to a given signal with less precision.

6.5.1 Temperature Comfort with Zero Mean Targets

Large and fast deviations from baseline temperatures are not desired as they will undermine occupants comfort. Constraints on room temperature deviation for the target trajectory above, in Fig. 23, are not violated as seen in Fig. 25 below.

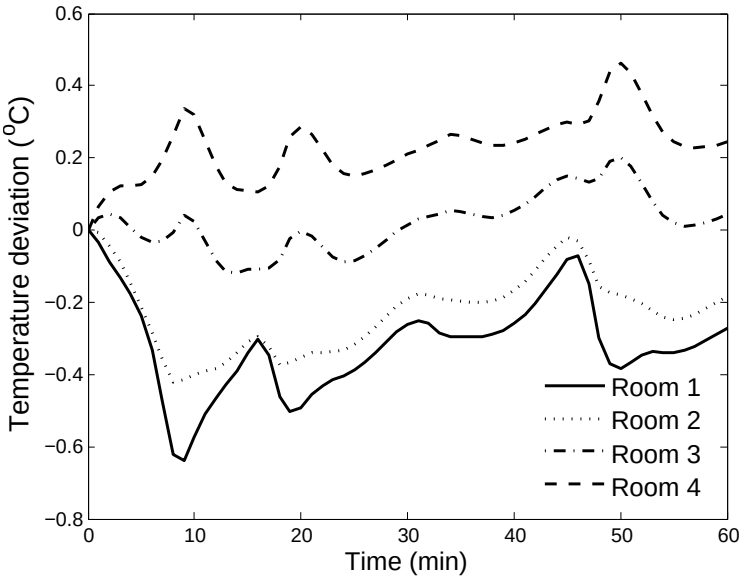

Figure 25: Temperature deviations in the building as a result of following signal shown in Figure 23

In order to compare temperature deviations associated with all target trajectories, the norm, $|\theta|_2$, and maximum value, $|\theta|_\infty$, of θ for each run is computed and recorded.

Table 38 shows the mean (and standard deviation) of $|\theta|_2$ and $|\theta|_\infty$ across all runs within each respective limits.

Limits	±10%	±15%	±20%	±25%
$\|\theta\|_2$	0.21 (0.03)	0.23 (0.04)	0.25 (0.06)	0.34 (0.13)
$\|\theta\|_\infty$	0.40 (0.07)	0.46 (0.09)	0.54 (0.14)	0.73 (0.24)

Table 38: $|\theta|_2$ and $|\theta|_\infty$ associated with zero mean target's within specified limits

There is an increasing temperature deviation from baseline as the requested target range increases. Interestingly, both the mean and standard deviations of $|\theta|_\infty$ are approximately double those of $|\theta|_2$. Assuming the air in the room is well mixed, then

the results for targets within $10, 15$, and 20% do not significantly disturb the occupants and would be therefore tolerated. Nevertheless, since both the mean and standard deviation for $|\theta|_\infty$ for targets within 25% are large enough to have a high likelihood of having temperature deviations hitting the constraints, buildings subscribing to such a large potential power deviation would probably affect occupant comfort negatively. Nevertheless, because the model considers air as the only thermal mass in the room, the estimate of the availability of power before incurring noticeable changes for the occupant would be more conservative than expected. A more detailed model is required to understand the fluid dynamics effects on occupant comfort.

6.5.2 Performance with Step Change Targets

For the set of step change target signals, multiple runs with different, negative and positive, targets were simulated. The performance error is defined in Eq. 6.5.1 above.

Figure 26 below shows four plots of target and actual power deviation model outputs with two runs on each of the plots. The top and bottom rows show the results of the runs with targets $\pm 10\%$ and $\pm 15\%$, and $\pm 20\%$ and $\pm 25\%$ from left to right respectively.

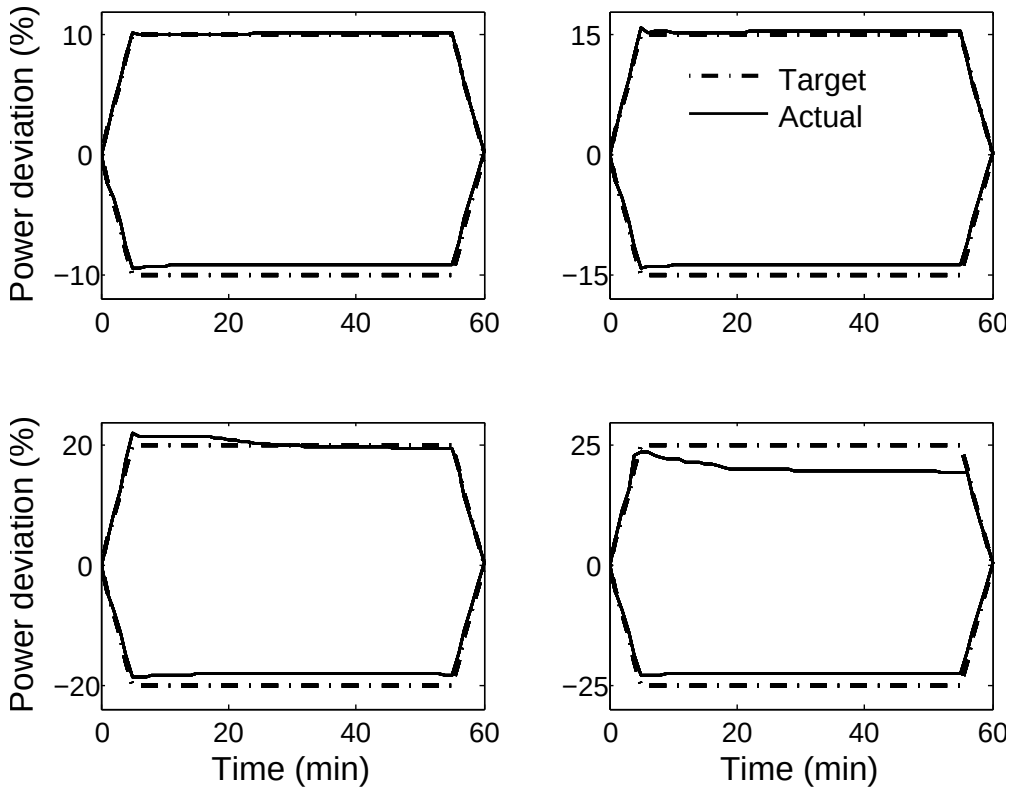

Figure 26: Sample of tracking results for step target requests

For each target signal $|\epsilon_{\%}|_2$ is calculated. Figure 27, below, shows $|\epsilon_{\%}|_2$ as a function

of the requested target. As the absolute value of the target increases so does $|\epsilon_{\%}|_2$. As in the results for the zero mean target set in Fig. 24, $|\epsilon_{\%}|_2$ is smaller for positive than for negative requests. But interestingly, an abrupt increase in $|\epsilon_{\%}|_2$ occurs after target requests exceed +20%. Targets around +20% and higher, hit the temperature constraints and therefore start decreasing the controllability of the cooling load.

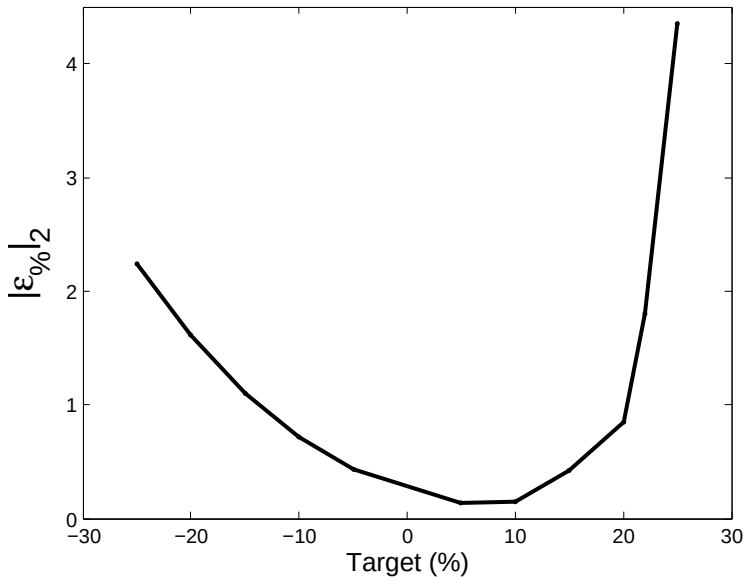

Figure 27: $|\epsilon_{\%}|_2$ as a function of step target request

6.5.3 Temperature Comfort with Step Targets

Complying to a step target is more taxing on the building's HVAC system than tracking a zero mean target. Maintaining a power deviation for extended periods of time will most likely cause the controller to take measures that affect occupants comfort. Traditional DR, like load shifting, often requires temperature setpoint changes for an extended period of time.

Figure 28 below, shows the temperature deviations in the rooms associated with tracking a +10% step target. Even when the largest temperature deviations are larger than for a zero mean target with ±20% limits, as in Fig. 25, they do not reach the imposed constraints.

Nevertheless, as Fig. 29 below shows, the temperature deviations associated with tracking a +20% step target are significantly larger. At least two rooms have reached the temperature constraints and would therefore feel as if the thermostat had been set a degree lower.

Figure. 30 shows that, in general, negative targets from baseline have less effect on temperature than positive targets. In addition, and a deciding factor on the reliability

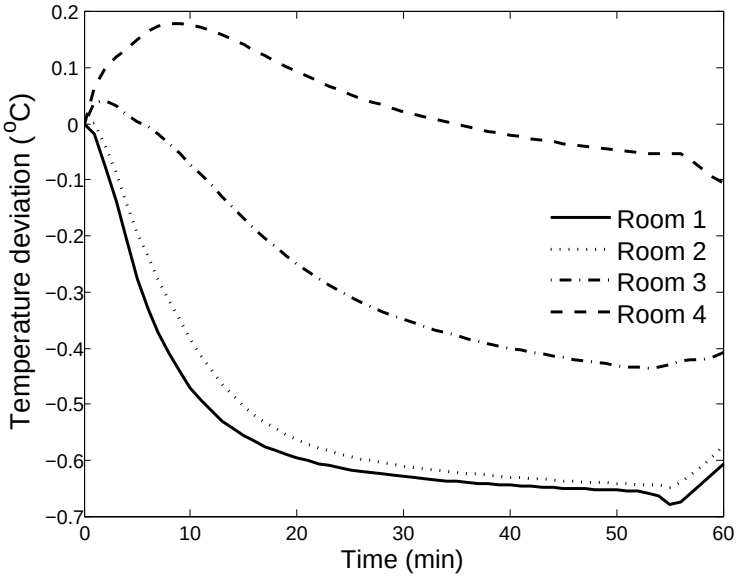

Figure 28: Temperature deviations in the building associated with a +10% step target

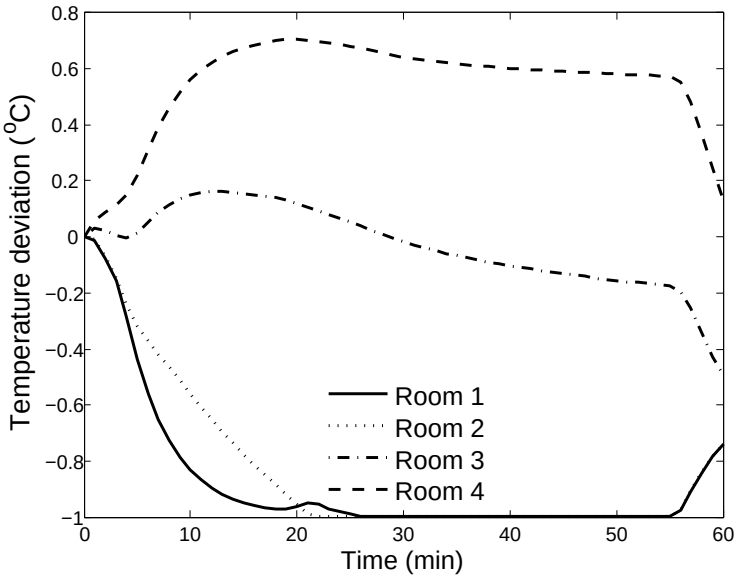

Figure 29: Temperature deviations in the building associated with a +20% step target

of the system to provide step deviations from baseline, targets above 20% seem to jeopardize occupants comfort.

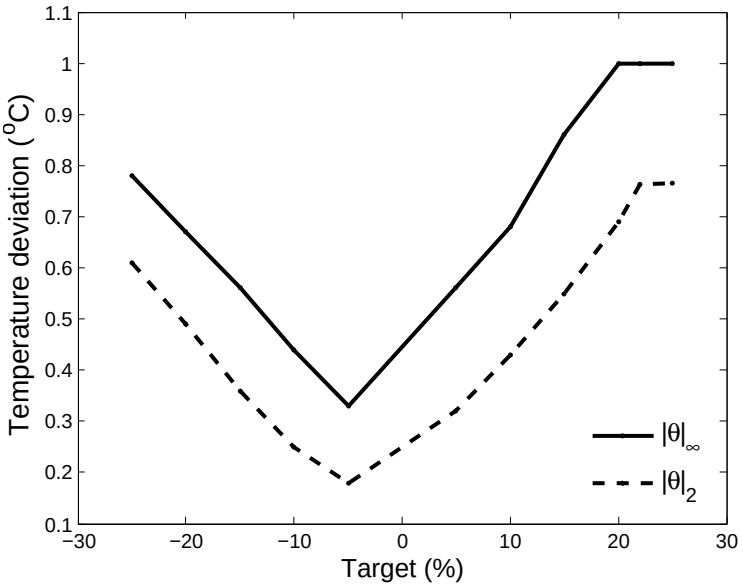

Figure 30: $|\theta|_2$ and $|\theta|_\infty$ as a function of step target

6.6 Climate Parameters

As of 2003, 30% of all commercial floor area in the United States used VAV HVAC systems for cooling and heating purposes and 24% included an EMCS[97], which enables measurement and control of system parameters relevant to the strategy presented in this paper. Industry buildings with an EMCS generally have newer and high capacity cooling equipment with digital controls [54]. Conservative estimates put at 4% of the total commercial floor area in the United States the available area that can make use of the control strategy presented above, without major equipment replacement or addition. Furthermore, the industry is shifting towards variable speed compressors and cooling in both chillers and packaged direct expansion units. This will allow a bigger percent of the total future building floor space to be able to implement this control strategy. Assuming a typical cooling load, system efficiency, and California load factor, continuously controllable air-based cooling systems represent roughly 50 GW peak (5% of installed capacity) and 10 GW average load (1% of installed capacity) in the United States [97, 98].

Despite the moderate effects on occupant comfort by allowing the system to track a zero mean target, not all systems are utilizable all the time. Energy codes now require VAV systems to have economizers. ASHRAE 90.1 requires this for all systems larger than 15.8 kW cooling capacity. Economizers reduce or eliminate cooling energy use

Zone	City	Zone	City
1	Miami	4.1	Albuquerque
2	Houston	4.2	Seattle
2.1	Phoenix	5	Chicago
3	Atlanta	5.1	Boulder
3.1	LA	6	Minneapolis
3.2	Las Vegas	6.1	Helena
3.3	San Francisco	7	Duluth
4	Baltimore	8	Fairbanks

Table 39: Climate zones in representative cities

when outdoor air conditions are favorable by using the cooler outside air for cooling. Depending upon the distribution strategy, all cooling consumption might be eliminated when outdoor temperature is below the 12.7-18.3°C range. Cooling electricity demand tends to be 2-5 times higher than fan electricity demand for VAV at full load. The ratio increases at part load. The controllable resource thus decrease dramatically when cooling power is not present. The best locations that maximize the available controllable resource have few hours below the critical 12.7-18.3°C.

It is assumed that most of the building's controllability can be achieved during the working hour periods, defined from 6 am to 6 pm. In order to estimate the availability of controllable resource during these hours, a climate analysis was performed with national level hourly temperature data for sixteen cities. Ambient (dry bulb) temperature data was collected[99] for each city in Table 39.

A measure of how often a temperature threshold is surpassed on any city for the 6 am - 6 pm period every day is defined by Eq. 6.6.1 below. This measure is useful to approximate the availability of power since the economizer will compromise controllability when ambient temperature, θ_{oa}, drops below somewhere on the 12.7-18.3°C range depending on the actual system set point. Since the precise temperature threshold chosen for the building is not constant across cities or buildings, the average availability per city or climate zone will fall in the $[P_{\theta>18.3°C}, P_{\theta>12.7°C}]$

$$P_{\theta>\alpha} = \frac{\text{Hours when } \theta_{oa} > \alpha}{\text{4335 Hours}} x100\% \tag{6.6.1}$$

Figure 31, below, shows that controllability ranges widely as a function of the geographic location. For example, the area around Miami could provide continuous DR between 93 and 99% of the time during the 6 am to 6 pm period. In contrast, a building in Fairbanks would most likely provide continuous DR between 10 and 30% of the time. In San Francisco, where the widest daily temperature swings occur among studied cities, the threshhold economizer position can substantively affect the

availability of cooling power, and therefore, controllability of the system.

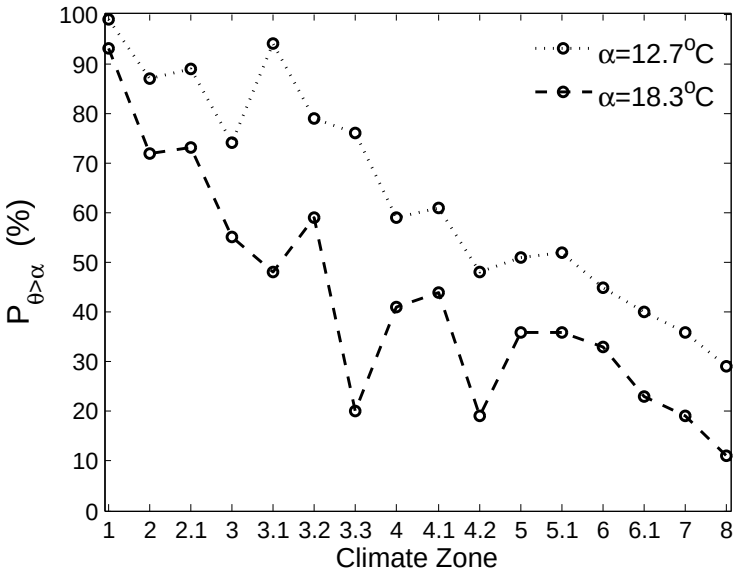

Figure 31: $P_{\theta>12.7°C}$ and $P_{\theta>18.3°C}$ for different US climate zones

6.7 Conclusion

This paper presented a linear model of an HVAC VAV system and a MPC algorithm that achieves controllability. The controllability of the model is tested against two types of power deviation signals. The zero mean target signal achieves controllability with less than 1% error for signals with amplitudes within ±20%, of power rating capacity, or up to ±2GW on a national scale with current infrastructure and technology. With newer variable speed compressors and cooling in both chillers and packaged direct expansion units replacing packaged direct-expansion units with staged cooling control, the potential will increase. Furthermore, the expected maximum temperature deviation in any of the rooms is less than 0.54°C. For step targets within ±20%, the controller achieves less than 2% error, and less than 1°C maximum temperature deviation in any of the rooms. Higher targets increase both the error and occupants' discomfort. Finally, a climate analysis was performed in order to assess the availability of controllable resources in sixteen cities in the US. This control strategy could be implemented up to 99% of the time in the hottest regions, but as low as 10% of the time in the coldest.

Chapter 7

Assessing DR flexibility provision potential from the commercial sector in China

7.1 Introduction

As presented in Chapter 6 of this dissertation, it is possible to provide regulation services by managing the HVAC system in a building and to maintain temperature comfort at the same time. Other research at the intersection of DR and renewables integration has focused on the potential of DR to provide flexibility and aid in the integration of renewables in other countries, like Germany [100], or from the residential sector in the US [101].

In this chapter, we will use the netload model described in Chapter 5 to investigate the potential flexibility provision from managing electricity at the commercial sector level across China in 2030. We first describe the model used to estimate the demand response available in Section 7.2 from the commercial sector. We then present the estimated DR impacts of managing the commercial sector across China for a specific base case netload scenario of a given set of parameters and a renewable penetration scenario in Section 7.3. Section 7.4 we analyze the results in the previous section, as well as provide a parameter and renewable scenario sensitivity analysis on the DR impact across all cases studied. We also compare two DR impact between two different netload scenarios to investigate the effect of parameters in tandem. Finally, we expand this comparison across all modeled netload scenarios to understand what commercial sector buildings' parameters are more important for the provision of demand response.

7.2 Model description

Quantifying the impacts of DR strategies at a regional level poses several challenges similar to those at the building level. Namely, estimation of a baseline is necessary

[102], utilizing a reliable physical model is critical, and, as we found out in our research, analyzing the resulting demand response is focus dependent. It's important to elaborate on the last point. DR estimates will be different for models that focus on controlling demand in intrahour or hour to hour timeframes as well as models controlling ramping or load. Furthermore, if DR events are called infrequently, then the expected deviation from baseline is likely to be larger than if the DR provider is continuously involved in flexibility provision.

The present model is built on a constructed country wide electricity demand baseline, presented in Chapter 3, that both grows as yearly consumption grows, and changes qualitatively as the energy consumption from different economic sectors change in importance over time. The baseline is a function of a physically constructed commercial sector model as explained in Chapter 2. As the system integrates renewables the difference between baseline load and renewable production will be qualitatively different than the load. As presented in Chapter 5, as more renewables are integrated the operation constraints become more challenging.

In this chapter, we use the model developed in Chapter 5 to build a netload baseline for a given set of global parameters. We then use this baseline to capture the times of highest netload or ramping flexibility need. In order to do that, we first define the ordered sequence of netload and ramping for a given set of global parameters as seen in Equations 7.2.1 and 7.2.2.

$$\mathbf{NL} = \{\min NL_{CH}, \cdots, \max NL_{CH}\} \tag{7.2.1}$$

$$\mathbf{NL}_{ramp} = \{\min NL_{CH,ramp}, \cdots, \max NL_{CH,ramp}\} \tag{7.2.2}$$

Since NL is an hourly function, and therefore indexable by hour of the year, we can obtain the hour index of $\min NL$, and $\max NL$ and any other member of the sequences $\mathbf{NL}$ and $\mathbf{NL}_{ramp}$ in between. The hour index set for $\mathbf{NL}$ and $\mathbf{NL}_{ramp}$ are then defined by Equations 7.2.3 and 7.2.4, respectively.

$$\mathbf{T} = \{t_{\min NL_{CH}}, \cdots, t_{\max NL_{CH}}\} \tag{7.2.3}$$

$$\mathbf{T}_{ramp} = \{t_{\min NL_{CH,ramp}}, \cdots, t_{\max NL_{CH,ramp}}\} \tag{7.2.4}$$

In this work, we are interested in finding the impact of providing demand response from the commercial sector. If we order the sequence of hourly commercial load according to $\mathbf{T}$ and $\mathbf{T}_{ramp}$ we get a set of ordered commercial load, $\mathbf{L}_{comm_c}$ and $\mathbf{L}_{comm_c,ramp}$ that correspond hour by hour to the sequences in $\mathbf{NL}$ and $\mathbf{NL}_{ramp}$.

In order to actuate change in the load, we modify the temperature setpoints by ΔT (^{o}C) in the commercial building sector's HVAC systems to provide flexibility for four specific netload cases $\Phi_{\mathbf{case}}$: high and low netload, and high up and down ramping rates. The modified temperature setpoints give rise to different commercial sector model load output and in turn used to build modified load and netload models. The

demand response impact on the system is defined as the difference between the baseline netload and the modified netload and is a function of the netload case $\Phi_{\mathbf{case}}$ for which DR is requested, and the temperature setpoint change ΔT across commercial HVAC systems as shown in Equation 7.2.5.

$$DR = NL_{CH,mod}(\xi, \theta, \chi, R_i, \Phi_{\mathbf{case}}, \Delta T) - NL_{CH}(\xi, \theta, \chi, R_i) \tag{7.2.5}$$

where NL_{CH} is the output of the national hourly netload model given by the chosen parameters, and $NL_{CH,mod}$ is the same model but constructed with temperature setpoint changes ΔT (^{o}C) actuated in accordance to the case of interest $\Phi_{\mathbf{case}}$.

Similarly, we can define the impact on the ramping of the system as a function of the same global parameters, the netload case $\Phi_{\mathbf{case}}$ of interest and the temperature setpoint change ΔT as the difference between the ramping of the modified netload model and the ramping of the baseline netload model as shown in Equation 7.2.6.

$$DR_{ramp} = NL_{CH,ramp,mod}(\xi, \theta, \chi, R_i, \Phi_{\mathbf{case}}, \Delta T) - NL_{CH,ramp}(\xi, \theta, \chi, R_i) \tag{7.2.6}$$

If we order the sequence of hourly demand response according to $\mathbf{T}$ and $\mathbf{T}_{ramp}$ we get a sequence of demand response in the year, $\mathbf{DR}$ and $\mathbf{DR}_{ramp}$ that correspond hour by hour to the sequences $\mathbf{NL}$ and $\mathbf{NL}_{ramp}$.

For each specific netload case we try to modify and manage the commercial load with a different set of goals and for different hours of the year. The function $\Phi_{\mathbf{case}}$ described below is used to decide how and when to manage the commercial load to achieve different purposes.

$$\Phi_{\mathbf{case}} = \begin{cases} \{decrease, \mathbf{T}^{(X)}\} & \text{if case = high netload} \\ \{increase, \mathbf{T}[1, \cdots, X]\} & \text{if case = low netload} \\ \{decrease, \mathbf{T}^{(X)}_{ramp}\} & \text{if case = high up ramping} \\ \{increase, \mathbf{T}_{ramp}[1, \cdots, X]\} & \text{if case = high down ramping} \\ \text{do nothing,} & \text{otherwise.} \end{cases}$$

where we define the X last hours $\mathbf{T}_{(-X)}$ as

$$\mathbf{T}_{(-X)} = \max(t \text{ such that } \#\{s \in \mathbf{T} | s \geq t\} = X)$$

and the sequence of X last hours is defined as

$$\mathbf{T}^{(X)} = \{t \in \mathbf{T} | t \geq \mathbf{T}_{(-X)}\}$$

In specific, for a high netload case scenario, the purpose of DR is to decrease load for the highest X netload hours of the year, $\mathbf{T}^{(X)}$. For a low netload scenario, the purpose of DR is to increase load for the lowest X netload hours of the year, $\mathbf{T}[1, \cdots, X]$. For the high up and down ramping scenarios, DR would be used to decrease ramping rates for the highest X ramping hours of the year $\mathbf{T}^{(X)}_{ramp}$ and increase ramping rates for the lowest X ramping hours of the year, $\mathbf{T}_{ramp}[1, \cdots, X]$. In this work, only effects on the highest 1% of netload hours, approximately 88, for any case will be studied.

7.2.1 Netload algorithms

Since for the two different extreme of the netload different effects are needed (i.e. decrease load at the highest netload hours and increase load at the lowest netload hours) two different algorithms for achieving these changes are used in our model. At times of extreme netload, demand response is actuated by changing the cooling, the heating or both setpoints of each building in the commercial sector model depending on the operation of the building.

By controlling the temperature setpoints in the building's HVAC system, commercial buildings could decrease their electricity consumption for a limited amont of time before temperature comfort is affected by increasing the temperature gap between cooling and heating setpoints.

Algorithm 1 Temperature setpoint changes to decrease load in hour $h \in \mathbf{T}^{(X)}$

if $C_{cool,b}(h) > 0$ **and** $C_{heat,b}(h) == 0$ **then**
  $\Delta T_{sp,cool,b}(h) \leftarrow +\Delta T$
  $\Delta T_{sp,heat,b}(h) \leftarrow 0$
else if $C_{heat,b}(h) > 0$ **and** $C_{cool,b}(h) == 0$ **then**
  $\Delta T_{sp,cool,b}(h) \leftarrow 0$
  $\Delta T_{sp,heat,b}(h) \leftarrow -\Delta T$
else if $C_{heat,b}(h) > 0$ **and** $C_{cool,b}(h) > 0$ **then**
  $\Delta T_{sp,cool,b}(h) \leftarrow +\Delta T$
  $\Delta T_{sp,heat,b}(h) \leftarrow -\Delta T$
else $\{C_{heat,b}(h) == 0$ **and** $C_{cool,b}(h) == 0\}$
  $\Delta T_{sp,cool,b}(h) \leftarrow 0$
  $\Delta T_{sp,heat,b}(h) \leftarrow 0$
end if

Algorithm 1 describes how the DR model decides on temperature setpoint changes for both the cooling and heating components of every building's HVAC system in order to decrease netload. If a decrease in load is requested at hour h (to reduce peak load for example), then each building, b, in our commercial model increases the cooling setpoint and, or, decreases the heating setpoint by ΔT in ^{o}C. If at hour h, building b is providing cooling, then the cooling setpoint is increased. Similarly, if at hour h, building b is providing heating, then the heating setpoint is decreased. If both processes are occurring simultaneously, then both setpoints are moved up and down respectively by ΔT in ^{o}C.

At times of low netload it is similarly possible to increase consumption by decreasing the temperature gap between cooling and heating temperature setpoints. We first define this temperature setpoint gap in Equation 7.2.7 and then describe the algorithm used to increase load in a given hour in Algorithm 2.

$$\Theta_{sp,cool-heat,b}(h) = T_{sp,cool,b}(h) - T_{sp,heat,b}(h) \tag{7.2.7}$$

$T_{sp,cool,b}(h)$ and $T_{sp,heat,b}(h)$ are the cooling and heating temperature setpoint for building b in hour h. If temperature in a given conditioned exceeds $T_{sp,cool,b}(h)$ for that room, then the cooling system starts cooling. If temperature in a given conditioned goes under $T_{sp,heat,b}(h)$ for that room, then the heating system starts heating.

Algorithm 2 Temperature setpoint changes to increase load in hour $h \in \mathbf{T}[1, \cdots, X]$

if $C_{cool,b}(h) > 0$ **and** $C_{heat,b}(h) == 0$ **then**
  $\Delta T_{sp,cool,b}(h) \leftarrow -\max\{\Delta T, \frac{\Delta T}{4} \cdot \Theta_{sp,cool-heat,b}(h)\}$
  $\Delta T_{sp,heat,b}(h) \leftarrow 0$
else if $C_{heat,b}(h) > 0$ **and** $C_{cool,b}(h) == 0$ **then**
  $\Delta T_{sp,cool,b}(h) \leftarrow 0$
  $\Delta T_{sp,heat,b}(h) \leftarrow +\max\{\Delta T, \frac{\Delta T}{4} \cdot \Theta_{sp,cool-heat,b}(h)\}$
else if $C_{heat,b}(h) > 0$ **and** $C_{cool,b}(h) > 0$ **then**
  $\Delta T_{sp,cool,b}(h) \leftarrow -\max\{\Delta T, \frac{\Delta T}{4} \cdot \Theta_{sp,cool-heat,b}(h)\}$
  $\Delta T_{sp,heat,b}(h) \leftarrow +\max\{\Delta T, \frac{\Delta T}{4} \cdot \Theta_{sp,cool-heat,b}(h)\}$
else $\{C_{heat,b}(h) == 0$ **and** $C_{cool,b}(h) == 0\}$
  $\Delta T_{sp,cool,b}(h) \leftarrow 0$
  $\Delta T_{sp,heat,b}(h) \leftarrow 0$
end if

Algorithm 2 describes how the DR model decides on temperature setpoint changes for both cooling and heating components of every building's HVAC system in order to increase load. If an increase in load is requested at hour h (to increase load at times of high renewable production and low base load, for example) each building, b, in our commercial model increases their cooling setpoint and, or, increases the heating setpoint by the largest of ΔT and $\Delta T, \frac{\Delta T}{4} \cdot \Theta_{sp,cool-heat,b}(h)$ in ^{o}C. If the building is cooling and not heating, then the cooling setpoint is decreased by the largest of ΔT or $\Delta T, \frac{\Delta T}{4} \cdot \Theta_{sp,cool-heat,b}(h)$ at that hour h. If the building is heating, and not cooling, then the heating setpoint is increased by the largest of ΔT or $\Delta T, \frac{\Delta T}{4} \cdot \Theta_{sp,cool-heat,b}(h)$ at that hour h. If both cooling at heating are happening in a given building at hour h, then both the cooling and heating setpoints are decreased and increased by the largest of ΔT or $\Delta T, \frac{\Delta T}{4} \cdot \Theta_{sp,cool-heat,b}(h)$ at that hour h, respectively.

In this model we only experiment with ΔT of 1 or 2 ^{o}C and therefore use the term $\frac{\Delta T}{4}$ to bound the potential changes in cooling and heating temperature setpoints. The denominator, 4, could change to 6 if we increased our study range of ΔT to 1-3 ^{o}C or $2 \cdot \max(\Delta T)$ in general.

The resulting effects for a 1 and 2 ^{o}C change for the extreme 1% of high and low netload hours during the year (88 hours each) are summarized in Section 7.3.

7.2.2 Ramping algorithms

As with the extreme netload case, at times of extreme ramping, DR effects are estimated by changing the cooling, the heating or both setpoints of each buildings in the

commercial sector depending on the operation of the building. For both ramping up and down, we want to explore the impact of managing load in the commercial sector to effectively reduce ramping rates in times of highest need. In this report, only effects on the highest 1% of ramping hours will be studied.

For the highest ramping up hours of the year, if a decrease in ramping is requested at hour h, then the building follows the algorithm described in Algorithm 3. Since ramping cannot be controlled in a single hour, in this model we manage ramping in hour h by managing load in hours $h-1$ and h. Once we define our objective as managing load of the hours with the largest change, the algorithm for decreasing ramping up can be simplified as first increasing load at hour $h-1$ and then decreasing load at the following hour h.

Algorithm 3 Temperature setpoint changes to reduce ramping up in hour $h \in \mathbf{T}_{ramp}^{(X)}$

Perform Algorithm 2 (increase netload) for hour $h-1$ and a given ΔT
Perform Algorithm 1 (decrease netload) for hour h and a given ΔT

Similarly, if a decrease in ramping down rate is requested at hour h, then the building follows the algorithm described in Algorithm 4 by first decreasing load at hour $h-1$ and then increasing load at the following hour h.

Algorithm 4 Temperature setpoint changes to reduce ramping down in hour $h \in \mathbf{T}_{ramp}[1, \cdots, X]$

Perform Algorithm 1 (decrease netload) for hour $h-1$ and a given ΔT
Perform Algorithm 2 (increase netload) for hour h and a given ΔT

7.2.3 Base case scenario

In Section 7.3 we show the effects of a synchronized commercial sector wide change in temperature setpoint $\Delta T \in \{1, 2\}$ across the four types of demand response, $\Phi_{\mathbf{case}}$ (high and low netload, high up and down ramping), studied in this work on the netload base case defined by the parameters described in Table 40.

Parameter	Value
Standards	2020 (ξ_1), see Chapter 3
Schedules	MoHURD, 2014 [68] (θ_1)
Heating Electrification	Low Efficiency (χ_1)
Renewables	Historic growth, with curtailment (R_b)

Table 40: Parameters for the base case netload scenario

Under netload parameters described in Table 40 the netload curve can be described by the statistics in Table 41.

Statistic	Value
Load Factor	0.60
Netload, peak (GW)	1065
Netload, min (GW)	90
Ramping ↑, max (GW/h)	215
Ramping ↓, max (GW/h)	-121

Table 41: Statistics for base netload scenario

The peak and lowest netload of the year is 1,065 GW and 90 GW respectively. The highest ramping up and down rates of the year are 215 and -121 GW per hour and the overall netload factor is 0.6.

7.3 Results

In this section we present the results of changing the temperature setpoint by 1 and 2 across all commercial buildings to provide demand response for the four netload cases presented earlier: low and high netload, high up and down ramping.

7.3.1 DR impact statistics

In order to formalize the results from these changes in the operation of the commercial sector, we start by defining a group of sequences of interest within the ordered sequences $\mathbf{L}_{comm_c}$, **NL**, and **DR** and their ramping equivalents. In general, we want to find the subsets of the ordered commercial load, netload, and demand response hourly sequences in accordance to $\mathbf{T}$ and $\mathbf{T}_{ramp}$ that have been affected by demand response events. If we only affect the top 1% of hours for each netload case, then we have approximately 88 hours when demand response events are actuated. In order to measure the impact of the demand response events, we only look at the changes that occur on those hours when we need demand response.

We define the subset of the commercial load being affected by the demand response events as $\mathbf{L}^*_{comm_c}$ and $\mathbf{L}^*_{comm_c,ramp}$ for the hours that require changes in netload and ramping respectively.

$$\mathbf{L}^*_{comm_c} = \begin{cases} \mathbf{L}^{(X)}_{comm_c} & \text{if case = high netload} \\ \mathbf{L}_{comm_c}[1, \cdots, X] & \text{if case = low netload} \end{cases} \tag{7.3.1}$$

$$\mathbf{L}^*_{comm_c,ramp} = \begin{cases} \mathbf{L}^{(X)}_{comm_c,ramp} & \text{if case = high } \uparrow \text{ ramping} \\ \mathbf{L}_{comm_c,ramp}[1, \cdots, X] & \text{if case = high } \downarrow \text{ ramping} \end{cases} \tag{7.3.2}$$

The variable X describes the number of hours being affected by the demand response. If $X = 1$, then we are only interested in a single hour of the sequence. In the super script form, X refers to the last X hours in the sequence.

We define similar subsets for the netload sequences (Equations7.3.3 and 7.3.4) and for the demand response sequences (Equations 7.3.5 and 7.3.6).

$$\mathbf{NL}^* = \begin{cases} \mathbf{NL}^{(X)} & \text{if case = high netload} \\ \mathbf{NL}[1, \cdots, X] & \text{if case = low netload} \end{cases} \tag{7.3.3}$$

$$\mathbf{NL}^*_{ramp} = \begin{cases} \mathbf{NL}^{(X)}_{ramp} & \text{if case = high } \uparrow \text{ ramping} \\ \mathbf{NL}_{ramp}[1, \cdots, X] & \text{if case = high } \downarrow \text{ ramping} \end{cases} \tag{7.3.4}$$

$$\mathbf{DR}^* = \begin{cases} \mathbf{DR}^{(X)} & \text{if case = high netload} \\ \mathbf{DR}[1, \cdots, X] & \text{if case = low netload} \end{cases} \tag{7.3.5}$$

$$\mathbf{DR}^*_{ramp} = \begin{cases} \mathbf{DR}^{(X)}_{ramp} & \text{if case = high } \uparrow \text{ ramping} \\ \mathbf{DR}_{ramp}[1, \cdots, X] & \text{if case = high } \downarrow \text{ ramping} \end{cases} \tag{7.3.6}$$

As mentioned earlier in our work we only focused on DR events for the top 1% of hours for each netload case studied.

Using Equations 7.3.1-7.3.6 we can build a set of statistics that describe the impacts of the demand response events to provide flexibility in high and low netload cases (42) and for high down and up ramping cases (43).

Symbol	Statistic		Units
	Low Netload	High Netload	
$\dot{\delta}$	$\mathbf{DR}[1]$	$\mathbf{DR}^{(1)}$	GW
$\dot{\delta}_{\%,l}$	$\frac{\mathbf{DR}[1]}{\mathbf{NL}[1]}$	$\frac{\mathbf{DR}^{(1)}}{\mathbf{NL}^{(1)}}$	%
$\dot{\delta}_{\%,c}$	$\frac{\mathbf{DR}[1]}{\mathbf{L}_{comm_c}[1]}$	$\frac{\mathbf{DR}^{(1)}}{\mathbf{L}^{(1)}_{comm,c}}$	%
μ	$\langle \mathbf{DR}^* \rangle$		GW
$\mu_{\%,l}$	$\frac{\langle \mathbf{DR}^* \rangle}{\langle \mathbf{NL}^* \rangle}$		%
$\mu_{\%,c}$	$\frac{\langle \mathbf{DR}^* \rangle}{\langle \mathbf{L}^*_{comm,c} \rangle}$		%
σ	$\text{std}(\mathbf{DR}^*)$		GW

Table 42: DR impact statistics for the lowest and highest netloads in the year

In Tables 42 and 43 $\dot{\delta}$ captures the impact of the demand response signal for the highest (or lowest) netload or higest up (or down) ramping rate of the year in absolute terms, while $\dot{\delta}_{\%,l}$, and $\dot{\delta}_{\%,c}$ show the relative impact of the response to the size of the netload and commercial load at that time. To capture the impact of DR across all

Symbol	Statistic		Units
	↓ Ramping	↑ Ramping	
$\dot{\delta}$	$\mathbf{DR}_{ramp}[1]$	$\mathbf{DR}^{(1)}_{ramp}$	$\frac{\text{GW}}{\text{h}}$
$\dot{\delta}_{\%,l}$	$\frac{\mathbf{DR}_{ramp}[1]}{\mathbf{NL}_{ramp}[1]}$	$\frac{\mathbf{DR}^{(1)}_{ramp}}{\mathbf{NL}^{(1)}_{ramp}}$	%
$\dot{\delta}_{\%,c}$	$\frac{\mathbf{DR}_{ramp}[1]}{\mathbf{L}_{comm_c,ramp}[1]}$	$\frac{\mathbf{DR}^{(1)}_{ramp}}{\mathbf{L}^{(1)}_{comm_c,ramp}}$	%
μ	$\langle \mathbf{DR}^{*}_{ramp} \rangle$		$\frac{\text{GW}}{\text{h}}$
$\mu_{\%,l}$	$\frac{\langle \mathbf{DR}^{*}_{ramp} \rangle}{\langle \mathbf{NL}^{*}_{ramp} \rangle}$		%
σ	$\text{std}(\mathbf{DR}^{*}_{ramp})$		$\frac{\text{GW}}{\text{h}}$

Table 43: DR impact statistics for the highest ramping up and down rates in the year

hours when DR events are actuated, we use μ, $\mu_{\%,l}$, and $\mu_{\%,c}$. μ is the average response across all affected hours, in absolute terms, while, $\mu_{\%,l}$ and $\mu_{\%,c}$ show the relative impact of the response to the average of the netload and commercial load at those times. Finally, σ captures the standard deviation of the response across all responses, in absolute terms.

7.3.2 DR impacts on netload

We first study the DR impacts of a temperature setpoint deviation of 1 and 2^{o}C for the low and high netload cases of the base case netload scenario $NL_{CH}(\xi_1, \theta_1, \chi_1, R_b)$.

We call DR events on the lowest and highest 1% netload hours of the year. In Figure 32 we can see the impact of both signals on the netload for the lowest and highest 100 hours of the year. The dotted line shows the modified netload after actuating a 1^{o}C temperature setpoint change across all buildings of the commercial sector, while the dashed line shows the modified netload for a 2^{o}C change.

The descriptive statistics for both the low netload and high netload cases across both temperature setpoint changes are shown in Table 44.

DR impact on the lowest netload hour, $\dot{\delta}$, is a net increase of 5.8 and 15.3 GW for a 1 and 2 ^{o}C temperature setpoint change, respectively. This amounts to a 6.4 and 16.9% increase in the lowest netload hour in the base case scenario, or a 6.9 and 18.2% increase of the commercial load of that hour. Across all 88 hours, netload is increased, on average, by 3.8 and 8.2 GW for a 1 and 2 ^{o}C temperature setpoint change, respectively. This represents a 1.6 and 3.5% increase in average netload over

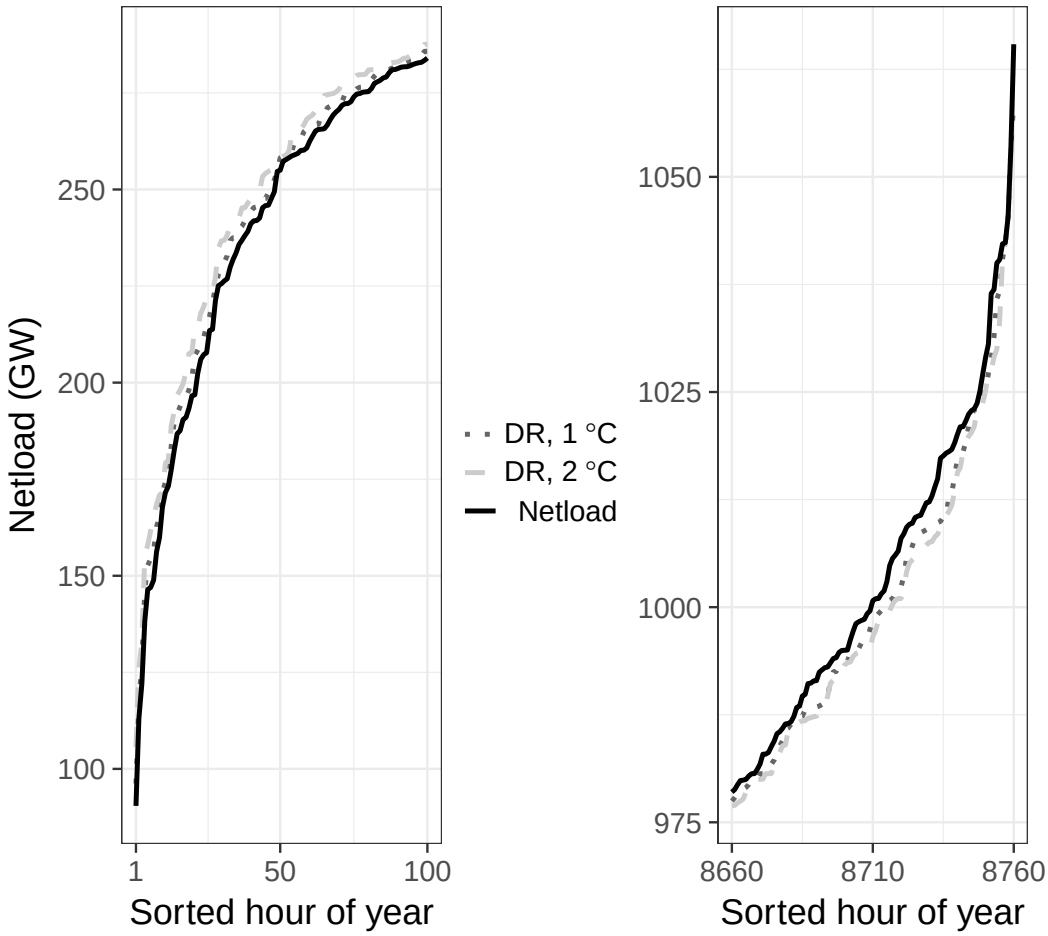

Figure 32: DR impact on netload for base netload scenario for the lowest and highest netload hours of the year, in GW

Statistic	Low Netload		High Netload	
	ΔT=1	ΔT=2	ΔT=1	ΔT=2
$\dot{\delta}$ (GW)	5.8	15.3	-6.8	-12.2
$\dot{\delta}_{\%,l}$ (%)	6.4	16.9	-0.6	-1.1
$\dot{\delta}_{\%,c}$ (%)	6.9	18.2	-3.3	-6.0
μ (GW)	3.8	8.2	-2.9	-4.0
$\mu_{\%,l}$ (%)	1.6	3.5	-0.3	-0.4
$\mu_{\%,c}$ (%)	3.3	7.3	-1.8	-2.5
σ (GW)	3.0	6.7	3.3	4.5

Table 44: Descriptive statistics for the impact of DR on the lowest and highest netload 1% of hours in the year, in GW or % terms)

those hours, or a 3.3 and 7.3% average increase in commercial load in those hours. The standard deviation across both responses is 3.0 and 6.7 GW for a 1 and 2 ^{o}C temperature setpoint change, respectively.

DR impact on the highest netload hours is slightly below the impact on the lowest netload hours in absolute terms, but much smaller in relative terms. DR impact on the highest netload hour, $\dot{\delta}$, is a net decrease of 6.8 and 12.2 GW for a 1 and 2 ^{o}C temperature setpoint change, respectively. This amounts to a 0.6 and 1.1% decrease in the peak netload in the base case scenario, or a 3.3 and 6.0% decrease of the commercial load of that hour. Across all 88 hours, netload is decreased, on average, by 2.9 and 4.0 GW for a 1 and 2 ^{o}C temperature setpoint change, respectively. This represents a 0.3 and 0.4% decrease in average netload over those high netload hours, or a 1.8 and 2.5% average decrease in commercial load across those hours. The standard deviation across both responses is 3.3 and 4.5 GW for a 1 and 2 ^{o}C temperature setpoint change, respectively.

7.3.3 DR impact on ramping

We call DR events on the highest 1% up and down ramping hours of the year. In Figure 33 we can see the impact of both signals on the ramping for the lowest and highest 100 hours of the year. The dotted line shows the modified ramping rates after actuating a 1^{o}C temperature setpoint change across all buildings of the commercial sector, while the dashed line shows the modified ramping for a 2^{o}C change.

The descriptive statistics for both the high down and up ramping netload cases across both temperature setpoint changes are shown in Table 45.

Statistic	High Ramp Down		High Ramp Up	
	ΔT=1	ΔT=2	ΔT=1	ΔT=2
$\dot{\delta}$ ($\frac{GW}{h}$)	14.3	25.1	-10.1	-16.7
$\dot{\delta}_{\%,l}$ (%)	11.8	20.8	-4.7	-7.8
$\dot{\delta}_{\%,c}$ (%)	12.6	22.1	-11.4	-18.8
μ ($\frac{GW}{h}$)	5.9	11.3	-14.1	-26.6
$\mu_{\%,l}$ (%)	5.3	10.1	-9.1	-17.3
σ ($\frac{GW}{h}$)	2.4	3.8	6.6	12.5

Table 45: Descriptive statistics for the impact of DR on the highest ramping down and up 1% of hours in the year, in GW per hour or % terms)

DR impact on the highest down ramping hour, $\dot{\delta}$, is a net increase of 14.3 and 25.1 GW per hour for a 1 and 2 ^{o}C temperature setpoint change, respectively. This amounts to a 11.8 and 20.8% increase in ramping rate in the netload base case scenario, or a 12.6 and 22.1% increase of the commercial load ramping of that hour. Across all 88 hours, ramping is increased, on average, by 5.9 and 11.3 GW per hour for a 1 and 2 ^{o}C temperature setpoint change, respectively. This represents a 5.3 and 10.1% increase in

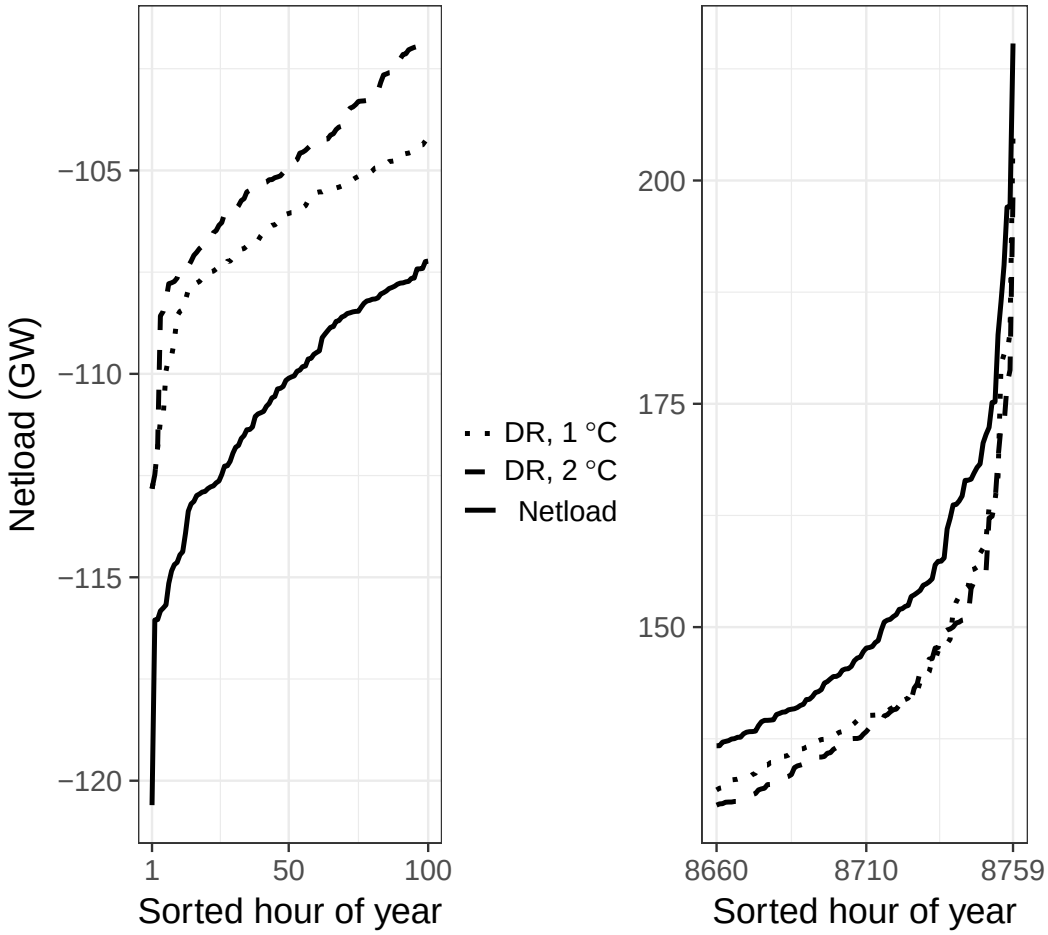

Figure 33: DR impact on ramping for base netload scenario for the highest ramping down and up hours of the year, in GW per hour

average ramping over those hours with respect to the average ramping in the base case scenario. The standard deviation across both responses in ramping is 2.4 and 3.8 GW per hour for a 1 and 2^oC temperature setpoint change, respectively.

DR impact on the highest up ramping hour, $\dot{\delta}$, is a net decrease of 10.1 and 16.7 GW per hour for a 1 and 2^oC temperature setpoint change, respectively. This amounts to a 4.7 and 7.8% decrease in the highest ramping rate in the base case scenario, or a 11.4 and 18.8% decrease in ramping of the commercial load of that hour. Across all 88 hours, ramping is decreased, on average, by 14.1 and 26.6 GW per hour for a 1 and 2^oC temperature setpoint change, respectively. This represents a 9.1 and 17.3% decrease in average ramping up rates over those high ramping hours. The standard deviation across both responses in ramping is 6.6 and 12.5 GW per hour for a 1 and 2 ^oC temperature setpoint change, respectively.

7.4 Discussion

In this section we analyze the impact of DR in providing flexibility for the operation of the electricity system. In Section 7.4.1 we contextualize the impacts of a 1 and 2^oC temperature setpoint change across all commercial buildings for all netload scenarios, under the renewable scenario R_b. In Section 7.4.2 we analyze the effect of the load model parameters in the DR impacts across the four different netload cases. Finally, we provide a comparison between DR impacts for a change in renewable scenarios in Section 7.4.3.

7.4.1 Impact Assessment

Decreasing peak netload

Reducing peak load reduces the need to build power plants that might only operate for a few hours a year in order to meet demand on the highest hours of the year. If we assume that each kW of added capacity cost the system 1,000 dlls, then reducing peak netload by providing DR from the commercial sector saves the system between 6 and 12 billion dollars for a 1 and 2^oC temperature setpoint deviation signal.

With approximately 10.7 billion m^2 of public building and commmercial space in China[77], reducing peak load using DR could pay itself if the cost falls between 0.60 to 1.10 USD per m^2 of floorspace affected. The costs can be distributed even further as the floorspace area of the commercial sector increases.

If we extend the reduction of high netload for the highest 1% of hours in the year, we can then reduce the peak load even further and decrease the time peaker plants run in the year. This extends the system savings between 276 and 377 GWh of electricity from the highest 1% of hours in our current model of the netload defined by $NL(\xi_1, \theta_1, \chi_1, R_b)$ for a 1 or 2^oC temperature setpoint change, respectively.

Using a 2010 study by the National Energy Technology Laboratory (NETL) [1] which estimated costs and performance for different fossil energy plants we can provide

an estimate for the carbon emissions and financial savings for a 276 and 377 GWh of electricity savings from peak netload hours reduction using the emissions and cost of electricity (COE) per megawatt-hour in Table 46 for a integrated gasification combined cycle (IGCC) and natural gas combined cycle (NGCC) power plant, respectively. We provide the emission and cost data for supercritical pulverized coal (PC) boiler for comparison.

Power plant type	CO_2 emissions (tons per MWh)	COE ($ per MWh)
IGCC	0.78	76.3
PC, Supercritical	0.80	58.9
NGCC	0.37	58.9

Table 46: Power plant CO_2 emissions and COE data

If we assume that this energy at the highest netload hours of the year would be provided by IGCC power plants in 2030, then by implementing DR events to decrease netload at the highest 1% of hours we could have a net reduction of 216 and 294 thousand tons of carbon emitted into the atmosphere by a ^oC temperature setpoint change DR signal, respectively. In addition, by reducing the electricity needed in those hours operation savings between 21 and 28 million dollars could be achieved with a 1 and 2^oC temperature setpoint change DR signal, respectively.

If we assume that this energy at the highest netload hours of the year would be provided by NGCC power plants, instead, then by implementing DR events to decrease netload at the highest 1% of hours we could have a net reduction of 100 and 138 thousand tons of carbon emitted into the atmosphere with a 1 and 2^oC temperature setpoint change DR signal, respectively. In addition, by reducing the electricity needed in those hours, operation savings between 16 and 22 million dollars could be achieved with a 1 and 2^oC temperature setpoint change DR signal, respectively.

Increasing low netload

In hours of very low netload, or at the extreme, renewable production that surpasses load, under current system flexibility circumstances renewable production most likely will be curtailed. The discussion about the benefits of raising the minimum netload in order to increase the role renewables play on the provision of electricity, should include a more nuanced analysis on who benefits and who loses when the minimum is increased.

From the point of view of renewable electricity suppliers, increasing the lowest netload of the system might reduce the need to have flexible provision for baseload hours, by effectively increasing the power that can be met from baseload (usually less flexible but cheaper) power plants. The second way that increasing the netload of the system with demand response facilitates the integration of renewables is by reducing the need for high capacity storage in hours of over production.

Nevertheless, the benefits and costs of a higher baseload capacity depend on the power plants meeting such capacity. If baseload is met with power production from coal power plants, then the impact on emissions by letting more coal plants operate is significant. If in 2030 the system baseload is met with a combination of nuclear and hydro then there is no significant impact on emissions.

Reducing high ramping rates

The introduction of renewables into the system will change the system's netload ramping down and up periods of the day. As large amounts of solar come into the grid, netload will decrease rapidly until solar production reaches a daily maximum and then increase rapidly until it reaches the daily peak later in the evening.

If maximizing electricity integration from renewables into the grid is an operational mandate, then, during hours of fast ramping up in solar production, netload system ramping rates will require hundreds of GW per hour of down ramping provision. This is equivalent to hundreds of large power plants being taken offline. If maintaining system stability, even at the expense of renewable production, then the most likely operational strategy to deal with such high rates of ramping would be to curtail solar production during these early morning hours.

By introducing DR to provide down ramping, system operators reduce the need to shut down plants, renewable or fossil, and therefore electricity providers benefit by having more production hours. If the hours a coal power supplier runs are agreed ahead of time in mid to long term contracts then preventing their sudden shutdown saves system operators money. On the other hand, curtailing renewables as the 'default option' as Martinot puts it [86], and allowing non-intermittent fossil power suppliers to continue producing electricity during periods of high production ramping from renewables increases carbon and other pollutants' emissions and affect the health of the general population.

On the other hand, when solar production ramps down during the early evening hours, netload system ramping rates will require hundreds of GW per hour of up ramping provision. This is equivalent to hundreds of large power plants coming online simultaneously. In order to prevent such a large increase in netload ramping after solar power reaches a maximum, system operators will most likely curtail the total production of solar to manage ramping around the solar production maximum. This reduces the overall contribution of renewables to the system and therefore has negative impacts on emissions.

By introducing DR to provide up ramping, system operators reduce the need to have idle power plants ready to be called within an hour, or plants already online running with suboptimal capacity factors in order to provide upwards flexibility. Reducing the extreme ramping rates by providing DR flexibility, also reduces the cost of building and maintaining fast ramping units idle that are called only a few hours a year.

7.4.2 Parameter sensitivity analysis

In this section we study the effects on demand response provision across the four different netload cases of changes in both the load model parameters and the temperature setpoint deviation signal sent across all building models.

Table 47 shows the percent difference in mean demand response impact from the netload base case scenario $NL(\xi_1, \theta_1, \chi_1, R_b)$ and the netload scenario where one of the parameters is different for a 1^oC temperature deviation for the first four columns, and the difference in percentage terms between the DR impact from the base case scenario under a 1 and 2^oC temperature deviation signals.

Case	Parameter change				
	$\Delta\xi$	$\Delta\theta$	$\chi_1 \rightarrow \chi_2$	$\chi_1 \rightarrow \chi_3$	ΔT
High Netload	-2.8	100	-32	-23	39
Low Netload	3.4	24	-73	-47	120
High Ramp Up	-4.6	55	-61	-44	89
High Ramp Down	2.8	69	-73	-64	91

Table 47: Effect of changing parameter on the mean demand response to a 1^oC temperature setpoint signal across different DR scenarios, as a percent of original response

Impact of improving efficiency standards in commercial buildings

As seen from the $\Delta\xi$ column, a change in efficiency gains measured in compliance to efficiency standards from 2020 to 2025 has mild impacts on the demand response provision across all netload cases. Decreasing load and ramping up rates is affected by a decrease of 2.8 and 4.6% in a system with higher efficiency standards. Nevertheless, increasing load and decreasing ramping down rates see a 3.4 and 2.8% improvement on average response for a 1^oC temperature setpoint change across the commercial sector. From these results we see that the relationship between efficiency and DR is not necessarily inversely proportional. Two of the four types of services that could be provided by DR in the facilitation of renewable integration see a negative impact as efficiency increases, but the other two see proportionate increases in the DR impact.

The estimated average commercial sector building intensity under 2020 standards is 138 $\frac{\text{kWh}}{m^2}$, while the same average across all buildings and climate zones in China for 2025 standards is 134 $\frac{\text{kWh}}{m^2}$. Therefore, there is a 4 $\frac{\text{kWh}}{m^2}$ difference between the two standards, or a 2.3% improvement.

If we divide the effect of changing efficiency standards on the mean demand response to a 1^oC temperature setpoint signal across all netload cases as a percent of the original response by the percent improvement in efficiency, we can approximate the effect of a percent efficiency gains on the DR impact. DR to reduce peak load is reduced by 1% for every percent gained in efficiency. DR to increase load at the lowest netload hours is increased by 1.2% for every percent gained in efficiency improvements. DR to reduce

ramping up and down rates at the hours of highest ramping rates is reduced by 1.59% and increased by 1% for every percent gained in efficiency improvements.

Impact of adopting US operational schedules in commercial buildings

As discussed in Chapter 2, MOHURD construction and operation standards outline a suggested a set of operational schedules across different building loads for the different building types modeled in this work [68]. The results in Section 7.3 show the DR impacts across different netload cases for the base case netload scenario that assumes buildings operate with MOHURD 2014 schedules. Nevertheless, a shift towards schedules that resemble those of their American counterparts, outlined by the PNNL commercial building prototype models, will impact the ability of the commercial sector to provide flexibility across the four different netload cases.

The impact of such a transition across the four different netload cases is shown under the θ parameter in Table 47. We can see that a transition towards a more Americanized building operation for all building types across all climate zones will lead to an increase in the DR provision of flexibility for all netload cases. The largest change in average response from a 1^oC temperature deviation signal across all buildings in the commercial sector occurs for the high netload cases with 100% increase in the average netload reduced across all hours affected by the DR events. Increasing netload sees a 24% increase in mean netload from a 1^oC change in temperature setpoint. DR provision of ramping rate alleviation is improved for both up and down ramping with a 55 and 69% increase in the mean response from a 1^oC temperature setpoint change across all buildings in the commercial sector.

Although a transition towards more Americanized building operation will require some increased costs in energy consumption in the year of about 123 TWh or 2.2% more than the base case scenario. DR provision is also non-uniformly increased, with a remarkable doubling in average load reduction at the highest netload hours of the year. The decision to transition towards operating schedules that resemble those in the US has to take into consideration not only the increased energy consumption that it entails, but also the increased occupant comfort and, in particular, increased DR flexibility provision from the commercial building sector.

Impact of de-electrification and higher efficiency electrification of heating in commercial buildings

The electrification of heating across all buildings in the commercial sector will alleviate pollution problems from coal and gas burning in densely populated areas and especially in cities in Northern China [76]. Moving towards meeting heating demand with electricity will have direct positive impacts on the people's health and happiness by reducing smog and other pollutants that cause respiratory diseases [29]. In tandem with alleviating pollution problems, the electrification of heating across the commercial sector could potentially increase the role of renewable electricity in the provision

of total energy demand across China [75].

In this section we study the impacts of moving back to traditional fuel-combustion at the local or city level and increase the efficiency of electric heat supply on the mean DR flexibility provision across the four different netload cases.

If heating is not provided by electricity or heating is provided by more efficient heat pumps across all buildings in the commercial sector, the average DR impact for all hours affected by DR events decrease across all four netload cases. Under parameter χ_{12} we see the impact in DR flexibility provision of de-electrifying the heating load across all buildings in the commercial sector for a 1^oC temperature setpoint deviation. Mean demand reduction at the highest netload hours is reduced by 32%. Mean increases in low netload and mean decreases in down ramping rates by DR provision is reduced by 73% both when the heating is not provided by electricity. Finally, DR impacts on reduction of high ramping up rates is reduced by 61% across all hours affected by DR events.

Keeping electrification of heating but improving the efficiency of the supply by retrofitting boilers into heat pumps will also decrease the availability of DR from the commercial sector when compared to the basecase netload scenario. Nevertheless, as seen under column χ_{13} the impact of such an efficiency improvement is a more limited decrease in DR availability as compared with the complete de-electrification of heating provision. DR impact on the reduction and increase of netload is reduced by 23 and 47% respectively. Mean DR impact on ramping up and down at the highest 88 hours of the year provision is reduced by 44 and 64% respectively.

In general, we can see that the changes in the way heating is provided have the largest impacts on DR provision of increasing low netload and decreasing ramping down services. Reducing the electricity consumption to provide heating across the commercial sector has a disproportionately large effect on the lowest netload hours of the year, which are usually colder than average and require heating. The disproportionately large impact on the ability to reduce ramping down rates by DR events by de-electrification or increase efficiency in the electric heating component of buildings can be explained by increased difficulty in increasing load effectively in the hours of highest down ramping. These hours are usually earlier in the day when solar production starts ramping up, causing netload to ramp down rapidly. Since these ramping rates occur earlier in the day, if they fall in the winter like the highest ramping down rate under the base case netload scenario (occurring in late November) then increasing efficiency of heating, or de-electrifying it completely, does diminish the ability to rapidly increase ramping in those hours of the year.

Impact of increasing the DR temperature setpoint signal

In order to understand the impact of increasing the control signal across all buildings we compare the effects of a 1 and 2^oC temperature setpoint deviation on the DR provision across all netload cases for the basecase netload scenario.

As expected, increasing the disturbance signal increases the response from the sys-

tem. Nevertheless, the response is not linear and even varies among the different netload cases. Increasing the temperature deviation from 1 to 2^{o}C increases the mean reduction of load at the highest 88 netload hours by 39%. This means that the relationship between average reduction in load and temperature setpoint deviation signal is sub-linear. Increasing the temperature deviation signal increases the mean increase of load at the lowest netload hours by 120% making the relationship supralinear. For ramping up and down rates, increasing the temperature setpoint change increases the mean reduction on up and down ramping rates by 89 and 91% respectively, making it approximately linear.

It is clear from the analysis that there are diminishing returns for increasing temperature deviation signals if the purpose of DR is to reduce netload at the highest netload hours. Since different netload models NL, will have moderately different load shapes, but perhaps largely different commercial load models (for example with a different of operational schedules) then it's not clear from just looking at the effect of temperature deviation changes for a specific model on the linearity between temperature deviation signal and average reduction of load. What we can say for this specific model is that high netload hours do not seem as flexible when you try to reduce load within an hour.

7.4.3 Renewable Scenario Effect

If parameters and temperature setpoint signal affect the average DR available to provide flexibility under the four netload cases, then it follows that the renewable penetration scenario also affects the availability of DR.

In this section we study the difference in DR impact as a percentage from the DR impact for 1^{o}C temperature setpoint deviation for the basecase netload scenario, as seen in Section 7.3. Table 48 compares the DR availability difference when the renewable scenario is different from the one outlined in scenario R_b: Historical growth with curtailment in the highest potential regions.

Case	Renewable scenario change	
	$R_b \rightarrow R_a$	$R_b \rightarrow R_c$
High Netload	21	-5.2
Low Netload	-45	1.5
High Ramp Up	2.9	-9.3
High Ramp Down	2.6	95

Table 48: Effect of different renewable scenarios on the mean demand response to a 1^{o}C centigrade temperature setpoint signal across different DR scenarios, as a percent of original response

Impact of reducing renewables penetration

If renewable penetration in 2030 at the province level was only that on the 2020 government goals, then DR across the four different netload cases will be different. The ability to reduce high netload in a lower penetration scenario (2020 goals, R_a) is increased by 21% when we compare the mean reduction across the two renewable scenarios R_a and R_b. Increasing low netload is significantly harder with an over all reduction of 45% on the average increase from the same 1^oC temperature setpoint deviation signal. Meanwhile, ramping rate flexibility provision is not significantly affected when the renewable penetration decreases with only a 2.9 and 2.6 % increase in response for the reduction of ramping up and down DR events.

In a system with both higher netload and netload not as directly linked to renewable penetration reducing load at the highest netload hours is significantly easier. The opposite is true at low netload hours since those low netload hours are also low load hours where it's harder to increase due other factors independent of renewable production. For example if the lowest netload hours occur in the middle of the night when HVAC systems are off for some buildings and regions, then increasing the load from those buildings under the current strategy of changing the temperature setpoint will see reduced responses.

Impact of increasing renewables penetration

If renewable penetration in 2030 exceeded that of our moderately ambitious base case renewable scenario and the provinces with the highest potential grew at proportional rates as the rest of the country (as in R_c) then the response from the same temperature deviation signal for three of the four netload cases is not expected to be dramatically different as for the base case renewable scenario. Reducing netload under a higher renewable penetration scenario is a slightly harder as there is a 5.2% in average response across all hours affected by DR events. Similarly, increasing netload at the hours of lowest netload with a higher penetration of renewable only sees a 1.5% increase in average increase from the DR events. Reducing high ramping up rates is slightly harder as there is a 9.3% reduction in average response from the 1^oC temperature deviation signal. The biggest change in DR impact occurs when trying to reduce the ramping down at the highest ramping down hours of the year. For such hours, a system with higher penetration of renewables will see their average DR response decrease in ramping rates go up by 95%.

The relative small changes in DR availability for the same 1^oC temperature setpoint change signal across the commercial sector between renewable scenarios R_b and R_c for the high and low netload, and the high ramping up netload cases is due to the similarities between the highest 1% of hours in those netload cases. As renewable production increases, specifically solar, the hours of highest ramping down rates shift towards the peak solar ramping up hours (between 9 am and noon) and away from evening hours. Commercial buildings have more ability to increase electricity consumption, and there-

fore manage their ramping rates in the hours of the new highest ramping down hours (9 am -12 pm) than during hours when offices, retail buildings, and schools are closed or closing. This shift in the period of the day explains the dramatic 95% increase in DR availability to decrease down ramping.

7.5 Scenario Comparison

In this section we compare the DR availability for a 1^oC temperature setpoint change signal across all buildings in the commercial sector of two different netload scenarios across multiple load parameters and renewable scenarios. In particular we compare the DR availability between the base case netload scenario, $NL(\xi_1, \theta_1, \chi_1, R_b)$, and a more efficient scenario with higher renewable penetration, $NL(\xi_2, \theta_1, \chi_3, R_c)$. While the base case scenario assumes that buildings on average comply with the estimated 2020 standards, the comparison scenario assumes that buildings are constructed slightly more efficient, complying with the estimated 2025 standards. In addition, buildings in the comparison scenario have high-efficiency heating provision, while buildings in the basecase scenario have low efficiency heating provision. Finally, the basecase and comparison scenarios have increasing penetration of renewables following R_b and R_c scenarios, respectively. We label the basecase scenario as Scenario A, and the more efficient scenario with higher renewable penetration as Scenario B.

We first compare the descriptive statistics and the netload curves for the 24 hour periods around the highest and lowest netload, and highest up and down ramping hour of the year, between these two netload scenarios in Section 7.5.1. We then analyze the difference in DR for a 1^oC temperature setpoint change signal across all buildings in the commercial sector for the two netload scenarios for all four netload cases in Section 7.5.2.

7.5.1 Netload Comparison

In Figure 34 we see a comparison of the lowest and highest 100 hours of netload of Scenario A and B. Scenario B has a higher penetration of renewables combined with a more efficient commercial building sector. This adds up to both lower lowest and highest netload hours when compared with the base case scenario (Scenario A). Figure 35 shows a 24 hour close up around the lowest and highest netload hour of the year. Although both curves across share similar characteristics, Scenario B's netload is shifted down across all hours. In the left panel we see a different of almost 400 GW between the lowest netload points of each graph. In contrast, the right panel shows more similarities.

In Figure 36 we see a comparison of the lowest and highest 100 hours of ramping of Scenario A and B. Given the increased renewable penetration, Scenario B's netload has higher up and down ramping throughout the year with an increased 25 GW per hour rates on the highest down and up ramping when compared to the base case scenario.

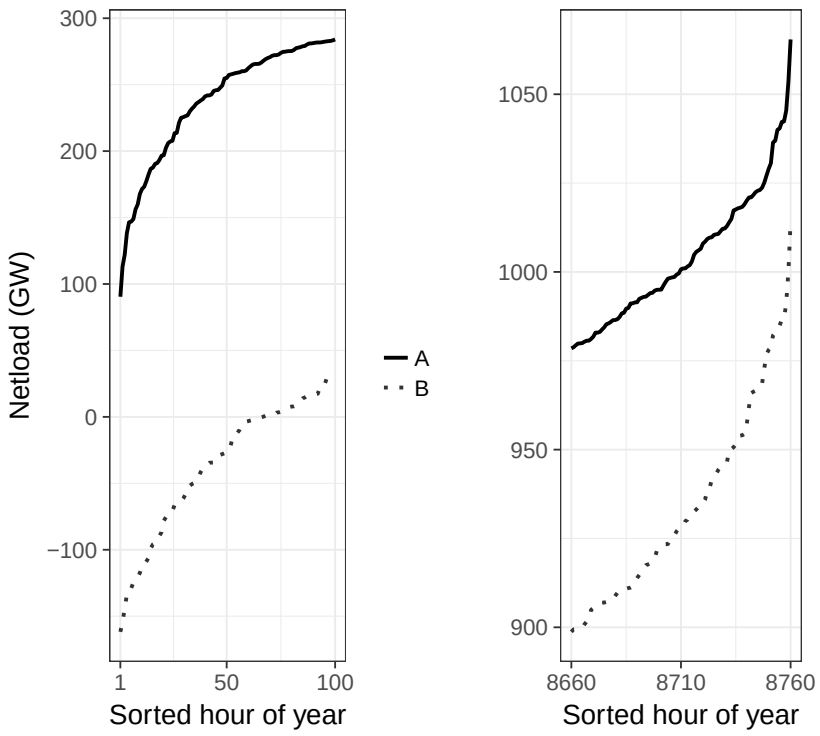

Figure 34: Load duration curve details on the lowest and highest 1% of hours in the year for the base case netload (Scenario A) and a comparison netload scenario (Scenario B).

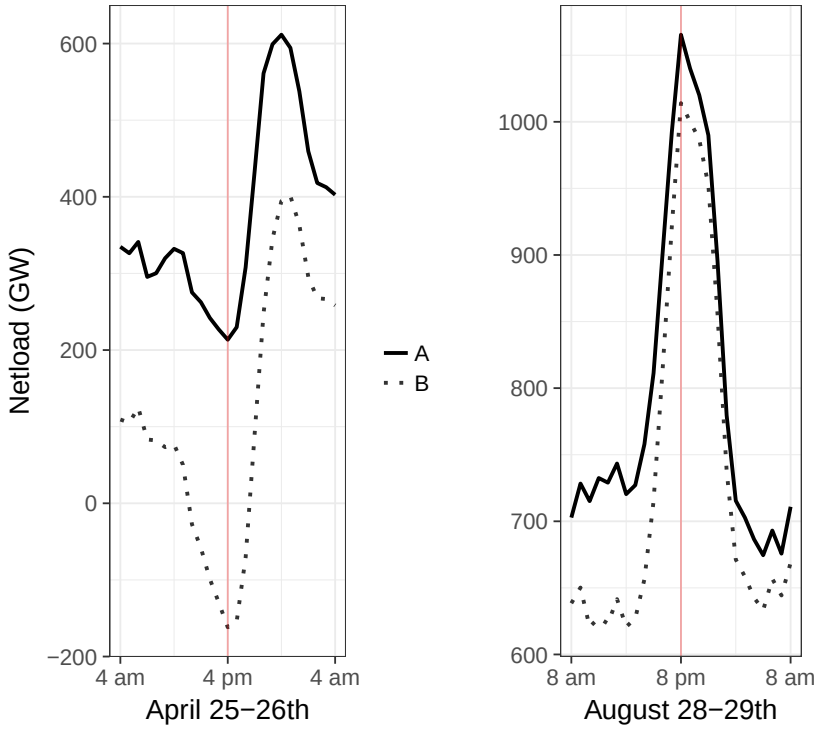

Figure 35: Netload scenarios comparison of the 24 hours around the lowest and highest netload hour for the netload model $NL(\xi_2, \theta_1, \chi_3, R_c)$, (Scenario B).

Figure 37 shows a 24 hour close up around those same lowest and highest ramping hours of the year in the left and right panels, respectively.

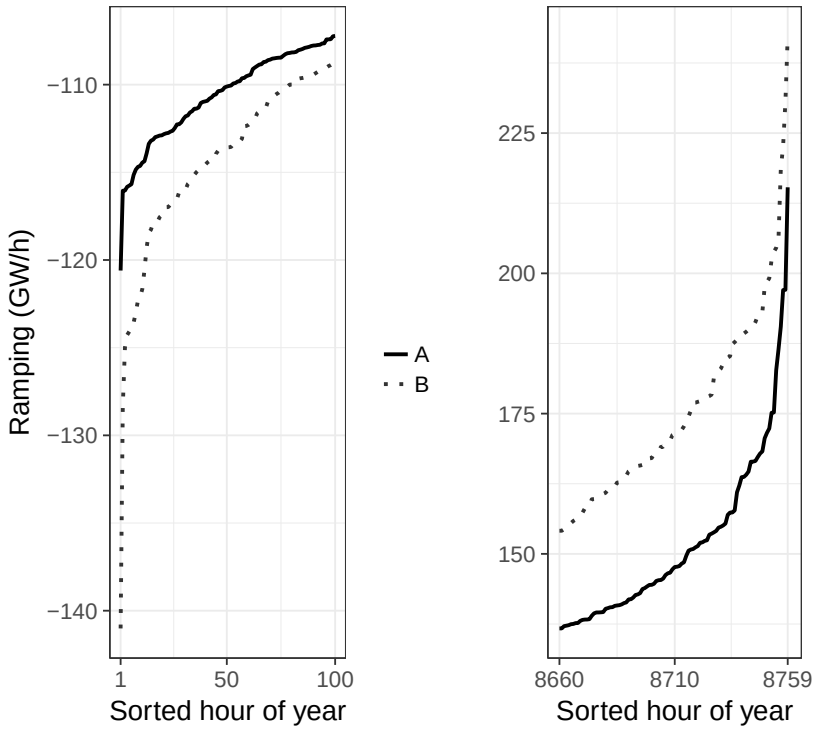

Figure 36: Ramping duration curve details on the lowest and highest 1% of hours in the year for the base case netload (Scenario A) and a comparison netload scenario (Scenario B).

7.5.2 DR Impact Comparison

In the tables below we label the basecase scenario as Scenario A, and the more efficient scenario with higher renewable penetration as Scenario B. We will first study the differences in DR impact on the reduction and increase of high and low netload respectively for the two netload scenarios. Then we will compare the DR impacts on ramping rates for the two scenarios.

Effect on Netload

As shown in Table 49, the absolute value of the increase in load for the lowest netload hours (left half of the table) is smaller for the more efficient scenario with higher penetration of renewables than for our basecase netload scenario. Although the absolute magnitude of the increase at the hour of lowest netload of the year, $\dot{\delta}$, is approximately the same between the two scenarios, the average increase across all 88 hours of the year

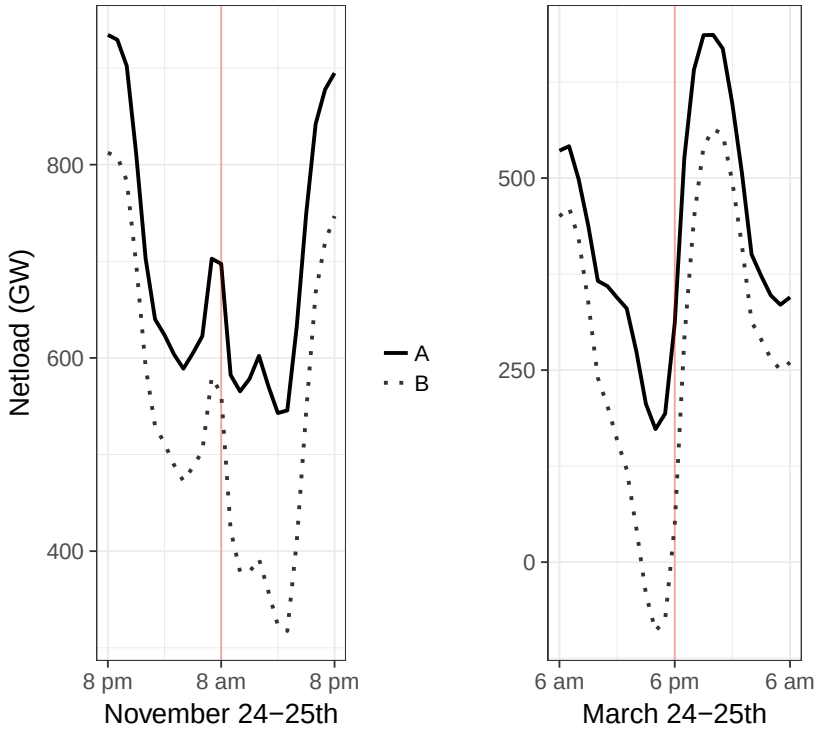

Figure 37: Netload scenarios comparison of the 24 hours around the lowest and highest ramping hour for the netload model $NL(\xi_2, \theta_1, \chi_3, R_c)$, (Scenario B).

affected by DR events, μ, do show a 1.7 GW (44%) decrease in DR availability in the comparison scenario.

Similarly, the absolute value of the decrease in load for the highest netload (right half of Table 49) hours is smaller for the more efficient scenario with higher penetration of renewables than for our basecase netload scenario. The absolute magnitude of the decrease at the hour of highest netload of the year, $\dot{\delta}$, is approximately 1 GW (13%) smaller for Scenario B. The average decrease across all 88 hours of the year affected by DR events, μ, have a 1 GW (34%) decrease in DR availability in the comparison scenario.

Statistic	Low Netload		High Netload	
	Scenario A	Scenario B	Scenario A	Scenario B
$\dot{\delta}$ (GW)	5.8	5.5	-6.8	-5.9
$\dot{\delta}_{t,\%}$ (%)	6.4	-3.4	-0.6	-0.6
$\dot{\delta}_{c,\%}$ (%)	6.9	3.5	-3.3	-3.0
μ (GW)	3.8	2.1	-2.9	-1.9
$\mu_{t,\%}$ (%)	1.6	-4.8	-0.3	-0.2
$\mu_{c,\%}$ (%)	3.3	1.9	-1.8	-1.4
σ (GW)	3.0	1.6	3.3	2.3

Table 49: Netload impact of a 1^{o}C temperature setpoint change across two different netload scenarios

Effect on Ramping

As shown in Table 50 and following the decreases seen for the high and low netload cases, the absolute value for the decrease in ramping rates across for the up and down ramping cases is smaller for Scenario B than for Scenario A. For the high ramp down highest hours, we see a decrease of over 10 GW (about 72%) in absolute DR availability at the highest ramping down hour, $\dot{\delta}$, of each netload scenario. The mean decrease in ramping down rates across all ramping down hours affected by DR events, μ, see a difference of 3.7 GW (62% decrease) between Scenarios A and B.

For the high ramp up highest hours, we see a decrease of 6 GW (about 60%) in absolute DR availability at the highest ramping down hour, $\dot{\delta}$, of each netload scenario. The mean decrease in ramping up rates across all ramping up hours affected by DR events, μ, see a difference of 6.4 GW (45% decrease) between Scenarios A and B.

7.6 Maximizing DR impact

In this section we expand the comparison of DR impacts across all the 32 different netload scenarios studied to find the set of variables that maximize the average DR availability across all hours affected by DR events for the four netload cases of interest.

Statistic	High Ramp Down		High Ramp Up	
	Scenario A	Scenario B	Scenario A	Scenario B
$\dot{\delta}$ (GW)	14.3	4.0	-10.1	-4.1
$\dot{\delta}_{t,\%}$ (%)	11.8	2.8	-4.9	-1.7
$\dot{\delta}_{c,\%}$ (%)	12.6	5.1	-12.1	-5.2
μ (GW)	5.9	2.2	-14.1	-7.7
$\mu_{t,\%}$ (%)	5.3	1.9	-8.7	-4.3
σ (GW)	2.4	1.7	6.6	5.2

Table 50: Ramping impact of a 1^oC temperature setpoint change across two different netload scenarios

7.6.1 Maximum high netload decrease

As shown in Table 51, across all renewable scenarios (R_a, R_b, R_c) the parameters that maximize the reduction of load at the highest netload hours as a percent of actual netload of those hours are ξ_1, θ_2, and χ_1, GB-2020 efficiency standards, ASHRAE recommended operational schedules and low-efficiency heating electrification across all commercial buildings.

A maximum mean decrease of about 0.6% of netload, or 6.1, 5.7, and 4.9 GW, is accomplished with a 1^oC temperature setpoint change signal across all commercial buildings for netload scenarios $NL(\xi_1, \theta_2, \chi_1, R_a)$, $NL(\xi_1, \theta_2, \chi_1, R_b)$, and $NL(\xi_1, \theta_2, \chi_1, R_c)$ respectively.

Netload Scenario	μ (GW)	$\mu_{t,\%}$
$NL(\xi_1, \theta_2, \chi_1, R_a)$	-6.1	-0.6
$NL(\xi_2, \theta_2, \chi_1, R_a)$	-6.0	-0.6
$NL(\xi_1, \theta_2, \chi_1, R_b)$	-5.7	-0.6
$NL(\xi_1, \theta_2, \chi_1, R_c)$	-4.9	-0.5

Table 51: Maximum mean decrease in load in GW (μ) and as a percentage of netload ($\mu_{t,\%}$) across all hours affected by DR events across all parameters and renewable penetration scenarios studied

7.6.2 Maximum high ramping up decrease

As shown in Table 52, the maximum mean decrease in high ramping up rates across all 32 netload scenarios studied, occurs for the netload scenario $NL(\xi_1, \theta_2, \chi_1, R_b)$ (2020 efficiency standards, ASHRAE/PNNL operational schedules, low-efficiency heating electrification, and the basecase renewable scenario R_b) with a maximum mean reduction across all hours affected by DR events of 21.8 GW per hour, equivalent of a 14.4% average reduction in ramping rates.

A scenario with more efficient commercial building construction (2025 standards) as the only differing parameter ($NL(\xi_2, \theta_2, \chi_1, R_b)$) achieves the second highest mean decrease in high ramping up rates with an average decrease of 21.3 GW per hour, equivalent to a 14% average reduction in ramping rates.

Netload Scenario	μ ($\frac{\text{GW}}{h}$)	$\mu_{t,\%}$
$NL(\xi_1, \theta_2, \chi_1, R_b)$	-21.8	-14.4
$NL(\xi_2, \theta_2, \chi_1, R_b)$	-21.3	-14.0
$NL(\xi_1, \theta_2, \chi_1, R_c)$	-14.8	-8.4
$NL(\xi_2, \theta_2, \chi_1, R_c)$	-14.7	-7.8

Table 52: Maximum mean decrease in ramping up rates in $\frac{\text{GW}}{h}$ (μ) and as a percentage of ramping ($\mu_{t,\%}$) across all hours affected by DR events across all parameters and renewable penetration scenarios studied

As shown in the third and fourth row of Table 52, as the penetration of renewables increases, the mean reduction in high ramping up rates for the same two previous load scenarios decreases to 14.8 and 14.7 GW per hour for $NL(\xi_1, \theta_2, \chi_1, R_c)$ and $NL(\xi_2, \theta_2, \chi_1, R_c)$ respectively.

7.6.3 Maximum high ramping down decrease

As shown in Table 53, the maximum mean decrease in high ramping down rates across all 32 netload scenarios studied occurs for the netload scenario $NL(\xi_1, \theta_2, \chi_1, R_c)$ with a maximum mean reduction across all hours affected by DR events of 13.8 GW per hour, equivalent of a 11.4% average reduction in down ramping rates.

A scenario with more efficient commercial building construction as the only differing parameter ($NL(\xi_2, \theta_2, \chi_1, R_c)$) (2025 vs 2020 standards) achieves the second highest mean decrease in high ramping up rates with an average decrease of 12.0 GW per hour, equivalent to a 10% average reduction in ramping rates.

Netload Scenario	μ ($\frac{\text{GW}}{h}$)	$\mu_{t,\%}$
$NL(\xi_1, \theta_2, \chi_1, R_c)$	-13.8	-11.4
$NL(\xi_2, \theta_2, \chi_1, R_c)$	-12.0	-10.0
$NL(\xi_1, \theta_2, \chi_1, R_a)$	-14.8	-9.7
$NL(\xi_1, \theta_2, \chi_1, R_b)$	-14.7	-8.5

Table 53: Maximum mean decrease in ramping down rates in $\frac{\text{GW}}{h}$ (μ) and as a percentage of ramping ($\mu_{t,\%}$) across all hours affected by DR events across all parameters and renewable penetration scenarios studied

Table 53 also shows the two following highest ramping down decreases across all netload scenarios. The only difference between these two netload scenarios and the

netload scenario with the highest ramping down decrease across all netload scenarios are the renewable scenarios. Instead of including the most aggressive renewable penetration scenario, R_c, they follow renewable scenarios R_a and R_b, respectively.

7.6.4 Key parameters in maximizing DR impact

As shown in the results of the previous section 7.6 there are some common commercial sector parameters that provide DR impacts consistently higher than the base case netload scenario. If we wanted to design buildings that are able to provide higher amounts of DR flexibility in both absolute and relative (to the netload at that time) we should then consider the possibility of designing buildings that have operational schedules that resemble more the ASHRAE than the MOHURD schedules.

7.7 Conclusion

In this Chapter we introduced a model to characterize the impact of demand response events across the commercial sector to provide flexibility across four netload cases: hours of high and low netload, and hours of high down and up ramping. We describe the methodology to actuate demand response by managing the buildings' HVAC system and explain the expected metrics.

We find that for the base case netload scenario as characterized by a commercial sector with 2020 efficiency standards, Chinese operational schedules, and low-efficiency electrified heating, and a renewable penetration scenario that has curtailment issues in the provinces with the largest potential (scenario R_b) we can decrease peak netload between 7-12 GW, saving the system between 7 and 12 billion dollars in deferred capacity expansion. Extending demand response to the highest 1% of netload hours in the year we get a 3-4 GW decrease in needed capacity, equivalent to a 276 to 377 GWh reduction in demand and additional operation savings of between 21 to 28 million dollars. Calculating the cost and benefits of increasing netload at the lowest hours requires further analysis on the potential generation portfolio in 2030 that is likely to benefit from an increased operational baseload. In addition, demand response can provide flexibility to alleviate extreme ramping down and up throughout the year. Actuating demand response on the highest 1% ramping hours of the year can provide, on average, between 6 to 11 GW per hour and -14 to -27 GW per hour for the extreme down and up ramping hours of the year.

In general, we find that demand response impact depends on the service that is requested as well as the operational schedules and heating efficiency of the building sector on which it relies on. We find that an operational schedule, across all buildings types in China, that resembles those of their American counterparts can provide increased flexibility to the system at a cost of higher electricity demand through the year. In addition, buildings with electrified heating systems are able to provide more flexibility than buildings that rely on boilers to meet heating demand. Increasing the efficiency

of electrification reduces the building sector's ability to provide demand response.

Finally, in order commercialize this technology and institutional barriers, including the lack of competitive electricity market and the resistance by the state grid corporations, need to be addressed. Without commercialization of demand response it will be difficult order to fully realize the smart grid's potential. We recommend China to consider demand response in their path towards reforming the electricity sector and establishing an open access electricity market so the pollution-free demand response resources may compete with power generators on leveled field [103].

Bibliography

[1] National Energy Technology Laboratory (NETL). Cost and performance baseline for fossil energy plants, volume 1: Bituminous coal and natural gas to electricity. Technical report, United States Department of Energy.

[2] U.S. Energy Information Administration (EIA), 2018.

[3] Michael R. Davidson, Da Zhang, Weiming Xiong, Xiliang Zhang, and Valerie J. Karplus. Modelling the potential for wind energy integration on China's coal-heavy electricity grid. *Nature Energy*, 1:16086, June 2016.

[4] R.K. Morse and G. He. The World's Greatest Coal Arbitrage: China's Coal Import Behavior and Implications for the Global Coal Market. *Program on Energy and Sustainable Development, Stanford*, 2010.

[5] Junnan Yang, Xiaoyuan Li, Wei Peng, Fabian Wagner, and Denise L Mauzerall. Climate, air quality and human health benefits of various solar photovoltaic deployment scenarios in China in 2030. *Environmental Research Letters*, 13(6):064002, 2018.

[6] AC Goodrich et al. Assessing the drivers of regional trends in solar photovoltaic manufacturing. *Energy Environ Sci*, 6, 2013. Environmental Challenges and Potential Solutions of Chinas Power Sector.

[7] International Energy Agency. International Energy Agency: Renewable Energy Law of the People's Republic of China.

[8] F. Birol et al. World Energy Outlook. *International Energy Agency, Paris, France*, 2017.

[9] China. China 13th wind energy development five year plan (2016-2020), November 2016.

[10] China. China 13th solar energy development five year plan (2016-2020), December 2016.

[11] Omar Ellabban, Haitham Abu-Rub, and Frede Blaabjerg. Renewable energy resources: Current status, future prospects and their enabling technology. *Renewable and Sustainable Energy Reviews*, 39:748 – 764, 2014.

[12] T.J. Hammons. Integrating renewable energy sources into European grids. *International Journal of Electrical Power & Energy Systems*, 30(8):462 – 475, 2008.

[13] D.S. Callaway and Hiskens I.A. Achieving controllability of electric loads. *Proceedings of the IEEE*, 2011.

[14] Y.V. Makarov, P.V. Etingov, Z. Huang, J. Ma, B.B. Chakrabarti, K. Subbarao, C. Loutan, and R.T. Guttromson. Integration of wind generation and load forecast uncertainties into power grid operations. In *Transmission and Distribution Conference and Exposition, 2010 IEEE PES*, pages 1–8. IEEE, 2009.

[15] Wen Liu, Henrik Lund, and Brian Vad Mathiesen. Large-scale integration of wind power into the existing Chinese energy system. *Energy*, 36(8):4753 – 4760, 2011. PRES 2010.

[16] OECD/IEA. 2014 Statistics, 2014.

[17] Bonnie West. Chinese coal-fired electricity generation expected to flatten as mix shifts to renewables. *U.S. EIA, Today in Energy.*

[18] M Forsythe. China Aims to Spend at Least $360 Billion on Renewable Energy by 2020. *New York Times.*

[19] Jiang Lin, Gang He, and Alexandria Yuan. Economic rebalancing and electricity demand in China. *The Electricity Journal*, 29(3):48 – 54, 2016.

[20] National Bureau of Statistics, China. 2016 Statistics, December 2016.

[21] China Electricity Council, 2017.

[22] Hongyi Harry Lai. China's western development program: Its rationale, implementation, and prospects. *Modern China*, 28(4):432–466, 2002.

[23] Michael Greenstone. Four years after declaring war on pollution, China is winning. *New York Times*, Mar 2018.

[24] Edward Wong. Nearly 14,000 companies in China violate pollution rules. *New York Times*, June 2017.

[25] Helen Roxburgh. How clean indoor air is becoming China's latest luxury must-have. *The Guardian*, Mar 2018.

[26] Jianlin Hu, Lin Huang, Mindong Chen, Gang He, and Hongliang Zhang. Impacts of power generation on air quality in China Part II: Future scenarios. *Resources, Conservation and Recycling*, 121:115 – 127, 2017. Environmental Challenges and Potential Solutions of Chinas Power Sector.

[27] Haidong Kan, Bingheng Chen, Changhong Chen, Qingyan Fu, and Minghua Chen. An evaluation of public health impact of ambient air pollution under various energy scenarios in Shanghai, China. *Atmospheric Environment*, 38(1):95 – 102, 2004.

[28] World Bank. The Cost of Pollution in China: economic estimates of physical damages. *World Bank and The State Environmental Protection Administration PR of China.*, 2007.

[29] Xiaoyuan Li, Fabian Wagner, Wei Peng, Junnan Yang, and Denise L. Mauzerall. Reduction of solar photovoltaic resources due to air pollution in China. *Proceedings of the National Academy of Sciences*, 114(45):11867–11872, 2017.

[30] Janssens-Maenhout G. Muntean M. Olivier, J.G.J. and J.A.H.W. Peters. Trends in global CO2 emissions: 2016 report. November 2016.

[31] Zeke Hausfather. Analysis: Global CO2 emissions set to rise 2% in 2017 after three-year 'plateau'. *CarbonBrief*, 2017.

[32] Fei Teng and et al. Pathways to deep decarbonization in China. 2015.

[33] NRDC. The road from Paris: China's progress towards its climate pledge. *Issue Brief*, November 2017.

[34] Ye Qi and Jiaqi Lu. China's coal consumption has peaked. *The Brookings Institution*, Jan 2018.

[35] Emily Feng. China's annual coal consumption rises for first time in 3 years. *Financial Times*, Feb 2018.

[36] Climate Action Tracker. China's country summary. 2018.

[37] Michael B. McElroy, Xi Lu, Chris P. Nielsen, and Yuxuan Wang. Potential for wind-generated electricity in China. *Science*, 325(5946):1378–1380, 2009.

[38] Gang He and Daniel M. Kammen. Where, when and how much wind is available? A provincial-scale wind resource assessment for China. *Energy Policy*, 74:116 – 122, 2014.

[39] Qu Hang, Zhao Jun, Yu Xiao, and Cui Junkui. Prospect of concentrating solar power in China - the sustainable future. *Renewable and Sustainable Energy Reviews*, 12(9):2505 – 2514, 2008.

[40] Gang He and Daniel M. Kammen. Where, when and how much solar is available? A provincial-scale solar resource assessment for China. *Renewable Energy*, 85:74 – 82, 2016.

[41] Gang He, Anne-Perrine Avrin, James H. Nelson, Josiah Johnston, Ana Mileva, Jianwei Tian, and Daniel M. Kammen. SWITCH-China: A systems approach to decarbonizing China's power system. *Environmental Science & Technology*, 50(11):5467–5473, 2016. PMID: 27157000.

[42] The White House Office of the Press Secretary. President Obama announces ambitious 2025 target to cut U.S. climate pollution by 26-28 percent from 2005 levels. *US-China joint announcement on climate change and clean energy cooperation*, 2014.

[43] China's National Energy Agency. 2017 Chinese electric power industry summary statistics. *China Energy Portal*, January 2018.

[44] Joern Huenteler, Tian Tang, Gabriel Chan, and Laura Diaz Anadon. Why is Chinas wind power generation not living up to its potential? *Environmental Research Letters*, 13(4):044001, 2018.

[45] Global Wind Energy Council. Global wind report: Annual market update 2016. *GWEC*, 2017.

[46] Danish Energy Agency. Flexibility in the power system - Danish and European experiences. Technical report, Danish Energy Agency.

[47] J. Wang, C.N. Bloyd, Z. Hu, and Z. Tan. Demand response in China. *Energy*, 35(4):1592–1597, 2010.

[48] Z. Hu, D. Moskovitz, and J. Zhao. Demand-Side Management in China's Restructured Power Industry. *Energy Sector Management Assistance Program (ESMAP), The World Bank, Washington, DC*, 2005.

[49] Pedro S. Moura and Anbal T. de Almeida. The role of demand-side management in the grid integration of wind power. *Applied Energy*, 87(8):2581 – 2588, 2010.

[50] Ken Dragoon. Chapter 18 - DM for integrating variable renewable energy: A northwest perspective. In Lawrence E. Jones, editor, *Renewable Energy Integration (Second Edition)*, pages 245 – 259. Academic Press, Boston, second edition edition, 2017.

[51] Mingtao Yao, Zhaoguang Hu, Froylan Sifuentes, and Ning Zhang. Integrated power management of conventional units and industrial loads in China's ancillary services scheduling. *Energies*, 8(5):3955–3977, 2015.

[52] J. H. Yoon, R. Baldick, and A. Novoselac. Dynamic demand response controller based on real-time retail price for residential buildings. *IEEE Transactions on Smart Grid*, 5(1):121–129, Jan 2014.

[53] Z. Zhou, F. Zhao, and J. Wang. Agent-based electricity market simulation with demand response from commercial buildings. *IEEE Transactions on Smart Grid*, 2(4):580–588, Dec 2011.

[54] Taylor Keep. Continuous demand response: Using loads to manage real-time energy imbalance on the electricity grid, 2011.

[55] Wei Feng and Angela Xu and LBL China Energy Group. Personal communication, 2018.

[56] Jianjun Xia, Tianzhen Hong, Qi Shen, Wei Feng, Le Yang, Piljae Im, Alison Lu, and Mahabir Bhandari. Comparison of building energy use data between the United States and China. *Energy and Buildings*, 78:165 – 175, 2014.

[57] IEA World Energy Outlook, China 2014.

[58] Energy Foundation. China 2050 high renewable energy penetration scenario and roadmap study, 2015.

[59] R. Deng, Z. Yang, M. Chow, and J. Chen. A survey on demand response in smart grids: Mathematical models and approaches. *IEEE Transactions on Industrial Informatics*, 11(3):570–582, June 2015.

[60] Jun Dong, Guiyuan Xue, and Rong Li. Demand response in China: Regulations, pilot projects and recommendations A review. *Renewable and Sustainable Energy Reviews*, 59:13 – 27, 2016.

[61] Pacific Northwest National Laboratory U.S. Department of Energy. US DOE, Building Energy Codes Program.

[62] EnergyPlus website: https://energyplus.net/. Accesed, 2018.

[63] Taylor Simon Lomas Kevin J. Liddiard Rob Witt, Henry. Simulation of energy use in UK supermarkets using EnergyPlus. *Proceedings of the 14th International Conference of the International Building Performance Simulation Association (BS2015)*, pages 1095–1102, December 2015.

[64] Vishal Garg, Shikher Somal, Rathish Arumugam, and Aviruch Bhatia. Development for cool roof calculator for India. *Energy and Buildings*, 114:136 – 142, 2016. SI: Countermeasures to Urban Heat Island.

[65] Ivan Oropeza-Perez and Poul Alberg Ostergaard. Energy saving potential of utilizing natural ventilation under warm conditions a case study of Mexico. *Applied Energy*, 130:20 – 32, 2014.

[66] Jing Hou, Yisheng Liu, Yong Wu, Nan Zhou, and Wei Feng. Comparative study of commercial building energy-efficiency retrofit policies in four pilot cities in China. *Energy Policy*, 88:204 – 215, 2016.

[67] Ministry of Housing and Urban-Rural Development, China. Design standard for energy efficiency of public building – GB 50189. Ministry of Housing and Urban-Rural Development, China P.R (in Chinese), 2005.

[68] Ministry of Housing and Urban-Rural Development, China. Design standard for energy efficiency of public building – GB 50189. Ministry of Housing and Urban-Rural Development, China P.R (in Chinese), 2014.

[69] Liu Yang, Joseph C. Lam, and C.L. Tsang. Energy performance of building envelopes in different climate zones in China. *Applied Energy*, 85(9):800 – 817, 2008.

[70] Joseph C. Lam, C.L. Tsang, L. Yang, and Danny H.W. Li. Weather data analysis and design implications for different climatic zones in China. *Building and Environment*, 40(2):277 – 296, 2005.

[71] *Evaluation of Energy Savings of the New Chinese Commercial Building Energy Standard*, Pacific Grove, CA, 08/2014 2014. The American Council for an Energy-Efficient Economy.

[72] Yong Geng, Huijuan Dong, Bing Xue, and Jia Fu. An overview of Chinese green building standards. *Sustainable Development*, 20(3):211–221.

[73] James H. Williams, B. Haley, F. Kahrl, J. Moore, A.D. Jones, M.S Torn, and H. McJeon. Pathways to deep decarbonization in the United States. 2014.

[74] Wei Peng, Junnan Yang, Xi Lu, and Denise L. Mauzerall. Potential co-benefits of electrification for air quality, health, and CO2 mitigation in 2030 China. *Applied Energy*, 218:511 – 519, 2018.

[75] Xinyu Chen, Xi Lu, Michael B. McElroy, Chris P. Nielsen, and Chongqing Kang. Synergies of Wind Power and Electrified Space Heating: Case Study for Beijing. *Environmental Science & Technology*, 48(3):2016–2024, 2014. PMID: 24383490.

[76] Ning Zhang, Xi Lu, Michael B. McElroy, Chris P. Nielsen, Xinyu Chen, Yu Deng, and Chongqing Kang. Reducing curtailment of wind electricity in China by employing electric boilers for heat and pumped hydro for energy storage. *Applied Energy*, 184:987 – 994, 2016.

[77] Da Yan. *China Building Energy Use 2016*. Tsinghua University, 12 2016.

[78] Ning Zhang, Zhaoguang Hu, Bo Shen, Gang He, and Yanan Zheng. An integrated source-grid-load planning model at the macro level: Case study for China's power sector. *Energy*, 126:231 – 246, 2017.

[79] Da Liu, Liang Ruan, Jinchen Liu, Huang Huan, Guowei Zhang, Yi Feng, and Ying Li. Electricity consumption and economic growth nexus in Beijing: A causal analysis of quarterly sectoral data. *Renewable and Sustainable Energy Reviews*, 82:2498 – 2503, 2018.

[80] Jian Zhang, Zhaoguang Hu, Yanan Zheng, Yuhui Zhou, and Ziwei Wan. Sectoral electricity consumption and economic growth : The time difference case of China , 2006 - 2015. 2017.

[81] Y.V. Makarov, C. Loutan, Jian Ma, and P. de Mello. Operational impacts of wind generation on California power systems. *IEEE Transactions on Power Systems*, 24(2):1039 –1050, May 2009.

[82] J. Ma, S. Lu, P. V. Etingov, and Y. V. Makarov. Evaluating the impact of solar generation on balancing requirements in Southern Nevada system. In *2012 IEEE Power and Energy Society General Meeting*, pages 1–7, July 2012.

[83] Mingjian Cui, Jie Zhang, Cong Feng, Anthony R. Florita, Yuanzhang Sun, and Bri-Mathias Hodge. Characterizing and analyzing ramping events in wind power, solar power, load, and netload. *Renewable Energy*, 111:227 – 244, 2017.

[84] Hannele Holttinen, Juha Kiviluoma, Ana Estanqueiro, Emilio Gmez-Lzaro, Barry Rawn, Jan Dobschinski, Peter Meibom, Eamonn Lannoye, Tobias Aigner, Yih-Huei Wan, and Michael Milligan. Variability of load and net load in case of large scale distributed wind power. In *IEEE Transactions on Sustainable Energy*, volume 3, pages 853–861, 10 2011.

[85] M.L. Kubik, P.J. Coker, and J.F. Barlow. Increasing thermal plant flexibility in a high renewables power system. *Applied Energy*, 154:102 – 111, 2015.

[86] Eric Martinot. Grid integration of renewables in China: Learning from the cases of California, Germany, and Denmark. pages 3955–3977, 2015.

[87] Spyros Chatzivasileiadis, Damien Ernst, and Gran Andersson. Chapter 12 - global power grids for harnessing world renewable energy. In Lawrence E. Jones, editor, *Renewable Energy Integration (Second Edition)*, pages 161 – 174. Academic Press, Boston, second edition edition, 2017.

[88] T.M. Keep, F.E. Sifuentes, D.M. Auslander, and D.S. Callaway. Using load switches to control aggregated electricity demand for load following and regulation. In *2011 PES General Meeting Proceeding*, 2010.

[89] Rongxin Yin, Peng Xu, Mary Ann Piette, and Sila Kiliccote. Study on Auto-DR and pre-cooling of commercial buildings with thermal mass in California. *Energy and Buildings*, 42(7):967–975, 2010.

[90] Yudong Ma, F. Borrelli, B. Hencey, B. Coffey, S. Bengea, and P. Haves. Model predictive control for the operation of building cooling systems. *Control Systems Technology, IEEE Transactions on*, 20(3):796–803, May 2012.

[91] Sorin C. Bengea, Anthony D. Kelman, Francesco Borrelli, Russell Taylor, and Satish Narayanan. Implementation of model predictive control for an HVAC system in a mid-size commercial building. *HVAC&R Research*, 20(1):121–135, 2014.

[92] C. Underwood. *HVAC Control Systems: Modeling, Analysis, and Design*. London Spon Press, 1999.

[93] Johnson Controls. *Application Specific Controllers Technical Manual, Variable Air Volume (VAV) Controller*, 1997.

[94] Johnson Controls. *VisSim Tutorial Series: Heating, Ventilation and Air Conditioning (HVAC) Controls: Variable Air Volume (VAV) Systems*, 1997.

[95] Z. Fan. Dynamic Performance of Control Loops and their Interactions in a VAV HVAC System, 2002.

[96] Jeff Stein. Advanced variable air volume system design guide. Technical report, Taylor Engineering, 2007.

[97] R.E. Brown and J.G. Koomey. Electricity use in California: past trends and present usage patterns. *Energy Policy*, 31(9):849–864, 2003.

[98] US Energy Information Administration. *Commercial Building Energy Consumption Survey*, 2003.

[99] Department of Energy. Energy.gov. EnergyPlus: Weather Data.

[100] M. Klobasa. Analysis of demand response and wind integration in Germany's electricity market. *IET Renewable Power Generation*, 4(1):55–63, 2010.

[101] W. Burke and D. Auslander. Robust control of residential demand response network with low bandwidth input. In *Proceedings of the ASME Dynamic Systems and Control Conference*, Ann Arbor, MI, October 2008.

[102] Do A., Auslander D., Burke W., White R., Wright P. Technical review of residential programmable communicating thermostat implementation for title 24-2008. Technical report, California Energy Commission, PIER Buildings End-Use Energy Efficiency Program. CEC-500-2007-XXX, 2007.

[103] Chi-Jen Yang. Opportunities and barriers to demand response in China. *Resources, Conservation and Recycling*, 121:51 – 55, 2017. Environmental Challenges and Potential Solutions of China's Power Sector.

Appendix A

Netload model parameters

Parameter	Value: Description
ξ, Efficiency standards	ξ_1: Buildings follow 2020 standards in 2030 ξ_2: Buildings follow 2025 standards in 2030
θ, Operation schedules	θ_1: Buildings follow Chinese operational schedules guidelines θ_2: Buildings follow US operational schedules guidelines
χ, Heating electrification	χ_1: Heating is provided by low efficiency electric boilers χ_2: Heating is provided by gas or coal boilers χ_3: Heating is provided by high efficiency electric heat pumps
R_i, Renewable penetration	R_a: Renewable capacity stays constant after 2020 (installed capacity = 394 GW) R_b: Capacity continues to grow to 2030, high potential provinces have limited additional capacity installations (1230 GW) R_c: Capacity continues to grow to 2030 for all provinces (1890 GW)

Table 54: Global parameters for the national hourly netload model

Appendix B

Building Standards

	Severe Cold Standards				Cold Standards				*Units*
	2005	2014	2020	2025	2005	2014	2020	2025	
U_{wall}	0.45	0.38	0.33	0.29	0.60	0.50	0.43	0.38	$\frac{W}{K \cdot m^2}$
U_{roof}	0.35	0.28	0.23	0.19	0.55	0.45	0.38	0.33	”
U_{window}	3.00	2.70	2.50	2.33	3.50	3.00	2.67	2.39	”
$SHGC$	0.70	0.70	0.70	0.70	0.70	0.70	0.70	0.70	–
f_{oa}	7.5	3.0	1.0	1.0	7.5	3.0	1.0	1.0	$\frac{m^3}{m^2 \cdot hr}$
η_b	0.89	0.89	0.91	0.91	0.89	0.89	0.91	0.91	–
COP_c	4.30	5.00	5.47	5.86	4.30	5.10	5.63	6.08	–
β_l	12.00	9.00	7.00	5.33	12.00	9.00	7.00	5.33	$\frac{W}{m^2}$
β_e	20.00	20.00	20.00	20.00	20.00	20.00	20.00	20.00	”
σ_p	5.00	8.00	10.00	11.67	5.00	8.00	10.00	11.67	$\frac{m^2}{person}$
	HSCW Standards				HSWW Standards				
	2005	2014	2020	2025	2005	2014	2020	2025	
U_{wall}	1.00	0.80	0.67	0.56	1.50	1.50	1.20	1.20	$\frac{W}{K \cdot m^2}$
U_{roof}	0.70	0.50	0.37	0.26	0.90	0.80	0.73	0.68	”
U_{window}	4.70	3.50	2.70	2.03	6.50	5.20	4.33	3.61	”
$SHGC$	0.70	0.70	0.70	0.70	0.70	0.52	0.40	0.30	–
f_{oa}	7.5	3.0	1.0	1.0	7.5	3.0	1.0	1.0	$\frac{m^3}{m^2 \cdot hr}$
η_b	0.89	0.89	0.91	0.91	0.89	0.9	0.91	0.91	–
COP_c	4.7	5.2	5.5	5.8	4.7	5.0	5.2	5.4	–
β_l	11.00	9.00	7.67	6.56	12.00	9.00	7.00	5.33	$\frac{W}{m^2}$
β_e	20.00	20.00	20.00	20.00	20.00	20.00	20.00	20.00	”
σ_p	5.00	8.00	10.00	11.67	5.00	8.00	10.00	11.67	$\frac{m^2}{person}$

Table 55: Chinese hospital building standards over time and across climate regions

	Severe Cold Standards				Cold Standards				*Units*
	2005	2014	2020	2025	2005	2014	2020	2025	
U_{wall}	0.45	0.38	0.33	0.29	0.60	0.50	0.43	0.38	$\frac{W}{K \cdot m^2}$
U_{roof}	0.35	0.28	0.23	0.19	0.55	0.45	0.38	0.33	”
U_{window}	2.80	2.50	2.30	2.13	3.00	2.70	2.50	2.33	”
$SHGC$	0.70	0.70	0.70	0.70	0.70	0.52	0.40	0.30	–
f_{oa}	7.5	3.0	1.0	1.0	7.5	3.0	1.0	1.0	$\frac{m^3}{m^2 \cdot hr}$
η_b	0.89	0.89	0.91	0.91	0.89	0.89	0.91	0.91	–
COP_c	2.60	2.80	2.93	3.04	2.60	2.80	2.93	3.04	–
β_l	15.00	7.00	6.00	5.00	15.00	7.00	6.00	5.00	$\frac{W}{m^2}$
β_e	20.00	15.00	11.67	8.89	20.00	15.00	11.67	8.89	”
σ_p	15.00	25.00	31.67	37.22	15.00	25.00	31.67	37.22	$\frac{m^2}{person}$
	HSCW Standards				HSWW Standards				
	2005	2014	2020	2025	2005	2014	2020	2025	
U_{wall}	1.00	0.80	0.67	0.56	1.50	1.50	1.20	1.20	$\frac{W}{K \cdot m^2}$
U_{roof}	0.70	0.50	0.37	0.26	0.90	0.80	0.73	0.68	”
U_{window}	3.50	3.00	2.67	2.39	4.70	4.00	3.53	3.14	”
$SHGC$	0.55	0.44	0.37	0.31	0.50	0.44	0.40	0.37	–
f_{oa}	7.5	3.0	1.0	1.0	7.5	3.0	1.0	1.0	$\frac{m^3}{m^2 \cdot hr}$
η_b	0.89	0.89	0.91	0.91	0.89	0.9	0.91	0.91	–
COP_c	2.60	2.90	3.10	3.27	2.60	2.90	3.10	3.27	–
β_l	15.00	7.00	6.00	5.00	15.00	7.00	6.00	5.00	$\frac{W}{m^2}$
β_e	20.00	15.00	11.67	8.89	20.00	15.00	11.67	8.89	”
σ_p	15.00	25.00	31.67	37.22	15.00	25.00	31.67	37.22	$\frac{m^2}{person}$

Table 56: Chinese hotel building standards over time and across climate regions

	HSWW Standards				HSCW Standards				*Units*
	2005	2014	2020	2025	2005	2014	2020	2025	
U_{wall}	1.5	1.5	1.5	1.5	1.0	0.8	0.66	0.55	$\frac{W}{K \cdot m^2}$
U_{roof}	0.9	0.8	0.73	0.68	0.7	0.5	0.37	0.26	”
U_{window}	3.5	3.0	2.7	2.4	3.0	2.6	2.3	2.1	”
$SHGC$	0.45	0.35	0.28	0.22	0.5	0.4	0.33	0.28	–
f_{oa}	7.5	3.0	1.0	1.0	7.5	3.0	1.0	1.0	$\frac{m^3}{m^2 \cdot hr}$
η_b	0.89	0.89	0.91	0.91	0.89	0.89	0.91	0.91	–
COP_c	5.1	5.7	6.1	6.4	5.1	5.6	5.9	6.2	–
β_l	11	9	7.7	6.6	11	9	7.7	6.6	$\frac{W}{m^2}$
β_e	20	15	11.7	8.9	20	15	11.7	8.9	”
σ_p	8	10	11.3	12.4	8	10	11.3	12.4	$\frac{m^2}{person}$
	Cold Standards				Severe Cold Standards				
	2005	2013	2020	2025	2005	2014	2020	2025	
U_{wall}	0.6	0.5	0.43	0.38	0.45	0.38	0.33	0.29	$\frac{W}{K \cdot m^2}$
U_{roof}	0.55	0.45	0.38	0.21	0.35	0.28	0.23	0.19	”
U_{window}	2.7	2.4	2.2	2.0	2.5	2.2	2.0	1.8	”
$SHGC$	0.7	0.48	0.33	0.21	0.7	0.7	0.7	0.7	–
f_{oa}	7.5	3.0	1.0	1.0	7.5	3.0	1.0	1.0	$\frac{m^3}{m^2 \cdot hr}$
η_b	0.89	0.89	0.91	0.91	0.89	0.9	0.91	0.91	–
COP_c	4.7	5.2	5.5	5.8	4.7	5.0	5.2	5.4	–
β_l	11.0	9.0	7.7	6.6	11.0	9.0	7.7	6.6	$\frac{W}{m^2}$
β_e	20.0	15.0	11.7	8.9	20.0	15.0	11.7	8.9	”
σ_p	8	10	11.3	12.4	8	10	11.3	12.4	$\frac{m^2}{person}$

Table 57: Chinese office building standards over time and across climate regions

	Severe Cold Standards				Cold Standards				*Units*
	2005	2014	2020	2025	2005	2014	2020	2025	
U_{wall}	0.45	0.38	0.33	0.29	0.60	0.50	0.43	0.38	$\frac{W}{K \cdot m^2}$
U_{roof}	0.35	0.28	0.23	0.19	0.55	0.45	0.38	0.33	”
U_{window}	3.00	2.70	2.50	2.33	3.50	3.00	2.67	2.39	”
$SHGC$	0.70	0.70	0.70	0.70	0.70	0.70	0.70	0.70	–
f_{oa}	7.5	3.0	1.0	1.0	7.5	3.0	1.0	1.0	$\frac{m^3}{m^2 \cdot hr}$
η_b	0.89	0.89	0.91	0.91	0.89	0.89	0.91	0.91	–
COP_c	2.60	2.80	2.93	3.04	2.60	2.80	2.93	3.04	–
β_l	12.00	10.00	8.67	7.56	12.00	10.00	8.67	7.56	$\frac{W}{m^2}$
β_e	13.00	13.00	13.00	13.00	13.00	13.00	13.00	13.00	”
σ_p	4.00	8.00	10.67	12.89	4.00	8.00	10.67	12.89	$\frac{m^2}{person}$
	HSCW Standards				HSWW Standards				
	2005	2014	2020	2025	2005	2014	2020	2025	
U_{wall}	1.00	0.80	0.67	0.56	1.50	1.50	1.20	1.20	$\frac{W}{K \cdot m^2}$
U_{roof}	0.70	0.50	0.37	0.26	0.90	0.80	0.73	0.68	”
U_{window}	4.70	3.50	2.70	2.03	6.50	5.20	4.33	3.61	”
$SHGC$	0.70	0.70	0.70	0.70	0.70	0.52	0.40	0.30	–
f_{oa}	7.5	3.0	1.0	1.0	7.5	3.0	1.0	1.0	$\frac{m^3}{m^2 \cdot hr}$
η_b	0.89	0.89	0.91	0.91	0.89	0.9	0.91	0.91	–
COP_c	2.60	2.90	3.10	3.27	2.60	2.90	3.10	3.27	–
β_l	12.00	10.00	8.67	7.56	12.00	10.00	8.67	7.56	$\frac{W}{m^2}$
β_e	13.00	13.00	13.00	13.00	13.00	13.00	13.00	13.00	”
σ_p	4.00	8.00	10.67	12.89	4.00	8.00	10.67	12.89	$\frac{m^2}{person}$

Table 58: Chinese retail building standards over time and across climate regions

	Severe Cold Standards				Cold Standards				*Units*
	2005	2014	2020	2025	2005	2014	2020	2025	
U_{wall}	0.45	0.38	0.33	0.29	0.60	0.50	0.43	0.38	$\frac{W}{K \cdot m^2}$
U_{roof}	0.35	0.28	0.23	0.19	0.55	0.45	0.38	0.33	”
U_{window}	2.50	2.20	2.00	1.83	2.70	2.40	2.20	2.03	”
$SHGC$	0.70	0.70	0.70	0.70	0.70	0.48	0.33	0.21	–
f_{oa}	7.5	3.0	1.0	1.0	7.5	3.0	1.0	1.0	$\frac{m^3}{m^2 \cdot hr}$
η_b	0.89	0.89	0.91	0.91	0.89	0.89	0.91	0.91	–
COP_c	2.60	2.80	2.93	3.04	2.60	2.80	2.93	3.04	–
β_l	11.00	9.00	7.67	6.56	11.00	9.00	7.67	6.56	$\frac{W}{m^2}$
β_e	5.00	5.00	5.00	5.00	5.00	5.00	5.00	5.00	”
σ_p	2.50	6.00	8.33	10.28	2.50	6.00	8.33	10.28	$\frac{m^2}{person}$
	HSCW Standards				HSWW Standards				
	2005	2014	2020	2025	2005	2014	2020	2025	
U_{wall}	1.00	0.60	0.33	0.11	1.50	0.80	0.50	0.50	$\frac{W}{K \cdot m^2}$
U_{roof}	0.70	0.40	0.30	0.25	0.90	0.50	0.30	0.25	”
U_{window}	3.00	2.60	2.33	2.11	3.50	3.00	2.67	2.39	”
$SHGC$	0.50	0.40	0.33	0.28	0.45	0.35	0.28	0.23	–
f_{oa}	7.5	3.0	1.0	1.0	7.5	3.0	1.0	1.0	$\frac{m^3}{m^2 \cdot hr}$
η_b	0.89	0.89	0.91	0.91	0.89	0.9	0.91	0.91	–
COP_c	2.60	2.90	3.10	3.27	2.60	2.90	3.10	3.27	–
β_l	11.00	9.00	7.67	6.56	11.00	9.00	7.67	6.56	$\frac{W}{m^2}$
β_e	5.00	5.00	5.00	5.00	5.00	5.00	5.00	5.00	”
σ_p	2.50	6.00	8.33	10.28	2.50	6.00	8.33	10.28	$\frac{m^2}{person}$

Table 59: Chinese school building standards over time and across climate regions

Appendix C

Electricity intensities for all commercial building models

Each building model is a function of three parameters: efficiency standards, operational schedules, and heating electrification (ξ,θ,χ, respectively). Building's energy consumption is assumed independent from renewable scenario. For crossreference, see Appendix A. Each table presents the building intensity for a building type across all four climate zones under the twelve different parameter choices available.

	Severe Cold		Cold	
Scenario	2020 (ξ_1)	2025 (ξ_2)	2020 (ξ_1)	2025 (ξ_2)
$\theta_1\chi_1$	386.0	380.1	361.5	355.7
$\theta_1\chi_2$	288.3	283.9	294.3	290.2
$\theta_1\chi_3$	320.8	316.0	316.7	312.0
$\theta_2\chi_1$	360.9	359.6	334.5	330.3
$\theta_2\chi_2$	263.7	258.1	266.9	261.2
$\theta_2\chi_3$	296.1	292.0	289.5	284.3

	HSCW		HSWW	
Scenario	2020 (ξ_1)	2025 (ξ_2)	2020 (ξ_1)	2025 (ξ_2)
$\theta_1\chi_1$	352.6	347.7	361.9	355.5
$\theta_1\chi_2$	290.5	285.9	307.5	301.3
$\theta_1\chi_3$	311.2	306.5	325.7	319.4
$\theta_2\chi_1$	322.3	316.7	329.5	322.8
$\theta_2\chi_2$	261.8	256.7	276.3	269.3
$\theta_2\chi_3$	282.0	276.7	294.0	287.2

Table 60: Hospital building intensity, $\frac{kWh}{m^2}$

	Severe Cold		Cold	
Scenario	2020 (ξ_1)	2025 (ξ_2)	2020 (ξ_1)	2025 (ξ_2)
$\theta_1\chi_1$	199.3	196.7	173.6	169.1
$\theta_1\chi_2$	133.1	128.7	144.3	140.3
$\theta_1\chi_3$	155.2	151.4	154.1	149.9
$\theta_2\chi_1$	199.0	197.2	174.2	170.4
$\theta_2\chi_2$	135.9	132.4	147.1	143.9
$\theta_2\chi_3$	156.9	154.0	156.1	152.8

	HSCW		HSWW	
Scenario	2020 (ξ_1)	2025 (ξ_2)	2020 (ξ_1)	2025 (ξ_2)
$\theta_1\chi_1$	183.8	176.8	200.5	195.3
$\theta_1\chi_2$	156.1	151.0	182.7	177.7
$\theta_1\chi_3$	165.4	159.6	188.7	183.6
$\theta_2\chi_1$	185.0	178.6	202.2	197.6
$\theta_2\chi_2$	159.4	155.1	186.4	182.1
$\theta_2\chi_3$	168.0	162.9	191.7	187.3

Table 61: Hotel building intensity, $\frac{kWh}{m^2}$

	Severe Cold		Cold	
Scenario	2020 (ξ_1)	2025 (ξ_2)	2020 (ξ_1)	2025 (ξ_2)
$\theta_1\chi_1$	211.0	208.4	194.2	191.3
$\theta_1\chi_2$	180.9	177.9	185.5	181.6
$\theta_1\chi_3$	191.0	188.0	188.4	184.9
$\theta_2\chi_1$	240.2	237.3	221.5	220.5
$\theta_2\chi_2$	199.6	196.1	206.3	201.3
$\theta_2\chi_3$	213.1	209.8	211.4	207.7

	HSCW		HSWW	
Scenario	2020 (ξ_1)	2025 (ξ_2)	2020 (ξ_1)	2025 (ξ_2)
$\theta_1\chi_1$	189.4	185.2	194.3	189.2
$\theta_1\chi_2$	185.5	181.4	194.0	189.0
$\theta_1\chi_3$	186.8	182.7	194.1	189.1
$\theta_2\chi_1$	211.2	206.1	216.4	210.6
$\theta_2\chi_2$	204.2	199.5	215.5	209.8
$\theta_2\chi_3$	206.5	201.7	215.8	210.1

Table 62: Office building intensity, $\frac{kWh}{m^2}$

	Severe Cold		Cold	
Scenario	2020 (ξ_1)	2025 (ξ_2)	2020 (ξ_1)	2025 (ξ_2)
$\theta_1\chi_1$	109.9	109.3	90.9	87.5
$\theta_1\chi_2$	77.8	76.8	80.8	76.4
$\theta_1\chi_3$	88.5	87.6	84.1	80.1
$\theta_2\chi_1$	141.5	138.9	117.5	117.1
$\theta_2\chi_2$	98.7	95.6	101.1	97.8
$\theta_2\chi_3$	113.0	110.0	106.6	104.2

	HSCW		HSWW	
Scenario	2020 (ξ_1)	2025 (ξ_2)	2020 (ξ_1)	2025 (ξ_2)
$\theta_1\chi_1$	82.4	78.2	84.2	79.3
$\theta_1\chi_2$	77.4	73.2	83.8	79.0
$\theta_1\chi_3$	79.0	74.9	84.0	79.1
$\theta_2\chi_1$	103.3	98.1	104.8	99.0
$\theta_2\chi_2$	95.0	90.3	103.7	98.0
$\theta_2\chi_3$	97.8	92.9	104.1	98.3

Table 63: Office with no data center intensity, $\frac{kWh}{m^2}$

	Severe Cold		Cold	
Scenario	2020 (ξ_1)	2025 (ξ_2)	2020 (ξ_1)	2025 (ξ_2)
$\theta_1\chi_1$	120.7	113.2	114.7	107.5
$\theta_1\chi_2$	82.2	77.2	90.3	83.4
$\theta_1\chi_3$	95.1	89.2	98.4	91.4
$\theta_2\chi_1$	142.6	134.5	142.7	135.9
$\theta_2\chi_2$	86.2	81.4	93.7	88.0
$\theta_2\chi_3$	105.0	99.1	110.0	104.0

	HSCW		HSWW	
Scenario	2020 (ξ_1)	2025 (ξ_2)	2020 (ξ_1)	2025 (ξ_2)
$\theta_1\chi_1$	98.9	98.9	109.4	100.8
$\theta_1\chi_2$	92.2	92.2	106.9	98.2
$\theta_1\chi_3$	94.5	94.5	107.7	99.1
$\theta_2\chi_1$	110.7	110.7	119.2	110.8
$\theta_2\chi_2$	98.2	98.2	113.8	105.3
$\theta_2\chi_3$	102.3	102.3	115.6	107.2

Table 64: Retail building intensity, $\frac{kWh}{m^2}$

	Severe Cold		Cold	
Scenario	2020 (ξ_1)	2025 (ξ_2)	2020 (ξ_1)	2025 (ξ_2)
$\theta_1\chi_1$	70.7	69.0	81.0	77.1
$\theta_1\chi_2$	56.5	55.4	58.1	56.7
$\theta_1\chi_3$	61.2	59.9	65.7	63.5
$\theta_2\chi_1$	100.9	97.5	125.1	116.9
$\theta_2\chi_2$	78.3	76.2	81.5	77.9
$\theta_2\chi_3$	85.8	83.3	96.0	90.9

	HSCW		HSWW	
Scenario	2020 (ξ_1)	2025 (ξ_2)	2020 (ξ_1)	2025 (ξ_2)
$\theta_1\chi_1$	68.8	67.1	73.9	71.9
$\theta_1\chi_2$	65.4	63.9	73.2	71.0
$\theta_1\chi_3$	66.5	65.0	73.4	71.3
$\theta_2\chi_1$	96.3	91.9	102.0	98.1
$\theta_2\chi_2$	88.7	85.1	99.6	95.2
$\theta_2\chi_3$	91.2	87.3	100.4	96.2

Table 65: School building intensity, $\frac{kWh}{m^2}$

Appendix D

DR flexibility provision potential from the commercial sector for all netload scenarios

Statistics

Symbol	Description
$\dot{\delta}$	impact of the demand response signal for the highest (or lowest) netload or highest up (or down) ramping rate of the year in absolute terms
$\dot{\delta}_{\%,t}$	relative impact of the response to the netload
$\dot{\delta}_{\%,c}$	relative impact of the response to the commercial sector's load
μ	average response across all affected hours, in absolute terms
$\mu_{\%,t}$	relative impact of the response to the average of the netload
$\mu_{\%,c}$	relative impact of the response to the average of the commercial sector's load
σ	standard deviation of the response across all responses, in absolute terms

Table 66: Definitions for DR flexibility provision statistics

Results

The statistics defined in Talbe 66 are presented for all netload model developed. We arrange the result tables in the following manner. We first present the results for each of the netload cases (high and low netload, and high up and down ramping) in both absolute and relative terms for the R_a, R_b, and R_c respectively. Tables 67 to 74 present the results for DR events across all netload cases for the renewable scenario R_a. Tables 75 to 82 and 83 to 90 present the results in the same order for the R_b and R_c, respectively.

For crossreference on the meaning of the global parameters of which netload, and therefore DR flexibility provision, are a function of, see Appendix A.

Scenario		ξ_1			ξ_2		
	ΔT	$\hat{\delta}$	μ	σ	$\hat{\delta}$	μ	σ
$\theta_1\chi_1$	1	-4.9	-3.4	4.1	-4.1	-3.1	3.7
	2	-8.8	-5.7	6.6	-8.4	-4.9	6.1
$\theta_1\chi_2$	1	-3.7	-2.5	2.8	-3.0	-2.3	2.6
	2	-7.1	-4.3	4.8	-6.9	-3.6	4.1
$\theta_1\chi_3$	1	-4.1	-2.6	2.9	-3.4	-2.5	2.7
	2	-7.7	-4.5	5.1	-7.4	-4.0	4.4
$\theta_2\chi_1$	1	-15.7	-6.0	6.4	-14.0	-6.1	6.2
	2	-29.7	-9.9	10.7	-26.2	-10.0	10.3
$\theta_2\chi_2$	1	-5.1	-3.6	3.5	-5.5	-3.5	3.4
	2	-9.3	-6.0	5.8	-9.6	-5.7	5.4
$\theta_2\chi_3$	1	-5.7	-4.0	3.8	-6.4	-4.0	3.7
	2	-10.1	-6.4	6.1	-10.6	-6.4	5.9

Table 67: DR flexibility provision: netload decrease, for high netload case and renewable scenario R_a, in GW

Scenario		ξ_1				ξ_2			
	ΔT	$\hat{\delta}_{t,\%}$	$\mu_{t,\%}$	$\hat{\delta}_{c,\%}$	$\mu_{c,\%}$	$\hat{\delta}_{t,\%}$	$\mu_{t,\%}$	$\hat{\delta}_{c,\%}$	$\mu_{c,\%}$
$\theta_1\chi_1$	1	-0.4	-0.3	-2.4	-2.0	-0.4	-0.3	-2.1	-1.8
	2	-0.8	-0.6	-4.3	-3.3	-0.8	-0.5	-4.3	-2.9
$\theta_1\chi_2$	1	-0.3	-0.2	-1.8	-1.5	-0.3	-0.2	-1.5	-1.4
	2	-0.7	-0.4	-3.5	-2.6	-0.6	-0.4	-3.5	-2.3
$\theta_1\chi_3$	1	-0.4	-0.3	-2.0	-1.6	-0.3	-0.2	-1.7	-1.6
	2	-0.7	-0.4	-3.8	-2.7	-0.7	-0.4	-3.8	-2.6
$\theta_2\chi_1$	1	-1.4	-0.6	-6.3	-3.1	-1.3	-0.6	-5.8	-3.3
	2	-2.7	-0.9	-12.0	-5.2	-2.4	-0.9	-10.8	-5.3
$\theta_2\chi_2$	1	-0.5	-0.3	-2.6	-2.0	-0.5	-0.3	-2.9	-2.0
	2	-0.8	-0.6	-4.7	-3.3	-0.9	-0.5	-5.1	-3.4
$\theta_2\chi_3$	1	-0.5	-0.4	-2.9	-2.2	-0.6	-0.4	-3.4	-2.3
	2	-0.9	-0.6	-5.1	-3.6	-1.0	-0.6	-5.6	-3.7

Table 68: DR flexibility provision: netload decrease, for high netload case and renewable scenario R_a, in percentage deviation

Scenario		ξ_1			ξ_2		
	ΔT	$\hat{\delta}$	μ	σ	$\hat{\delta}$	μ	σ
$\theta_1\chi_1$	1	2.5	2.1	1.7	2.1	2.0	1.6
	2	5.2	4.2	3.4	4.6	4.0	3.2
$\theta_1\chi_2$	1	0.2	0.2	0.2	0.1	0.1	0.2
	2	0.4	0.3	0.3	0.4	0.3	0.3
$\theta_1\chi_3$	1	1.0	0.8	0.7	0.8	0.8	0.7
	2	2.0	1.6	1.3	1.8	1.6	1.2
$\theta_2\chi_1$	1	0.0	0.1	0.5	0.0	0.0	0.6
	2	0.1	0.1	0.9	0.0	0.0	1.0
$\theta_2\chi_2$	1	0.2	0.2	0.3	0.4	0.1	0.5
	2	0.8	0.6	0.8	1.0	0.7	0.9
$\theta_2\chi_3$	1	0.5	0.6	0.6	0.6	0.6	0.7
	2	1.6	1.6	1.4	1.8	1.7	1.5

Table 69: DR flexibility provision: netload increase, for low netload case and renewable scenario R_a, in GW

Scenario		ξ_1				ξ_2			
	ΔT	$\hat{\delta}_{t,\%}$	$\mu_{t,\%}$	$\hat{\delta}_{c,\%}$	$\mu_{c,\%}$	$\hat{\delta}_{t,\%}$	$\mu_{t,\%}$	$\hat{\delta}_{c,\%}$	$\mu_{c,\%}$
$\theta_1\chi_1$	1	0.56	0.42	4.74	3.59	0.47	0.40	4.01	3.45
	2	1.13	0.84	9.66	7.20	1.02	0.81	8.73	7.07
$\theta_1\chi_2$	1	0.03	0.03	0.32	0.35	0.02	0.03	0.24	0.31
	2	0.09	0.05	0.85	0.55	0.08	0.06	0.82	0.61
$\theta_1\chi_3$	1	0.21	0.17	1.94	1.62	0.17	0.16	1.61	1.56
	2	0.44	0.32	4.06	3.12	0.40	0.32	3.71	3.16
$\theta_2\chi_1$	1	0.00	0.02	0.00	0.13	0.00	0.01	0.00	0.04
	2	0.01	0.01	0.09	0.08	0.00	0.01	0.00	0.07
$\theta_2\chi_2$	1	0.05	0.03	0.41	0.26	0.09	0.02	0.73	0.20
	2	0.18	0.13	1.43	1.09	0.21	0.15	1.77	1.27
$\theta_2\chi_3$	1	0.11	0.12	0.83	0.97	0.13	0.13	1.07	1.05
	2	0.34	0.32	2.65	2.63	0.39	0.33	3.13	2.74

Table 70: DR flexibility provision: netload increase, for low netload case and renewable scenario R_a, in percentage deviation

Scenario		ξ_1			ξ_2		
	ΔT	$\hat{\delta}$	μ	σ	$\hat{\delta}$	μ	σ
$\theta_1\chi_1$	1	-14.9	-14.5	7.0	-14.0	-11.3	4.7
	2	-25.9	-25.3	12.2	-23.8	-19.7	8.4
$\theta_1\chi_2$	1	-1.2	-1.1	0.5	-1.1	-1.1	0.6
	2	-2.6	-2.0	1.0	-3.6	-1.9	1.1
$\theta_1\chi_3$	1	-4.8	-4.0	1.7	-5.6	-3.5	1.6
	2	-9.1	-7.0	2.7	-9.0	-6.1	2.8
$\theta_2\chi_1$	1	-43.1	-2.2	13.1	-38.6	-2.1	11.6
	2	-83.1	-4.3	25.7	-76.6	-4.0	22.4
$\theta_2\chi_2$	1	-13.1	-4.6	3.9	-12.0	-4.5	4.0
	2	-27.1	-8.4	7.4	-25.1	-8.2	7.4
$\theta_2\chi_3$	1	-2.2	-6.5	4.3	-4.4	-5.7	3.2
	2	-5.6	-12.4	8.2	-9.1	-11.1	6.0

Table 71: DR flexibility provision: ramping decrease, for high ramping up case and renewable scenario R_a, in $\frac{GW}{h}$

Scenario		ξ_1			ξ_2		
	ΔT	$\hat{\delta}_{t,\%}$	$\mu_{t,\%}$	$\hat{\delta}_{c,\%}$	$\hat{\delta}_{t,\%}$	$\mu_{t,\%}$	$\hat{\delta}_{c,\%}$
$\theta_1\chi_1$	1	-9.4	-11.0	-8.5	-8.8	-8.7	-8.5
	2	-16.3	-19.1	-14.8	-15.0	-15.2	-14.5
$\theta_1\chi_2$	1	-1.1	-1.1	-1.8	-1.0	-1.1	-1.7
	2	-2.3	-2.0	-3.8	-3.2	-1.9	-5.6
$\theta_1\chi_3$	1	-4.1	-3.7	-4.3	-4.7	-3.3	-5.1
	2	-7.7	-6.5	-8.0	-7.7	-5.8	-8.3
$\theta_2\chi_1$	1	-27.2	-1.8	-21.7	-24.2	-1.7	-20.6
	2	-52.4	-3.5	-41.9	-48.0	-3.1	-40.9
$\theta_2\chi_2$	1	-12.8	-5.0	-11.5	-12.3	-5.0	-11.0
	2	-26.7	-9.1	-23.9	-25.6	-9.1	-23.0
$\theta_2\chi_3$	1	-2.0	-6.6	-1.7	-4.0	-5.7	-3.6
	2	-5.1	-12.4	-4.4	-8.3	-11.1	-7.4

Table 72: DR flexibility provision: ramping decrease, for high ramping up case and renewable scenario R_a, in percentage deviation

Scenario		ξ_1			ξ_2		
	ΔT	$\hat{\delta}$	μ	σ	$\hat{\delta}$	μ	σ
$\theta_1\chi_1$	1	4.6	6.1	1.3	5.1	6.4	0.9
	2	10.4	11.6	1.2	10.8	11.7	0.9
$\theta_1\chi_2$	1	2.5	1.9	0.9	2.2	1.7	0.6
	2	5.5	3.6	2.0	2.9	3.1	1.4
$\theta_1\chi_3$	1	3.2	2.5	1.5	3.0	2.4	1.5
	2	7.1	4.8	2.9	6.4	4.4	2.7
$\theta_2\chi_1$	1	36.4	11.2	6.5	27.0	10.4	5.6
	2	64.9	23.6	11.5	62.9	21.8	9.5
$\theta_2\chi_2$	1	7.7	4.7	3.7	4.8	3.9	2.7
	2	17.1	11.1	6.8	14.8	10.2	5.9
$\theta_2\chi_3$	1	8.6	4.6	3.7	6.0	4.2	3.0
	2	19.0	10.9	7.8	17.2	10.2	7.1

Table 73: DR flexibility provision: ramping increase, for high ramping down case and renewable scenario R_a, in $\frac{GW}{h}$

Scenario		ξ_1			ξ_2		
	ΔT	$\hat{\delta}_{t,\%}$	$\mu_{t,\%}$	$\hat{\delta}_{c,\%}$	$\hat{\delta}_{t,\%}$	$\mu_{t,\%}$	$\hat{\delta}_{c,\%}$
$\theta_1\chi_1$	1	-4.1	-5.6	5.0	-4.5	-5.9	5.6
	2	-9.2	-10.7	11.2	-9.6	-10.7	11.9
$\theta_1\chi_2$	1	-2.3	-1.7	2.8	-2.0	-1.5	3.4
	2	-4.9	-3.3	6.0	-2.6	-2.8	4.5
$\theta_1\chi_3$	1	-2.9	-2.3	3.5	-2.7	-2.2	3.4
	2	-6.3	-4.4	7.8	-5.7	-4.1	7.2
$\theta_2\chi_1$	1	-26.8	-9.7	17.8	-21.1	-9.2	14.0
	2	-47.8	-20.6	31.7	-49.2	-19.2	32.5
$\theta_2\chi_2$	1	-6.4	-4.1	7.0	-4.0	-3.4	4.5
	2	-14.3	-9.7	15.6	-12.5	-9.0	13.9
$\theta_2\chi_3$	1	-7.2	-4.1	7.8	-5.1	-3.7	5.6
	2	-15.9	-9.5	17.2	-14.5	-9.0	16.0

Table 74: DR flexibility provision: ramping increase, for high ramping down case and renewable scenario R_a, in percentage deviation

Scenario		ξ_1			ξ_2		
	ΔT	$\hat{\delta}$	μ	σ	$\hat{\delta}$	μ	σ
$\theta_1\chi_1$	1	-6.8	-2.9	3.3	-6.7	-2.8	3.1
	2	-12.2	-4.0	4.5	-12.6	-3.8	4.1
$\theta_1\chi_2$	1	-5.5	-2.0	2.5	-5.5	-1.9	2.4
	2	-10.5	-2.6	3.2	-10.8	-2.5	3.0
$\theta_1\chi_3$	1	-5.9	-2.2	2.7	-5.9	-2.1	2.5
	2	-11.1	-3.0	3.5	-11.4	-2.9	3.2
$\theta_2\chi_1$	1	-10.2	-5.7	5.9	-10.6	-5.6	5.7
	2	-16.4	-9.3	9.8	-16.7	-8.9	9.2
$\theta_2\chi_2$	1	-8.2	-3.6	3.5	-7.8	-3.5	3.3
	2	-13.9	-5.7	5.5	-13.4	-5.5	5.3
$\theta_2\chi_3$	1	-8.9	-4.0	3.8	-8.7	-3.8	3.7
	2	-14.7	-6.3	5.9	-14.5	-6.0	5.8

Table 75: DR flexibility provision: netload decrease, for high netload case and renewable scenario R_b, in GW

Scenario		ξ_1				ξ_2			
	ΔT	$\hat{\delta}_{t,\%}$	$\mu_{t,\%}$	$\hat{\delta}_{c,\%}$	$\mu_{c,\%}$	$\hat{\delta}_{t,\%}$	$\mu_{t,\%}$	$\hat{\delta}_{c,\%}$	$\mu_{c,\%}$
$\theta_1\chi_1$	1	-0.6	-0.3	-3.3	-1.8	-0.6	-0.3	-3.4	-1.9
	2	-1.1	-0.4	-6.0	-2.5	-1.2	-0.4	-6.4	-2.6
$\theta_1\chi_2$	1	-0.5	-0.2	-2.7	-1.3	-0.5	-0.2	-2.8	-1.3
	2	-1.0	-0.3	-5.2	-1.8	-1.0	-0.2	-5.6	-1.7
$\theta_1\chi_3$	1	-0.6	-0.2	-2.9	-1.5	-0.6	-0.2	-3.0	-1.5
	2	-1.0	-0.3	-5.4	-2.0	-1.1	-0.3	-5.9	-2.0
$\theta_2\chi_1$	1	-0.9	-0.6	-5.1	-3.1	-1.0	-0.5	-5.5	-3.1
	2	-1.5	-0.9	-8.2	-5.0	-1.5	-0.9	-8.7	-4.9
$\theta_2\chi_2$	1	-0.8	-0.3	-4.2	-2.1	-0.7	-0.3	-4.1	-2.1
	2	-1.3	-0.6	-7.0	-3.3	-1.2	-0.5	-7.1	-3.3
$\theta_2\chi_3$	1	-0.8	-0.4	-4.5	-2.3	-0.8	-0.4	-4.6	-2.3
	2	-1.3	-0.6	-7.4	-3.6	-1.3	-0.6	-7.7	-3.6

Table 76: DR flexibility provision: netload decrease, for high netload case and renewable scenario R_b, in percentage deviation

Scenario		ξ_1			ξ_2		
	ΔT	$\hat{\delta}$	μ	σ	$\hat{\delta}$	μ	σ
$\theta_1\chi_1$	1	5.1	3.6	2.9	4.1	4.1	3.1
	2	14.0	8.3	6.6	13.3	8.9	6.9
$\theta_1\chi_2$	1	1.8	0.8	1.3	0.9	0.8	1.1
	2	3.6	1.9	2.5	1.4	1.7	2.3
$\theta_1\chi_3$	1	3.0	2.0	1.6	2.0	2.0	1.5
	2	7.1	4.4	3.4	5.2	4.3	3.3
$\theta_2\chi_1$	1	2.3	4.5	4.0	2.9	4.4	4.0
	2	6.3	10.6	9.2	7.0	10.4	9.2
$\theta_2\chi_2$	1	0.7	1.8	2.4	0.3	1.6	2.2
	2	1.4	4.5	5.8	1.0	4.3	5.4
$\theta_2\chi_3$	1	1.4	2.7	2.7	1.1	2.6	2.7
	2	3.1	6.8	6.5	2.9	6.5	6.2

Table 77: DR flexibility provision: netload increase, for low netload case and renewable scenario R_b, in GW

Scenario		ξ_1				ξ_2			
	ΔT	$\hat{\delta}_{t,\%}$	$\mu_{t,\%}$	$\hat{\delta}_{c,\%}$	$\mu_{c,\%}$	$\hat{\delta}_{t,\%}$	$\mu_{t,\%}$	$\hat{\delta}_{c,\%}$	$\mu_{c,\%}$
$\theta_1\chi_1$	1	5.7	1.6	6.1	3.2	4.7	1.8	5.0	3.7
	2	15.4	3.6	16.7	7.4	14.9	3.9	16.2	8.1
$\theta_1\chi_2$	1	2.3	0.4	2.5	0.8	1.2	0.4	1.3	0.8
	2	4.5	0.9	5.0	1.8	1.9	0.8	2.0	1.7
$\theta_1\chi_3$	1	3.7	0.9	4.0	1.8	2.5	0.9	2.7	1.9
	2	8.6	2.0	9.3	4.1	6.5	2.0	7.1	4.1
$\theta_2\chi_1$	1	2.0	1.8	2.2	3.4	2.5	1.8	2.7	3.5
	2	5.6	4.4	5.9	8.2	6.1	4.3	6.5	8.2
$\theta_2\chi_2$	1	0.8	0.8	0.8	1.6	0.3	0.7	0.3	1.5
	2	1.4	2.0	1.5	4.0	1.1	1.9	1.1	3.8
$\theta_2\chi_3$	1	1.3	1.2	1.4	2.3	1.1	1.1	1.2	2.2
	2	3.0	2.9	3.2	5.6	2.9	2.8	3.1	5.5

Table 78: DR flexibility provision: netload increase, for low netload case and renewable scenario R_b, in percentage deviation

Scenario		ξ_1			ξ_2		
	ΔT	$\hat{\delta}$	μ	σ	$\hat{\delta}$	μ	σ
$\theta_1\chi_1$	1	-10.1	-14.1	6.6	-10.5	-13.4	6.9
	2	-16.7	-26.6	12.5	-16.2	-25.4	13.3
$\theta_1\chi_2$	1	-0.4	-5.5	6.1	-0.9	-5.4	5.7
	2	-1.8	-11.4	12.2	-1.9	-11.1	11.6
$\theta_1\chi_3$	1	-3.7	-7.9	5.8	-4.1	-7.7	5.0
	2	-6.8	-15.7	11.8	-6.7	-15.1	10.7
$\theta_2\chi_1$	1	-16.4	-21.8	10.9	-15.9	-21.3	9.8
	2	-25.1	-39.7	20.4	-24.5	-38.2	18.0
$\theta_2\chi_2$	1	-3.5	-10.8	10.9	-3.4	-10.1	10.6
	2	-4.9	-19.0	17.8	-4.8	-17.5	17.6
$\theta_2\chi_3$	1	-7.8	-13.3	10.1	-7.4	-13.0	9.6
	2	-11.6	-23.7	16.8	-11.4	-22.9	15.9

Table 79: DR flexibility provision: ramping decrease, for high ramping up case and renewable scenario R_b, in $\frac{GW}{h}$

Scenario		ξ_1			ξ_2		
	ΔT	$\hat{\delta}_{t,\%}$	$\mu_{t,\%}$	$\hat{\delta}_{c,\%}$	$\hat{\delta}_{t,\%}$	$\mu_{t,\%}$	$\hat{\delta}_{c,\%}$
$\theta_1\chi_1$	1	-4.7	-9.1	-11.4	-4.9	-8.7	-12.1
	2	-7.8	-17.3	-18.8	-7.5	-16.5	-18.7
$\theta_1\chi_2$	1	-0.2	-3.6	-0.5	-0.4	-3.5	-1.2
	2	-0.8	-7.5	-2.3	-0.9	-7.3	-2.5
$\theta_1\chi_3$	1	-1.7	-5.2	-4.5	-1.9	-5.0	-5.2
	2	-3.1	-10.3	-8.2	-3.1	-9.9	-8.4
$\theta_2\chi_1$	1	-8.0	-14.4	-16.7	-7.7	-14.0	-16.6
	2	-12.2	-26.2	-25.5	-11.9	-25.1	-25.6
$\theta_2\chi_2$	1	-1.7	-7.3	-4.0	-1.7	-6.8	-4.1
	2	-2.4	-12.8	-5.7	-2.4	-11.8	-5.8
$\theta_2\chi_3$	1	-3.8	-9.0	-8.7	-3.6	-8.7	-8.5
	2	-5.7	-15.9	-13.0	-5.6	-15.3	-13.1

Table 80: DR flexibility provision: ramping decrease, for high ramping up case and renewable scenario R_b, in percentage deviation

Scenario		ξ_1			ξ_2		
	ΔT	$\hat{\delta}$	μ	σ	$\hat{\delta}$	μ	σ
$\theta_1\chi_1$	1	14.3	5.9	2.4	12.3	6.1	2.3
	2	25.1	11.3	3.8	23.4	11.0	4.0
$\theta_1\chi_2$	1	0.9	1.6	0.9	2.2	1.5	0.7
	2	0.9	3.1	2.1	2.9	2.7	1.5
$\theta_1\chi_3$	1	4.1	2.1	1.8	4.5	3.3	0.4
	2	6.3	3.9	3.4	6.7	6.0	0.8
$\theta_2\chi_1$	1	36.3	9.9	6.8	27.0	9.4	5.9
	2	66.8	21.1	13.0	62.9	19.6	10.9
$\theta_2\chi_2$	1	2.4	4.2	3.6	0.2	3.4	2.6
	2	3.2	10.2	7.2	2.7	9.0	6.1
$\theta_2\chi_3$	1	4.6	6.1	3.2	2.3	5.3	2.3
	2	6.9	14.0	6.1	6.1	12.6	5.5

Table 81: DR flexibility provision: ramping increase, for high ramping down case and renewable scenario R_b, in $\frac{GW}{h}$

Scenario		ξ_1			ξ_2		
	ΔT	$\hat{\delta}_{t,\%}$	$\mu_{t,\%}$	$\hat{\delta}_{c,\%}$	$\hat{\delta}_{t,\%}$	$\mu_{t,\%}$	$\hat{\delta}_{c,\%}$
$\theta_1\chi_1$	1	-11.8	-5.3	12.6	-10.3	-5.5	11.2
	2	-20.8	-10.1	22.1	-19.5	-9.9	21.2
$\theta_1\chi_2$	1	-0.8	-1.4	1.4	-1.9	-1.3	3.4
	2	-0.8	-2.8	1.4	-2.5	-2.4	4.5
$\theta_1\chi_3$	1	-3.5	-1.9	5.8	-3.8	-3.0	6.5
	2	-5.3	-3.5	8.9	-5.7	-5.4	9.7
$\theta_2\chi_1$	1	-25.9	-8.5	17.8	-20.4	-8.1	14.0
	2	-47.6	-18.0	32.7	-47.5	-16.8	32.5
$\theta_2\chi_2$	1	-1.9	-3.6	2.8	-0.2	-2.9	0.3
	2	-2.6	-8.8	3.8	-2.2	-7.8	3.3
$\theta_2\chi_3$	1	-3.8	-5.3	5.2	-1.9	-4.6	2.6
	2	-5.6	-12.1	7.8	-5.0	-10.9	7.0

Table 82: DR flexibility provision: ramping increase, for high ramping down case and renewable scenario R_b, in percentage deviation

Scenario		ξ_1			ξ_2		
	ΔT	$\hat{\delta}$	μ	σ	$\hat{\delta}$	μ	σ
$\theta_1\chi_1$	1	-6.8	-2.7	3.0	-6.7	-2.5	2.7
	2	-12.2	-3.8	4.0	-12.6	-3.5	3.6
$\theta_1\chi_2$	1	-5.5	-1.9	2.4	-5.5	-1.7	2.1
	2	-10.5	-2.6	3.1	-10.9	-2.2	2.7
$\theta_1\chi_3$	1	-5.9	-2.2	2.6	-5.9	-1.9	2.3
	2	-11.1	-3.0	3.3	-11.4	-2.6	2.9
$\theta_2\chi_1$	1	-10.3	-4.9	5.2	-10.7	-4.7	5.0
	2	-16.4	-7.8	8.6	-16.8	-7.2	7.9
$\theta_2\chi_2$	1	-8.2	-3.2	3.4	-7.8	-3.0	3.2
	2	-13.9	-5.1	5.3	-13.5	-4.8	5.0
$\theta_2\chi_3$	1	-8.9	-3.6	3.7	-8.8	-3.4	3.5
	2	-14.7	-5.6	5.7	-14.6	-5.3	5.5

Table 83: DR flexibility provision: netload decrease, for high netload case and renewable scenario R_c, in GW

Scenario		ξ_1				ξ_2			
	ΔT	$\hat{\delta}_{t,\%}$	$\mu_{t,\%}$	$\hat{\delta}_{c,\%}$	$\mu_{c,\%}$	$\hat{\delta}_{t,\%}$	$\mu_{t,\%}$	$\hat{\delta}_{c,\%}$	$\mu_{c,\%}$
$\theta_1\chi_1$	1	-0.7	-0.3	-3.3	-1.9	-0.7	-0.3	-3.4	-1.8
	2	-1.2	-0.4	-6.0	-2.6	-1.2	-0.4	-6.4	-2.5
$\theta_1\chi_2$	1	-0.5	-0.2	-2.7	-1.4	-0.5	-0.2	-2.8	-1.2
	2	-1.0	-0.3	-5.2	-1.9	-1.1	-0.2	-5.6	-1.7
$\theta_1\chi_3$	1	-0.6	-0.2	-2.9	-1.6	-0.6	-0.2	-3.0	-1.4
	2	-1.1	-0.3	-5.4	-2.2	-1.1	-0.3	-5.9	-1.9
$\theta_2\chi_1$	1	-1.0	-0.5	-5.1	-2.8	-1.0	-0.5	-5.6	-2.8
	2	-1.5	-0.8	-8.2	-4.5	-1.6	-0.7	-8.8	-4.4
$\theta_2\chi_2$	1	-0.8	-0.3	-4.2	-1.9	-0.7	-0.3	-4.2	-1.9
	2	-1.3	-0.5	-7.0	-3.1	-1.3	-0.5	-7.2	-3.0
$\theta_2\chi_3$	1	-0.8	-0.4	-4.5	-2.2	-0.8	-0.4	-4.6	-2.2
	2	-1.4	-0.6	-7.4	-3.4	-1.4	-0.6	-7.7	-3.4

Table 84: DR flexibility provision: netload decrease, for high netload case and renewable scenario R_c, in percentage deviation

Scenario		ξ_1			ξ_2		
	ΔT	$\hat{\delta}$	μ	σ	$\hat{\delta}$	μ	σ
$\theta_1\chi_1$	1	7.1	3.8	3.0	7.6	4.0	3.0
	2	13.7	8.5	6.7	14.4	8.7	6.9
$\theta_1\chi_2$	1	4.5	1.3	1.4	4.4	1.0	1.2
	2	8.9	2.5	2.8	8.1	2.2	2.5
$\theta_1\chi_3$	1	5.4	2.2	1.8	5.5	2.1	1.6
	2	10.5	4.6	3.8	10.2	4.5	3.6
$\theta_2\chi_1$	1	10.3	3.9	4.1	10.2	3.7	4.0
	2	23.3	9.1	9.3	23.8	8.9	9.1
$\theta_2\chi_2$	1	7.4	2.4	2.8	7.0	2.0	2.4
	2	17.5	5.7	6.4	17.6	5.3	5.8
$\theta_2\chi_3$	1	8.4	3.3	3.2	8.1	3.0	3.0
	2	19.4	7.7	7.4	19.7	7.4	6.9

Table 85: DR flexibility provision: netload increase, for low netload case and renewable scenario R_c, in GW

Scenario		ξ_1				ξ_2			
	ΔT	$\hat{\delta}_{t,\%}$	$\mu_{t,\%}$	$\hat{\delta}_{c,\%}$	$\mu_{c,\%}$	$\hat{\delta}_{t,\%}$	$\mu_{t,\%}$	$\hat{\delta}_{c,\%}$	$\mu_{c,\%}$
$\theta_1\chi_1$	1	-4.8	-12.4	4.3	3.2	-4.8	-11.6	4.7	3.5
	2	-9.1	-27.7	8.2	7.2	-9.1	-25.2	9.0	7.5
$\theta_1\chi_2$	1	-2.9	-2.9	2.8	1.2	-2.7	-2.1	2.9	1.0
	2	-5.6	-5.8	5.5	2.3	-4.9	-4.6	5.3	2.1
$\theta_1\chi_3$	1	-3.5	-5.6	3.3	2.0	-3.4	-4.8	3.5	1.9
	2	-6.8	-11.6	6.4	4.0	-6.3	-10.4	6.6	4.1
$\theta_2\chi_1$	1	-7.0	-19.2	6.1	2.9	-6.6	-15.9	6.3	2.9
	2	-15.8	-45.0	13.8	6.9	-15.5	-37.7	14.6	6.9
$\theta_2\chi_2$	1	-4.8	-7.0	4.5	2.0	-4.4	-5.2	4.5	1.7
	2	-11.4	-16.8	10.7	4.8	-11.0	-13.9	11.2	4.6
$\theta_2\chi_3$	1	-5.5	-11.1	5.1	2.6	-5.1	-9.1	5.1	2.5
	2	-12.8	-26.3	11.7	6.2	-12.4	-22.4	12.4	6.1

Table 86: DR flexibility provision: netload increase, for low netload case and renewable scenario R_c, in percentage deviation

Scenario		ξ_1			ξ_2		
	ΔT	$\hat{\delta}$	μ	σ	$\hat{\delta}$	μ	σ
$\theta_1\chi_1$	1	-10.1	-12.8	6.0	-10.5	-13.2	6.2
	2	-16.2	-24.4	12.1	-15.7	-25.0	12.0
$\theta_1\chi_2$	1	-0.4	-5.2	5.5	-0.9	-4.8	5.2
	2	-1.2	-10.9	11.1	-1.3	-9.9	10.5
$\theta_1\chi_3$	1	-3.7	-7.8	5.1	-4.1	-7.7	5.2
	2	-6.2	-15.5	10.6	-6.1	-15.2	10.5
$\theta_2\chi_1$	1	-16.4	-14.7	12.4	-15.9	-14.8	12.2
	2	-25.1	-26.3	21.5	-24.5	-26.2	20.7
$\theta_2\chi_2$	1	-3.1	-10.5	9.7	-3.0	-9.9	9.2
	2	-4.3	-19.0	16.3	-4.6	-17.5	15.3
$\theta_2\chi_3$	1	-7.0	-13.7	9.1	-6.7	-13.0	8.8
	2	-11.0	-24.7	15.5	-11.2	-23.0	14.9

Table 87: DR flexibility provision: ramping decrease, for high ramping up case and renewable scenario R_c, in $\frac{GW}{h}$

Scenario		ξ_1			ξ_2		
	ΔT	$\hat{\delta}_{t,\%}$	$\mu_{t,\%}$	$\hat{\delta}_{c,\%}$	$\hat{\delta}_{t,\%}$	$\mu_{t,\%}$	$\hat{\delta}_{c,\%}$
$\theta_1\chi_1$	1	-4.2	-7.2	-11.4	-4.4	-7.4	-12.1
	2	-6.7	-13.7	-18.2	-6.5	-14.0	-18.1
$\theta_1\chi_2$	1	-0.2	-2.9	-0.5	-0.4	-2.7	-1.2
	2	-0.5	-6.1	-1.6	-0.6	-5.6	-1.8
$\theta_1\chi_3$	1	-1.5	-4.4	-4.5	-1.7	-4.3	-5.2
	2	-2.6	-8.7	-7.6	-2.5	-8.5	-7.7
$\theta_2\chi_1$	1	-7.1	-8.3	-16.7	-6.9	-8.4	-16.6
	2	-10.8	-14.9	-25.5	-10.5	-14.8	-25.6
$\theta_2\chi_2$	1	-1.3	-6.1	-3.6	-1.3	-5.7	-3.6
	2	-1.9	-10.9	-5.0	-2.0	-10.1	-5.6
$\theta_2\chi_3$	1	-3.0	-7.8	-7.8	-2.9	-7.4	-7.7
	2	-4.8	-14.1	-12.2	-4.8	-13.1	-12.8

Table 88: DR flexibility provision: ramping decrease, for high ramping up case and renewable scenario R_c, in percentage deviation

Scenario		ξ_1			ξ_2		
	ΔT	$\hat{\delta}$	μ	σ	$\hat{\delta}$	μ	σ
$\theta_1\chi_1$	1	10.6	11.5	10.6	9.8	11.2	9.1
	2	17.1	20.9	19.2	15.8	19.6	16.1
$\theta_1\chi_2$	1	1.1	1.6	1.0	1.1	1.4	0.8
	2	1.3	3.0	2.3	1.3	2.6	1.6
$\theta_1\chi_3$	1	4.3	4.0	2.8	4.0	2.2	1.7
	2	6.6	7.5	5.1	6.1	3.9	3.0
$\theta_2\chi_1$	1	36.3	13.8	10.6	26.6	12.0	8.8
	2	66.8	26.9	18.9	48.9	23.3	15.6
$\theta_2\chi_2$	1	0.8	4.2	4.1	1.1	3.4	3.5
	2	1.9	9.5	7.8	2.1	8.2	6.8
$\theta_2\chi_3$	1	0.0	4.0	4.3	0.0	3.3	3.3
	2	0.0	8.7	8.7	0.0	7.8	7.6

Table 89: DR flexibility provision: ramping increase, for high ramping down case and renewable scenario R_c, in $\frac{GW}{h}$

Scenario		ξ_1			ξ_2		
	ΔT	$\hat{\delta}_{t,\%}$	$\mu_{t,\%}$	$\hat{\delta}_{c,\%}$	$\hat{\delta}_{t,\%}$	$\mu_{t,\%}$	$\hat{\delta}_{c,\%}$
$\theta_1\chi_1$	1	-7.4	-9.9	11.5	-6.8	-9.6	10.9
	2	-11.9	-17.9	18.6	-11.0	-16.9	17.5
$\theta_1\chi_2$	1	-0.8	-1.4	1.5	-0.8	-1.3	1.5
	2	-1.0	-2.6	1.8	-0.9	-2.3	1.8
$\theta_1\chi_3$	1	-3.0	-3.5	5.3	-2.8	-1.9	5.1
	2	-4.7	-6.5	8.2	-4.3	-3.4	7.7
$\theta_2\chi_1$	1	-25.0	-11.4	17.8	-18.8	-10.0	13.2
	2	-46.0	-22.3	32.7	-34.4	-19.4	24.2
$\theta_2\chi_2$	1	-0.6	-3.5	1.0	-0.8	-2.9	1.4
	2	-1.4	-8.0	2.6	-1.5	-6.9	2.7
$\theta_2\chi_3$	1	0.0	-3.3	0.0	0.0	-2.8	0.0
	2	0.0	-7.3	0.0	0.0	-6.6	0.0

Table 90: DR flexibility provision: ramping increase, for high ramping down case and renewable scenario R_c, in percentage deviation